



HAL
open science

Traitement itératif et conjoint pour les systèmes radio-mobiles

Raphaël Visoz

► **To cite this version:**

Raphaël Visoz. Traitement itératif et conjoint pour les systèmes radio-mobiles. domain_other. Télécom ParisTech, 2002. Français. NNT : . pastel-00001292

HAL Id: pastel-00001292

<https://pastel.hal.science/pastel-00001292>

Submitted on 22 Nov 2010

HAL is a multi-disciplinary open access archive for the deposit and dissemination of scientific research documents, whether they are published or not. The documents may come from teaching and research institutions in France or abroad, or from public or private research centers.

L'archive ouverte pluridisciplinaire **HAL**, est destinée au dépôt et à la diffusion de documents scientifiques de niveau recherche, publiés ou non, émanant des établissements d'enseignement et de recherche français ou étrangers, des laboratoires publics ou privés.

Traitements itératif et conjoint pour les systèmes radio mobiles *

R. Visoz

Soutenue le 25 Mars 2002

Claude Berrou	Président
Pierre Humblet	
Pierre Duhamel	Rapporteurs
Daniel Duponteil	
Philippe Ciblat	Examineurs
Joseph Boutros	Directeur de Thèse

*English title: Iterative and Joint Processing for Wireless Mobile Systems

To my parents Jacques and Michelle Visoz.

"L'intelligence parcellarisée, compartimentée, mécanistique, disjonctive, réductionniste brise le complexe du monde en fragments disjoints, fractionne les problèmes, sépare ce qui est relié, unidimensionnalise le multidimensionnel", (Edgar Morin).

Acknowledgements

This work is the result of many influences, and meetings. The main contributors from a technical point of view to this thesis are Antoine Berthet (chapter 3,4,6,7), Elie Bejjani (chapter 2), Hatem Boujemaa (chapter 5), Nikolai Nefedov and Markku Pukkila (chapter 4), without their help and their enthusiasm this thesis would not exist. A special thank to Antoine, who is now a very good friend as well as my favorite fellow worker. I hope that our future collaborations will be as fruitful as they were during these last three years.

I am very grateful to Professor Joseph Boutros who accepted to supervise this thesis and gave me precious advice and orientations to improve its overall content.

I am also grateful to Bertrand Penther and Hiroshi Kubo whose contributions to the European Project Broadband Radio Access Network (BRAN) were very helpful to understand and master the Generalized Viterbi Algorithm (GVA) [61]. These contributions [89] [71] were specially important to me, since I consider them as the starting point of my work on efficient trellis search techniques.

I wish to thank Professor Pierre Humblet whose class notes [63] keeps being my reference work and were specially useful for chapter 1. I hope that these class notes will be published on account of their contents.

This thesis was made possible by Armand Levy who not only accepted that I carried out a PhD in parallel to my professional activities but also encouraged me. I also thank Daniel Duponteil for giving me interesting work which always lay between advanced engineering and research.

I am very grateful to the two reviewers Pierre Duhamel and Pierre Humblet who accepted to read carefully and correct the draft of this thesis. I wish to thank namely Professor Claude Berrou who accepted to be the president of the jury, Professor Joseph Boutros who was my efficient supervisor, Daniel Duponteil, and Professor Philippe Ciblat who accepted to be the other members of my jury.

Last but not least, thanks to Ainhoa for always being supportive, all the more during the difficult phases of this project.

Résumé

L'égalisation pour les systèmes monoporteuses est un vieux domaine qui paraît peu sujet à des innovations. Cependant, on peut se demander si la séparation fonctionnelle entre égalisation, décodage et estimation de canal est pertinente [40][37]. En effet, les traitements itératifs faisant dialoguer plusieurs entités d'une même chaîne de communication se sont avérés extrêmement fructueux dans le domaine du codage et, plus récemment, dans le domaine de l'estimation de canal et de l'égalisation. Le sujet de cette thèse est, en fonction des paramètres du système étudié (typiquement la taille de l'entrelacement, le type de canal radio mobile), d'essayer de combiner ces trois tâches de la façon la plus performante (la retransmission étant traitée comme une forme de codage canal). L'approche proposée ne s'attache pas seulement aux performances obtenues mais aussi au souci de complexité, afin de viser des applications industrielles. Trois contextes sont particulièrement étudiés: les réseaux radio haut débits du type ATM sans fil, le CDMA haut débit avec faible facteur d'étalement, les systèmes TDMA avancés (EDGE) avec modulation d'ordre élevé et/ou antennes d'émission et de réception multiple. Afin de conserver le critère Maximum A Posteriori (MAP), tout en gardant une complexité abordable, les techniques dites de traitement par survivant (sur treillis réduits) sont exhaustivement décrites et mises en pratiques pour les contextes précédemment cités. Il est notamment démontré que la généralisation du traitement par survivant, consistant très simplement à garder plus d'un survivant par noeud du treillis réduit, est très robuste à la propagation d'erreur même en présence de canaux à phase non minimale. Cette généralisation fut originellement introduite par Hashimoto [61] sous le nom d' algorithme de Viterbi généralisé (GVA), la technique elle même étant dans cette thèse dénommée traitement par survivant généralisé.

Contents

1	Introduction	11
2	Matched Filter Bound for Multichannel Diversity over Frequency-Selective Rayleigh-Fading Mobile Channels	15
2.1	Introduction	15
2.2	General Approach	17
2.2.1	System Model	17
2.2.2	Error Probability Lower Bound	20
2.2.3	Asymptotic Behavior	21
2.3	Unitary Transformation Effect In Micro-Diversity	22
2.4	Polarization vs. Spatial Micro-Diversity	24
2.4.1	Polarization Diversity	24
2.4.2	\mathbf{K}_x Matrix for Space/Polarization Dual-Diversity	25
2.4.3	Space/Polarization Diversity for GSM and IS-95	26
2.4.4	Rotating the Base Station Antennas	27
2.5	Coded Matched Filter Bound	29
2.6	Conclusion	30
3	Joint Equalization and decoding using the Generalized Viterbi for broadband wireless applications.	37
3.1	Introduction	37
3.2	Proposed Algorithm	38
3.3	Applications	40
3.3.1	Application 1: Cyclic block codes, joint equalization and decoding on various full code trellises	40
3.3.2	Application 2: cyclic block codes, joint equalization and decoding on reduced code trellises	41
3.3.3	Application 3: Convolutional encoded signals, joint equalization and decoding process for broadband wireless applications.	43

3.4	Conclusions	46
4	Iterative Equalization and Estimation for Advanced TDMA Systems	53
4.1	Introduction	53
4.2	System Model	54
4.2.1	Notation	54
4.2.2	The equivalent discrete-time channel model	55
4.2.3	Conventional receiver	56
4.3	Low Complexity Q -ary SISO Equalizer	57
4.3.1	Decision Feedback Soft-In Soft-Out (DF-SISO) equalizer	57
4.3.2	DF-SISO equalizer with forward recursion	60
4.3.3	Minimum-phase pre-filtering	61
4.4	Iterative Receiver for EDGE	62
4.4.1	Turbo detection principle	62
4.4.2	Q -ary turbo-detection with DF-SISO equalizers	62
4.4.3	Iterative (turbo) channel estimation	64
4.4.4	Combined iterative estimation-equalization	65
4.4.5	Turbo equalization for retransmission schemes	66
4.5	Simulation Results	67
4.5.1	Turbo detection without channel re-estimation	67
4.5.2	Turbo detection and LS-based channel re-estimation	68
4.5.3	application of the Turbo equalization to GSM EDGE Radio Access Network	68
4.6	Conclusions	69
5	Iterative Low-Complexity Receiver for High Bit Rate CDMA	81
5.1	Introduction	81
5.2	System model	83
5.3	Equivalent channel Model at the Rake receiver output	83
5.4	Low-complexity iterative Receiver	85
5.4.1	Turbo Rake SISO DFSE receiver	85
5.5	Channel estimation improvement	85
5.5.1	MMSE channel estimates	85
5.5.2	iterative (turbo) channel estimation	87
5.6	Simulation results	87
5.7	Conclusion	88

6	Iterative Receivers for Bit-Interleaved Coded Modulation over Wireless Frequency-Selective Channels	93
6.1	Introduction and motivations	93
6.2	Communication model	95
6.3	Iterative multilayer data detection and channel decoding	96
6.3.1	SISO joint multilayer data detection	96
6.3.2	A generalized reduced-state SOVA-like algorithm	97
6.4	Iterative channel estimation	99
6.4.1	Initial channel estimation	99
6.4.2	LS-based turbo channel estimation	101
6.5	Performance analysis	102
6.5.1	Optimal receiver	102
6.5.2	Reduced-complexity multilayer data detector	102
6.5.3	Reduced-complexity receiver and its application to GERAN	103
6.6	Conclusion	104
7	Iterative Decoding of Serially Concatenated Multilayered Trellis-Coded Modulations in Multipath Rayleigh Fading Environment.	111
7.1	Introduction	111
7.1.1	Wireless transmission context	111
7.1.2	Efficiency and limits of full turbo detection	112
7.1.3	Improving spectral efficiency of serially concatenated space-time trellis coded modulation	113
7.1.4	Chapter organization	114
7.2	Serially concatenated multilayered space-time trellis coded modulation	114
7.2.1	Communication model	114
7.2.2	Iterative decoding	116
7.3	Discrete-time finite-state Markov model and associated possibly-reduced trellis	116
7.3.1	Discrete-time finite-state Markov model for elementary ST-TCM	116
7.3.2	Combined trellis associated with elementary ST-TCM	118
7.3.3	Multilayer discrete-time Markov model and multilayer combined trellis	118
7.3.4	Reduced-state multilayer combined trellis	119
7.4	SISO joint multilayer data detection and inner decoding	119
7.4.1	Reduced-state trellis search and generalized per-survivor processing	119
7.4.2	A generalized reduced-state SOVA-like algorithm	120
7.5	Performance analysis	122
7.5.1	Serially concatenated TCM (non minimum-phase time-invariant channel)	122

7.5.2	Design of inner ST-TCM in concatenated systems	124
7.5.3	Serially concatenated multilayered ST-TCM (BLAST-like approach) .	125
7.6	Conclusion and future research topics	126
8	Conclusions	133
A	Wide Sense Stationary (WSS) Random Processes	137
B	Karhunen-Loève Expansion for Circularly Symmetric Complex Variables	139
C	Calculus of U_n	141
D	CRLB for Iterative Channel Estimation	143

Chapter 1

Introduction

Equalization for single carrier wireless systems may appear at first sight as a worn out field, where few innovations remain to be done. However, one can wonder if the strict functional split between equalization, decoding and channel estimation that exists nowadays in classical receivers is judicious [40] [37]. Indeed, iterative processing making several entities of the same communication chain communicate was proved to be very profitable in the coding domain and more recently in the channel estimation and equalization domains. The topic of this thesis is to combine these reception basic tasks in the most efficient way taking into account the studied system constraints, i.e., interleaving size, wireless mobile channel type, and channel coding. The proposed approaches not only optimize the performance but also the complexity in order to aim at industrial applications.

Three main contexts are studied in this thesis:

- wireless Local Area Network (LAN) with very high data rate and granularity constraints,
- high data rate CDMA with low spreading factor,
- advanced wireless TDMA systems with high order modulation and/or Multiple Input Multiple Output channel.

In the **second chapter**, we analytically derive the performance of optimal receivers over wireless mobile channels. The chosen approach is the Matched Filter Bound (being a lower bound under idealized conditions, in particular perfect channel estimation and no Inter-Symbol Interference) for multichannel diversity over frequency selective Rayleigh fading mobile channels. It allows a better understanding of the diversity concept, which is important for mobile radio interface design; and to quantify, to a certain extent, the gains related to different diversity sources (i.e., antenna diversity, multipath diversity, and time diversity) that can be expected for a given set of system parameters such as the modulation

characteristics, the data rate, the radio channel properties. It also helps to explain the performance degradation due to InterSymbol Interference (ISI) and to identify sub-optimality in the receiver design. This bound serves as a valuable benchmark throughout this thesis.

The **third chapter** deals with wireless LAN, that is to say systems that have strong granularity constraints and no time diversity at all due to very high data rates, i.e, the channel coherence time is by far larger than the permitted interleaving size (e.g., much larger than an ATM cell length). A joint equalization and decoding approach without interleaving seems to be the most appropriate one for single carrier radio interfaces. However, the major problem lies here in the receiver complexity which increases exponentially with data rates. This chapter is, thus, naturally oriented towards suboptimal trellis search techniques applied to joint equalization and decoding that enable to reduce significantly the receiver trellis complexity. Finally, a new low-complexity receiver is proposed based on Generalized Per Survivor (GPSP) Processing technique derived from the Generalized Viterbi Algorithm (GVA). This technique revealed particularly robust to error propagation even in the case of non-minimum phase channels.

The **fourth chapter** looks into the gains brought by iterative processing or by the "turbo principle" applied to advanced TDMA systems with high order modulation and channel interleaving. We tried to include as many entities as possible into one iteration. A low complexity trellis based receiver is proposed, performing iteratively channel estimation, equalization and decoding.

The turbo detection/equalization scheme is original in the sense that it stands out from the classical approaches based on Decision Feedback Equalizers (DFE) or Maximum A Posteriori (MAP) equalizers. Here, we used a Soft-In Soft-Out (SISO) Decision Feedback Sequence Estimation (DFSE) equalizer with prefiltering to turn the channel into minimum phase.

Concerning channel re-estimation, many different methods can be used to tackle this issue. Once again in order to keep the receiver complexity as low as possible, we chose one of the simplest: a linear approach derived from the so-called bootstrap technique (using a Least Square (LS) estimator, often refers as LS-based channel re-estimation). A Cramer Rao bound is also presented and gives insights about its performance.

The **fifth chapter** deals with CDMA systems using low spreading factor or equivalently spreading sequences with bad correlation properties. It is well known that the Rake receiver performance degrades significantly for spreading factor lower than 16 entailing the need of an Interference canceller at its output. Fortunately, the Rake output can be formally identified to a convolution product enabling the transposition of the different techniques developed in the previous chapter to that context (i.e, Rake followed by SISO-DFSE).

The use of a low spreading factor also degrades the performance of the conventional channel estimator which relies heavily on spreading sequence properties. This issue is also addressed in this chapter by suggesting a new channel estimation algorithm that takes into account the ISI structure.

The **sixth chapter** aims at generalizing the previous approaches to a Multiple Input Multiple Output (MIMO) channel for TDMA systems. A reduced-complexity trellis-based receiver performing iteratively channel estimation, multilayer detection/equalization and channel decoding is derived. The SISO multilayered data detector/equalizer is based on the GPSP technique already introduced in the third chapter. Indeed this technique is well adapted to this context since a prefilter turning every single channel into minimum phase does not exist. The channel re-estimation is based on the generalization of the bootstrap technique of chapter 4.

Our approach presents two-fold advantages. It enables to cope with severe MIMO channel ISI and allows to use more transmit antennas than receive antennas. Focusing on the case of N transmit antennas and one receive antenna, which is particularly interesting for handset mobile at the receiver end, the equivalence in terms of data rate and receiver complexity between one 2^N -order modulation and N parallel transmitted BPSK is pointed out.

The **seventh chapter** investigates Iterative Decoding of Serially Concatenated Multilayered Trellis-Coded Modulations in a MIMO frequency selective radio channel . It can be viewed as an extension of chapter 3 and 6 in order to increase the spectral efficiency and the robustness of the GPSP-based sub-optimal receiver to strong ISI.

Chapter 2

Matched Filter Bound for Multichannel Diversity over Frequency-Selective Rayleigh-Fading Mobile Channels.

2.1 Introduction

In modern time-division multiple-access (TDMA) digital mobile radio systems, data signals are transmitted in bursts. If the channel can be assumed time invariant for the burst duration (slow fading channel) then the optimum L -channel diversity receiver is the Maximum Likelihood Sequence Estimation (MLSE) receiver [69]. The performance of such a receiver is given by averaging the error probability on all possible channel outcomes. For a given channel outcome the error probability (in white Gaussian noise) is assessed by the minimum Euclidian distance between all possible received sequences. This quantity is very difficult to calculate for arbitrary dispersive channels, so that only numerical performance results can be obtained via error trellis method [77, page 420].

A much simpler measure of performance can be obtained by neglecting the effect of Inter-Symbol-Interference (ISI) and deriving the Bit Error Probability (BEP) when a single symbol is transmitted over a perfectly known channel. In this way, an absolute BEP performance lower bound is obtained, which is commonly known as the Matched Filter Bound (MFB). Surprisingly, the MFB gives in many cases the same performances as the error trellis method, meaning that within a multiplicative constant the error probability of the MLSE is essentially the same as the MFB even in presence of ISI [77, page 448]. For Direct-Sequence Spread-Spectrum (DSSS) systems, the classical RAKE receiver approaches the MFB at the expense of very low symbol rate [92]. As a consequence, matched filter bounds (being lower

bounds under idealized conditions, in particular perfect channel estimation and no ISI) are very attractive because they are more easily derived in analytical form, and also because these bounds are generally found to be tight enough (in comparison with MLSE optimum receiver or RAKE receiver) to make them serve as valuable benchmarks for system design and evaluation.

In this chapter, a matched filter bound of the error probability for an L -branches diversity system that uses any linear modulation over multipath frequency-selective fading channels is derived. On the receiver side, it is assumed that L branches of diversity are obtained by the use of L distinct antennas. The lower bound is based on the principles of matched filter and Maximal Ratio Combining (MRC). Performance bounds have already been derived for several systems in the past [63], [4], [5], [98], [127],[66], [100], [78], [129], [35], [46]. For example, in [98] the problem has been formulated in its most general form, but only for the case of ideal linear equalization, while [66] treats the case of a single multipath Rayleigh fading channel with independent taps only.

In [35] the matched filter bound is calculated in the frequency domain for L uncorrelated diversity branches via a continuous Karhunen Loève transformation which allows both continuously dispersive channels and discrete multipath channels to be taken into account. Moreover [35] considers colored noise but having the same power spectral density on all branches. Finally, in [46], the matched filter bound results for uncorrelated L diversity branches are extended to Trellis Coded Modulation with perfect interleaving.

Our formulation is the first one which accounts at the same time for the following aspects: pulse shape, channel taps correlation, any number of diversity branches, power mismatch of the different branches (especially useful for polarization diversity), envelope correlation between the signals on different branches, and white noise with different power spectral density on each branch. Moreover, the presented matched filter bound derivation is the most straightforward as it relies on a unique Karhunen-Loève expansion. In comparison, the approach considered in [78] is composed of two successive transformations as it needs an extra Cholesky decomposition to take into account any kind of correlation. In this respect, it is shown here that the compactness of our analytical formulation allows us to get more insight in important issues related to antenna diversity, such as polarization diversity gain.

In Section 2.2, the considered system model is presented and the theoretical error probability lower bound using Karhunen-Loève expansion is derived, together with the asymptotic expression of the BER for BPSK. This result, already known for flat fading channels [101], is thus shown to apply for the more general case of frequency-selective fading channels.

In Section 2.3, with the use of our model, any unitary transformation on taps of equal delay is shown to leave the diversity gain unchanged for antenna diversity systems having the same noise spectral density on each branch. This is particularly interesting for polarization

diversity as it is shown that rotating the base station antennas represents a special case of unitary transformation. Thus, the widespread belief of added diversity gain for slanted antennas at the receiver is proven to be wrong from the matched filter bound point of view. In addition, by extending the work of Vaughan [117], the same result was numerically confirmed. Polarization diversity gain is invariant vs. antennas rotation.

In Section 2.4, polarization diversity is overviewed as there is a renewed interest for this kind of diversity, especially in mobile radio systems. Additionally, with the use of our theoretical model, the spatial and polarization dual-diversity gains for Global System for Mobile communication (GSM) [82] and Interim Standard 95 (IS-95 downlink) [114] mobile systems are compared in various cellular environments.

Finally, in section 2.5 the coded Matched Filter Bound is presented.

2.2 General Approach

In this section we give a detailed presentation of the system model and the computation of the matched filter error probability bound.

2.2.1 System Model

The considered base-band system model is depicted in Fig. 2.1. It consists of a one dimensional (complex or real) linear modulation with a pulse shape filter $g(t)$ at the transmitter side. The transmitted signal passes through L time-varying multipath channels $h_i(t, \tau)$ ($i = 1, \dots, L$), assumed to be perfectly known, and is received by L different antennas corresponding to L diversity branches. Each channel is modeled by a discrete K_i -taps time varying response

$$h_i(t, \tau) = \sum_{j=1}^{K_i} c_{ij}(t) \delta(\tau - \tau_{ij}), \quad (2.1)$$

where each $c_{ij}(t)$ is a zero mean complex Gaussian random variable (Rayleigh fading). The additive white Gaussian noise (AWGN) of the i -th branch $n_i(t)$ has a power spectral density N_i . The L different noise signals are assumed to be uncorrelated. In the sequel, c_{ij} and $c_{ij}(t)$ will be indistinctly used as the channel is assumed to be invariant for a symbol duration. The channel taps c_{ij} of the L branches can be arranged in the following vector form

$$\mathbf{x} = [c_{11} \dots c_{1K_1} c_{21} \dots c_{2K_2} \dots c_{L1} \dots c_{LK_L}]^T. \quad (2.2)$$

The covariance matrix \mathbf{K}_x of the vector \mathbf{x} is given by $\mathbf{K}_x = E(\mathbf{x}\mathbf{x}^\dagger)$, where \dagger denotes the conjugated transpose operator. It is important to note that, unlike previously published results [4] [5], [98], [127],[66], [100], [78], [129], [35], [46], no particular restriction on \mathbf{K}_x

is considered. This allows to treat, in the same framework, the most general case of tap correlation within one branch as well as between different branches.

As the matched filter bound is considered, only one symbol is transmitted and received [5]. In this case, for the i -th diversity branch the matched filter for each transmitted symbol —say a — is in fact matched to $M_i(t, \tau) = g(\tau) * h_i(t, \tau)$ where $*$ denotes the convolution operator. The optimal way to combine the L branches is to perform Maximal Ratio Combining (MRC). Therefore, as the noise signals of the branches have different flat power spectral densities N_i , any branch i must be weighted by a factor $1/N_i$, [101]. Then the outputs of the L matched filters are sampled at the symbol rate (perfect synchronization is supposed). We then obtain the samples

$$y_i = \frac{a}{N_i} \| M_i(t, \tau) \|^2 + b_i , \quad (2.3)$$

where b_i is the Gaussian noise sample of the i -th branch output and $\| M_i(t, \tau) \|^2$ is the total energy of $M_i(t, \tau)$ given by

$$\| M_i(t, \tau) \|^2 = \int d\tau \left[\sum_{j=1}^{K_i} c_{ij}(t) g^*(\tau - \tau_{ij}) \right] \left[\sum_{k=1}^{K_i} c_{ik}(t) g(\tau - \tau_{ik}) \right] . \quad (2.4)$$

Defining the autocorrelation function of $g(t)$ as

$$\rho_g(\tau) = \int g^*(t - \tau) g(t) dt , \quad (2.5)$$

y_i can now be written

$$y_i = \frac{a}{N_i} \sum_{j=1}^{K_i} \sum_{k=1}^{K_i} c_{ij}^* \rho_g(\tau_{ij} - \tau_{ik}) c_{ik} + b_i . \quad (2.6)$$

Let $\mathbf{c}_i = [c_{i1}, c_{i2}, \dots, c_{iK_i}]^T$, then we have

$$y_i = a \mathbf{c}_i^\dagger \mathbf{A}^i \mathbf{c}_i + b_i , \quad (2.7)$$

where \mathbf{A}^i is a $K_i \times K_i$ matrix with elements $A_{jk}^i = \rho_g(\tau_{ij} - \tau_{ik})/N_i$.

The L samples y_i are added together to give the final decision variable u

$$u = \sum_{i=1}^L y_i = az + b \quad (2.8)$$

with

$$z = \sum_{i=1}^L \mathbf{c}_i^\dagger \mathbf{A}^i \mathbf{c}_i \quad (2.9)$$

and

$$b = \sum_{i=1}^L b_i . \quad (2.10)$$

Recalling (2.2), it is easily observed that (2.9) can be expressed as

$$z = \mathbf{x}^\dagger \mathbf{H} \mathbf{x} \quad (2.11)$$

where the matrix \mathbf{H} is defined as

$$\mathbf{H} = \begin{pmatrix} \mathbf{A}^1 & 0 & 0 & \cdots & 0 \\ 0 & \mathbf{A}^2 & 0 & \cdots & 0 \\ \vdots & \vdots & \vdots & \vdots & \vdots \\ 0 & 0 & 0 & \cdots & \mathbf{A}^L \end{pmatrix}. \quad (2.12)$$

Consequently, the final decision variable is equal to the transmitted symbol a scaled by the coefficient z and added to a Gaussian noise sample b . The instantaneous signal-to-noise ratio (SNR) of the combiner output (i.e. the variable u), for given values of \mathbf{c}_i , is equal to

$$\gamma = \frac{|E(u)|^2}{E(|u - E(u)|^2)}. \quad (2.13)$$

Let us verify that the receiver really implements MRC combining. As b is a zero mean Gaussian noise, and assuming that $E(|a|^2) = 1$ we have

$$|E(u)|^2 = \left(\sum_{i=1}^L \frac{\|M_i(t, \tau)\|^2}{N_i} \right)^2. \quad (2.14)$$

The noise sample b_i at the output of i -th branch is expressed as

$$b_i = \frac{1}{N_i} \int d\tau n_i(\tau) M_i^*(t, \tau). \quad (2.15)$$

As a result the variance of the decision variable u can be written

$$E(|u - E(u)|^2) = \frac{1}{N_i N_j} \sum_{i=1}^L \sum_{j=1}^L \int \int du dv E[n_i(u) \times n_j^*(v)] M_i^*(t, u) M_j(t, v). \quad (2.16)$$

Using the properties of the noise signals, we have

$$E(n_i(u) \times n_j^*(v)) = N_i \delta(u - v) \delta_{ij}. \quad (2.17)$$

Thus we can write

$$E(|u - E(u)|^2) = \sum_{i=1}^L \frac{\|M_i(t, \tau)\|^2}{N_i}. \quad (2.18)$$

Equations (2.13), (2.14) and (2.18) yield

$$\gamma = \sum_{i=1}^L \frac{\|M_i(t, \tau)\|^2}{N_i}. \quad (2.19)$$

Finally, using (2.3) and (2.8), one can easily verify that

$$\gamma = z = \sum_{i=1}^L \gamma_i \tag{2.20}$$

where $\gamma_i = \| M_i(t, \tau) \|^2 / N_i = E_s^i / N_i$ is the instantaneous signal-to-noise ratio of the i -th branch (E_s^i is the instantaneous received symbol energy for the i -th branch). Thus, adding the samples is equivalent to performing MRC of the diversity branches [101]. Therefore, the combination of ideal matched filters and MRC leads to the best theoretical performance, meaning that it corresponds to the lowest bound of the error probability that a real life receiver can attain. However, as underlined before, this bound is very close to the optimum receiver performance.

2.2.2 Error Probability Lower Bound

As the autocorrelation function $\rho_g(t)$ has an Hermitian symmetry and is non-negative definite, it follows that matrix \mathbf{A}^i is Hermitian non-negative definite. By extension, matrix \mathbf{H} is also Hermitian non-negative definite, and of dimension $K \times K$ where $K = \sum_{i=1}^L K_i$. Therefore, $\sqrt{\mathbf{H}}$ exists so that z can be written $z = \mathbf{v}^\dagger \mathbf{v}$, where $\mathbf{v} = \sqrt{\mathbf{H}} \mathbf{x}$.

Knowing that \mathbf{x} is circularly symmetric (i.e., $E(\mathbf{x}\mathbf{x}^T) - E(\mathbf{x})E(\mathbf{x}^T) = 0$, T denoting the transpose operator) and that its covariance matrix is real (see Appendix A), \mathbf{v} is also circularly symmetric as it is obtained by a linear transformation of \mathbf{x} . Using the results of Appendix B, \mathbf{v} can be written as

$$\mathbf{v} = \sum_{i=1}^K q_i \mathbf{u}_i, \tag{2.21}$$

where q_i are complex circularly symmetric random variables with variances the eigenvalues of $\mathbf{K}_v = E(\mathbf{v}\mathbf{v}^\dagger)$, and \mathbf{u}_i are complex mutually orthonormal vectors. As a result, z can be written in the simple form

$$z = \sum_{i=1}^K |q_i|^2, \tag{2.22}$$

where $|q_i|^2$ are independent chi-square random variables with means the eigenvalues λ_i ($i = 1, \dots, K$) of $\mathbf{K}_v = \sqrt{\mathbf{H}}\mathbf{K}_x\sqrt{\mathbf{H}}$ or equivalently of $\mathbf{H}\mathbf{K}_x$, $\mathbf{K}_x = E(\mathbf{x}\mathbf{x}^\dagger)$ being the covariance matrix of \mathbf{x} . Note that the matrix \mathbf{H} takes into account the pulse shape characteristics in combination with the channel delay spread, whereas the matrix \mathbf{K}_x combines the effects of the power profiles of the L channels, the correlations (between taps of one branch as well as taps of different branches), and the power mismatch among the L branches.

In case of unequal eigenvalues, the probability distribution of z is given by

$$p_z(z) = \sum_{i=1}^K \frac{\pi_i}{\lambda_i} e^{-\frac{z}{\lambda_i}} \tag{2.23}$$

where π_i are the residues ($\pi_i = \prod_{k \neq i} \frac{\lambda_i}{\lambda_i - \lambda_k}$).

More generally, some eigenvalues may be equal, which is the case for instance when treating independent diversity branches having the same channel profile. This case was examined extensively in many papers such as [100]. Alternatively, one can artificially separate the equal eigenvalues by a very small amount. In this way, the distribution (2.23) can still be used and yields results very close to the exact approach.

We know from (2.20) that the instantaneous signal-to-noise ratio of the decision variable u is $\gamma = z$. Moreover, using (2.22), the mean signal-to-noise ratio when considering the channel variations is simply $\bar{\gamma} = \bar{z} = \sum_i \lambda_i$. Then the average error probability versus $\bar{\gamma}$ can be obtained as

$$P_e(\bar{\gamma}) = \int_0^\infty dz p_z(z) P_0(z) \quad (2.24)$$

where $P_0(\gamma)$ is the error probability of the chosen modulation in AWGN channel.

For BPSK modulation, (2.24) can be solved analytically, so the matched filter bound error probability can be expressed as [66], [100], [78]

$$P_e(\bar{\gamma}) = \frac{1}{2} \sum_{i=1}^K \pi_i \left[1 - \sqrt{\frac{\bar{\gamma}}{\bar{\gamma} + 1/\mu_i}} \right] \quad (2.25)$$

where $\mu_i = \lambda_i / \sum \lambda_i$ are the normalized eigenvalues.

One can check that in a flat Rayleigh fading channel ($K = 1$) the BER reduces to the well known equation [92]

$$P_e(\bar{\gamma}) = \frac{1}{2} \left[1 - \sqrt{\frac{\bar{\gamma}}{\bar{\gamma} + 1}} \right]. \quad (2.26)$$

2.2.3 Asymptotic Behavior

It is well known, in the case of K branches diversity with flat Rayleigh fading, that for large signal-to-noise ratio $\bar{\gamma}$, the BER behaves as $\bar{\gamma}^{-K}$. The order of diversity thus is said to be K . Moreover, when the signals on the branches are correlated or have different energy levels, the BER will still have the same asymptotic slope but suffers a degradation in SNR given by the amount of signal correlation and/or energy mismatch [101].

Our goal is to extend this notion to the general case of frequency-selective Rayleigh fading channels. The asymptotic error probability of BPSK for large SNR can be obtained by developing (2.25) in the following manner

$$P_e(\bar{\gamma}) = \frac{1}{2} \sum_{n=1}^{\infty} (-1)^n C_{-\frac{1}{2}}^n U_n \frac{1}{\bar{\gamma}^n} \quad (2.27)$$

where

$$U_n = \sum_{i=1}^K \frac{\pi_i}{\mu_i^n} \quad (2.28)$$

and

$$C_q^k = \frac{q(q-1)\cdots(q-k+1)}{k!}. \quad (2.29)$$

It is demonstrated in [14] (see Appendix C) that

$$\begin{cases} U_n = 1 & n = 0 \\ U_n = 0 & n = 1, \dots, K-1 \\ U_n = \frac{(-1)^{K+1}}{\prod_{i=1}^K \mu_i} & n = K \end{cases} \quad (2.30)$$

Thus, for sufficiently large $\bar{\gamma}$, (2.27) can be well approximated by its first non-zero term

$$P_e(\bar{\gamma}) \simeq \frac{(-1)^K}{2} \frac{C_{-\frac{1}{2}}^K}{\bar{\gamma}^K \prod_{i=1}^K \mu_i} \quad (2.31)$$

or in a more simple form

$$P_e(\bar{\gamma}) \simeq \frac{C_{2K-1}^K}{\prod_{i=1}^K (4\bar{\gamma}\mu_i)}. \quad (2.32)$$

Note that $\prod_{i=1}^K \mu_i$ is proportional to $\det(\mathbf{HK}_x)$. Of course, even in the presence of multipath, the asymptotic order of diversity remains equal to the total number of paths K (of the L branches), regardless of their relative time delays and power levels. More interesting, the product $\prod_{i=1}^K \mu_i$ is sufficient to determine the asymptotic SNR degradation caused by the pulse shape autocorrelation (via \mathbf{H}), the taps correlations, and the power mismatch between branches (via \mathbf{K}_x). The product of normalized eigenvalues appearing in (2.31) confirms the intuition that for diversity, it is better to have many small eigenvalues than a few large ones. The highest diversity gain is obtained when $\prod \mu_i$ is maximized, that is for $\mu_i = 1/K$ ($\sum_{k=1}^K \mu_k = 1$), in which case (2.31) reduces to the well known asymptotic error probability for K independent equal energy diversity branches [92]

$$P_e(\bar{\gamma}) = \left(\frac{K}{4\bar{\gamma}}\right)^K C_{2K-1}^K. \quad (2.33)$$

Unfortunately some very small eigenvalues often appear in the Karhunen-Loève expansion, making this asymptotic limit valid only for extremely high SNR values, far away from the range observed in practice (10 to 30 dB).

2.3 Unitary Transformation Effect In Micro-Diversity

Micro-diversity means that the antenna spacing is small enough to consider that the channels on the L branches have the same delay profile, i.e. $K_j = K_0$ and $\tau_{ij} = \tau_j$. This is actually the case for all multichannel diversity systems with antennas located in the same site (few wavelengths separation). As a consequence, the matrices \mathbf{A}^i defined in Section 2.2 (i denotes

the diversity branch number) will be all identical, i.e. $\mathbf{A}^i = \mathbf{A}$. It is also assumed that the noise signals have the same spectral density, which is the case for polarization and spatial diversity, most of the time.

In this section, it is shown that applying the same unitary matrix transformation on each of the K_0 L -taps vectors (each vector contains the taps of the same index) leaves the diversity gain unchanged.

Let \mathbf{U} be a unitary transformation matrix of dimension $L \times L$ (i.e. $\mathbf{U}^\dagger \mathbf{U} = \mathbf{I}$, where \mathbf{I} denotes the identity matrix), and $\mathbf{t}_i = [c_{1i} c_{2i} \cdots c_{Li}]^T$ be a vector of the L taps of the same delay τ_i .

$$\mathbf{t}_i' = \mathbf{U} \mathbf{t}_i \quad (2.34)$$

By noting from (2.2) that the taps in \mathbf{x} are arranged on a branch by branch basis, the new taps \mathbf{y} can be deduced from \mathbf{x} by an equivalent $LK_0 \times LK_0$ unitary transformation $\mathbf{\Gamma}$

$$\mathbf{y} = \mathbf{\Gamma} \mathbf{x} \quad (2.35)$$

where $\mathbf{\Gamma}$ is a block matrix of the form

$$\mathbf{\Gamma} = \begin{bmatrix} \mathbf{\Gamma}_{11} & \mathbf{\Gamma}_{12} & \cdots & \mathbf{\Gamma}_{1L} \\ \mathbf{\Gamma}_{21} & \mathbf{\Gamma}_{22} & \cdots & \mathbf{\Gamma}_{2L} \\ \vdots & \vdots & \vdots & \\ \mathbf{\Gamma}_{L1} & \mathbf{\Gamma}_{L2} & \cdots & \mathbf{\Gamma}_{LL} \end{bmatrix} \quad (2.36)$$

and $\mathbf{\Gamma}_{ij}$ are $K_0 \times K_0$ diagonal matrices related to the transformation \mathbf{U} by

$$\mathbf{\Gamma}_{ij} = U_{ij} \times \mathbf{I}. \quad (2.37)$$

By substituting \mathbf{y} as given in (2.35) into (2.11), we easily show that z becomes

$$z = \mathbf{x}^\dagger \mathbf{\Gamma}^\dagger \mathbf{H} \mathbf{\Gamma} \mathbf{x}. \quad (2.38)$$

Finally, referring to (2.12), \mathbf{H} is a block matrix of the form

$$\mathbf{H} = \begin{bmatrix} \mathbf{A} & 0 & \cdots & 0 \\ 0 & \mathbf{A} & \cdots & 0 \\ \vdots & \vdots & \vdots & \vdots \\ 0 & 0 & \cdots & \mathbf{A} \end{bmatrix} \quad (2.39)$$

It can be easily verified that \mathbf{H} and $\mathbf{\Gamma}$ commute. Using the fact that $\mathbf{\Gamma}$ is a unitary transformation we finally get

$$z = \mathbf{x}^\dagger \mathbf{H} \mathbf{x}. \quad (2.40)$$

Equation 2.40 is identical to 2.11, thus the quadratic form z remains unchanged, and consequently the diversity gain is invariant by any unitary transformation applied on taps of

the same index. In Section 2.4.4 we point out the fact that antenna rotation for polarization diversity is a particular case of such unitary transformation, and thus that it does not provide any additional gain.

2.4 Polarization vs. Spatial Micro-Diversity

In this section, the case of dual-diversity ($L = 2$) for both polarization and space diversity techniques is considered. It is assumed that the AWGN has the same power spectral density for the 2 branches (this is the case for almost all practical systems). The subject of space diversity has been widely studied for the past several decades [64], [101]. In general, the main disadvantage of space diversity is the existence of a non-negligible correlation between the different branches especially when the multipath angular spread of the channel is very narrow [1], [2]. However, the local mean power is generally the same on the two branches.

2.4.1 Polarization Diversity

Although polarization diversity has been well known for over 20 years [76], [117], [64], [101],[1], [2], space diversity schemes have been preferred as polarization diversity suffers from a strong imbalance between the local mean powers received on its two branches. This imbalance is commonly referred to as cross-polar-discrimination (XPD, denoted by χ hereafter) and is the ratio of the received vertical and horizontal polarization power. However, two main arguments can explain the increasing popularity of polarization diversity nowadays. First of all, the miniaturization of base stations makes the antenna spacing required by space diversity both costly and inconvenient. Secondly, polarization diversity is very attractive with handheld portables as their moving antennas are on the average closer to the horizontal, which decreases the XPD.

The nature of polarization diversity relies on the elementary processes responsible for the depolarization of electromagnetic waves. Three different processes are responsible for depolarization: scattering from rough surfaces, diffraction [124], and Fresnel reflection. As the later has the greatest impact in mobile channels, we will briefly present it.

Two Fresnel reflection coefficients R_{\perp} and R_{\parallel} are defined in reference to local axes.

- the orthogonal polarization (\perp) is defined by the electric field component included in the plane defined by the normal to the obstacle and the propagation vector,
- the parallel polarization (\parallel) is the electric field component parallel to the plane tangent to the obstacle.

In general, the propagation occurs mainly in the horizontal plane, either in microcells (where the antenna is well under roof tops) or in macrocells [64]. On the other hand, the scatterers are mainly vertical (especially in urban environments). In Fig. 2.2 it is obvious that the polarization parallel to the obstacle is less attenuated, therefore the vertical polarization is strongly favored at the expense of the horizontal one. This explains why the vertical polarization remains the strongest even when the portable mobile antenna is inclined at 70° from the vertical [79].

Moreover, the phase difference introduced by Fresnel coefficients between vertical and horizontal polarization (Fig. 2.2) ensures that the received horizontal and vertical polarized signals are merely uncorrelated [76]. Indeed, experimental results show an envelope correlation around 0.2 [76], [79]. It is well known that a correlation coefficient under 0.5 has small impact on diversity [64], [101], [1].

2.4.2 \mathbf{K}_x Matrix for Space/Polarization Dual-Diversity

As shown in Section 2.2, the matched filter bound performance is given by the eigenvalues of the matrix $\mathbf{H}\mathbf{K}_x$. The exact structure of matrix \mathbf{K}_x for both space/polarization dual-diversity is

$$\mathbf{K}_x = \begin{bmatrix} \mathbf{C}_1 & \mathbf{\Delta} \\ \mathbf{\Delta} & \mathbf{C}_2 \end{bmatrix}. \quad (2.41)$$

Assuming that the taps of each channel are uncorrelated, \mathbf{C}_1 , \mathbf{C}_2 and $\mathbf{\Delta}$ are $K_0 \times K_0$ diagonal matrices with diagonal elements $C_{1i} = E(|c_{1i}|^2)$, $C_{2i} = E(|c_{2i}|^2) = \beta_i^2 E(|c_{1i}|^2)$, and $\Delta_i = E(c_{1i}c_{2i}^*) = \beta_i\rho_i E(|c_{1i}|^2)$ respectively. The coefficient β_i^2 denotes the power mismatch between the i -th taps of the 2 channels, whereas ρ_i represents the correlation coefficient of those same taps.

Obviously, (2.41) covers the most general situation where power mismatch and correlation vary from one tap to another. Unfortunately, no such fine channel measurements are available, neither for space nor for polarization diversity. However, when the number of scatterers is relatively high and all the channel taps are Rayleigh fading, it is safe to consider these coefficients as constants —say β and ρ — for all the K_0 taps.

Space diversity presents no power mismatch between branches, thus $\beta^2 = 1$. Inversely, polarization diversity exhibits power mismatch between its two branches —as previously highlighted— given in terms of XPD χ (dB). This means that $\beta^2 = 10^{-\chi/10}$ for polarization diversity.

Finally, note that only the envelope correlation ρ_{env} is available experimentally. However, it is shown in [101] that ρ is very close to $\sqrt{\rho_{\text{env}}}$. From now on, all results will be given in terms of $\rho_{\text{env}} \approx \rho^2$.

2.4.3 Space/Polarization Diversity for GSM and IS-95

The GMSK modulation used in GSM is well approximated by binary linear modulation with the first pulse shape of Laurent development [75]. However the Minimum-Shift Keying (MSK) approximation is practically sufficient. MSK can be modeled as a linear OQPSK (Offset Quadrature Phase-Shift Keying) with a pulse shape filter $g(t) = \cos(\frac{\pi t}{2T_b})$ of time duration $2 \times T_b$, where T_b is the bit duration [88]. Indeed, in the range of the common delay spread of mobile radio channels, the autocorrelation function of the first Laurent pulse shape is very close to that of the MSK.

On the other hand, the IS-95 system uses a Raised-Cosine pulse shape $g(t)$ with a roll-off factor $\beta = 0.33$ and a binary modulation in downlink, at a chip rate of 1.2288 Mcps. Note that we do not consider power control for the IS-95 downlink. Ideally, it is assumed that the spreading sequences ensure a perfect Dirac $\delta(\tau)$ autocorrelation function, and that interfering users can be modeled by additive Gaussian noise (an acceptable approximation except for very low number of interferers). In this case, the performances are uniquely determined by the autocorrelation function $\rho_g(\tau)$ of the pulse shape, which is known to be [92]

$$\rho_g(\tau) = \frac{\sin(\pi\tau/T_c)}{\pi\tau/T_c} \frac{\cos(\pi\beta\tau/T_c)}{1 - 4\beta^2\tau^2/T_c^2}. \quad (2.42)$$

Although many authors still use the cumulative probability distribution of the received energy (i.e. the probability of the energy being greater than a given threshold) to evaluate the diversity gain [76], [117], we prefer to compare the polarization and space diversity schemes on the basis of the gain obtained for a given bit error probability. In fact, the later gain is much more relevant than the former in the case of digital systems [101]. In this respect, we consider that for uncoded bits (class II bits of the GSM frame) a BER equal to 5×10^{-3} is enough to ensure a good speech quality. The same value will be considered in the case of IS-95 in order to compare the two systems.

It is emphasized here that the relevant antenna diversity gain G_2 is the one obtained at 5×10^{-3} BER after excluding the inherent multipath diversity gain G_1 due to the multipath channel (as depicted in Fig. 2.3).

Experimental measurements showed that the average value of XPD in urban and suburban environments is between 1 and 10 dB with an average value of 6 dB [79], [76], and in rural environments (e.g. Hilly Terrain) that XPD is very high, ranging from 10 to 18 dB. This can be understood by the fact that a very small amount of energy is transposed from one polarization to another due to the lack of scatterers in rural areas (scatterers are responsible for depolarization via Fresnel coefficient, see Section 2.4.1). Polarization diversity is then uninteresting for this type of channel. In the following, a typical envelope correlation of 0.2 is considered for polarization diversity. Polarization and space dual diversity gains for various normalized mobile channels [36] are plotted in Figs. 2.4 and 2.5 respectively for

GSM, and in Figs. 2.6 and 2.7 for IS-95. As a reference, the diversity gain for a flat fading (1 tap) Rayleigh channel is plotted in each figure. The antenna diversity gain is the highest for this channel, which has no intrinsic multipath diversity.

One general observation is that antenna diversity gain is high when the multipath diversity gain is low and vice-versa. Note that multipath diversity gain is small either if the channel has a low intrinsic diversity, or if its diversity has not been exploited by the pulse shape. For IS-95, the multipath diversity is well resolved by the relatively short duration of the pulse $g(t)$ which makes antenna diversity useless in practice as its gain rarely exceeds 1 dB. However, multiple antennas are always useful for interference reduction [127], beside that of increasing the average signal to noise ratio.

Furthermore, our results show that the two branch polarization diversity gain is almost equivalent to that of spatial diversity in all urban/suburban environments. Spatial diversity clearly outperforms polarization diversity only in rural environments (e.g. Hilly Terrain HT).

2.4.4 Rotating the Base Station Antennas

The possible improvement of polarization diversity gain through spatial rotation of the two receiver's antennas is now analysed. In fact, slanted antenna polarization diversity is very popular nowadays [79], [117]. A great number of manufacturers claim that it achieves more diversity gain (up to 1.5 dB extra gain) than ordinary vertical/horizontal polarized antennas, the main reason advanced being the improvement of power balance between the two diversity branches.

The new XPD after rotation is first derived together with the new correlation coefficient after a rotation of the base station antennas by an angle α from the vertical (Fig. 2.8).

Let the horizontal and vertical received electric fields be respectively

$$\mathbf{E}_{x_1} = |x_1| \cos(\omega t + \phi_1) \quad (2.43)$$

$$\mathbf{E}_{x_2} = |x_2| \cos(\omega t + \phi_2) \quad (2.44)$$

where $x_1 = |x_1|e^{j\phi_1}$ and $x_2 = |x_2|e^{j\phi_2}$ are two correlated circularly symmetric complex Gaussian variables with an XPD equal to χ_1 and correlation coefficient ρ_1 .

After rotation the electric field received on the two rotated antennas, \mathbf{E}_{y_1} and \mathbf{E}_{y_2} , can be deduced from \mathbf{E}_{x_1} and \mathbf{E}_{x_2} by a rotation matrix. By linearity, the relation between the complex envelopes is the same. As a result, antenna rotation is equivalent to a rotation of any 2 channel taps of the same index. In a generic way, we have

$$\begin{bmatrix} y_1 \\ y_2 \end{bmatrix} = \begin{bmatrix} \cos \alpha & -\sin \alpha \\ \sin \alpha & \cos \alpha \end{bmatrix} \begin{bmatrix} x_1 \\ x_2 \end{bmatrix} \quad (2.45)$$

where (x_1, x_2) denotes the pair of initial taps, and (y_1, y_2) the pair of rotated taps. This transformation is a particular unitary transformation for $L = 2$ which has been shown not to have any impact on diversity gain (Section 2.3). Therefore, the widespread belief of added diversity gain is completely false from the matched filter bound point of view. It turns out that polarization diversity gain is invariant by antenna rotation.

Considering now the argument of a more balanced power distribution between the diversity branches, one should note that in reality there is a tradeoff between the power level balance and the correlation of the two branches. After rotation, the new taps exhibit new XPD and cross-correlation coefficients χ_2 and ρ_2 that are functions of the initial ones χ_1, ρ_1 and of the rotation angle α .

We must evaluate

$$\chi_2 = \frac{E(|y_2|^2)}{E(|y_1|^2)} \tag{2.46}$$

and

$$\rho_2 = \frac{E(y_1 y_2^*)}{\sqrt{E(|y_1|^2)E(|y_2|^2)}}. \tag{2.47}$$

After a straightforward development it is found

$$\chi_2 = \frac{f_1(\chi_1, \rho_1, \alpha)}{f_2(\chi_1, \rho_1, \alpha)} \quad (\text{see Fig. 2.9}) \tag{2.48}$$

$$\rho_2 = \frac{|(1 - \chi_1) \tan \alpha + \rho_1 \sqrt{\chi_1} (1 - \tan^2 \alpha)|}{\sqrt{f_1(\chi_1, \rho_1, \alpha) f_2(\chi_1, \rho_1, \alpha)}} \quad (\text{see Fig. 2.10}) \tag{2.49}$$

where $f_1(\chi_1, \rho_1, \alpha) = \tan^2 \alpha + \chi_1 + 2\rho_1 \sqrt{\chi_1} \tan \alpha$ and $f_2(\chi_1, \rho_1, \alpha) = 1 + \chi_1 \tan^2 \alpha - 2\rho_1 \tan \alpha \sqrt{\chi_1}$.

These results extend those of [117], where the effect of rotating the base station antennas was also studied but in the special case of independent Rayleigh fading signals ($\rho_1 = 0$).

By using (2.48) and (2.49) for various combinations of channel type, initial XPD, and initial correlation coefficient, to evaluate the diversity gain as before, it was noticed that the gain remained unchanged for whatever rotation angle α considered. This result confirms the one obtained above using the property of unitary transformations.

Consequently, even if the reported extra gains are valid, they should not be attributed to diversity itself, but rather to some imperfection or sub-optimality of the considered receivers which may be more sensitive to the power imbalance than to branch correlation. We believe that the measured diversity gain would be practically the same for vertical/horizontal and slanted polarization if the receiver is well designed. We conclude that the question of system performance with polarization diversity should not be limited to the study of signal propagation aspects (attenuation, spatial correlation, power mismatch), but should rather include the receiver signal processing algorithms. For instance, there may be some advantage for rotated antennas in systems where the receiver algorithms are constrained to be very

simple, and therefore far from optimal. To the best of our knowledge, no such combined investigations are available in the literature.

2.5 Coded Matched Filter Bound

This section is very inspired by [46] where the MFB is derived for trellis coded modulation. Consider the transmission of trellis coded symbols \mathbf{a} corresponding to a particular path through the code trellis. An error event of length \mathcal{T} of the decoded sequence $\tilde{\mathbf{a}}$ is taken to start with symbol $a_1 \neq \tilde{a}_1$ and end with symbol $a_{\mathcal{T}} \neq \tilde{a}_{\mathcal{T}}$. Along the error path, the $T \leq \mathcal{T}$ nonzero branch metrics $d_i^2 = |a_i - \tilde{a}_i|^2$ are accumulated leading to the Euclidian distance $d^2(T) = \sum_{i=1}^T d_i^2$, in the case of static channels, the error event with minimal euclidian distance d_{min}^2 is dominant but in fading environment the effective code length T_{min} (minimum number of branches with non-zero branch metrics) may be more important. Let consider an error event of length T , the individual SNR γ_i along the error path are to be weighted by d_i^2 and sum to form the effective SNR which enables to obtain the performances after the decoder. The effective SNR (at the output of the decoder) becomes

$$\gamma_e = \sum_{i=1}^{T_{min}} d_i^2 \cdot \gamma_i \quad (2.50)$$

One can see that the probability distribution of γ_e is easily derivable only in the two following cases:

- the γ_i are independent variables,
- the γ_i are completely correlated (i.e. $\forall i, \gamma_i = \gamma$), this is typically the situation of chapter 3.

These cases correspond to either no interleaving or perfect interleaving. Unfortunately, the reality lies always between these two cases. This is the reason why we preferred to focus on the uncoded MFB which is independent of the interleaving scheme. Moreover, simulations Fig. 2.11 show that the uncoded MFB is very close to reality for GSM and IS95 systems . As stated in the introduction, the MFB does not take into account the ISI. If the Uncoded MFB is attained at the output of the equalizer then it can only means that the distribution of the minimum distance associated to each channel outcome, has a large peak at the Gaussian distance (no ISI). This is particularly interesting to identify suboptimality in the receiver design (see chapter 4).

2.6 Conclusion

In this chapter, the matched filter and MRC bound for L -branch antenna diversity and linear modulation over frequency-selective Rayleigh fading multipath channels has been derived using a novel compact approach. The comparison of the space/polarization diversity gains for GSM and downlink IS-95 systems (binary modulation in both cases) shows that there is a trade-off between multipath diversity gain and antenna diversity gain. Polarization diversity has also been shown to provide almost the same gain as spatial diversity, especially in urban environments. Moreover, with the help of our general model, it has been possible to prove for the first time that polarization diversity gain is invariant by rotation of the receiver antennas, which is in contradiction with general belief. Some consideration were also given concerning the MFB extended to trellis coded modulation. It was finally concluded that the uncoded MFB was of more practical interest since the uncoded MFB is relatively tight to existing system performance (e.g., GSM and IS95) and is very useful to identify suboptimality in the receiver design independently of the channel coding scheme.

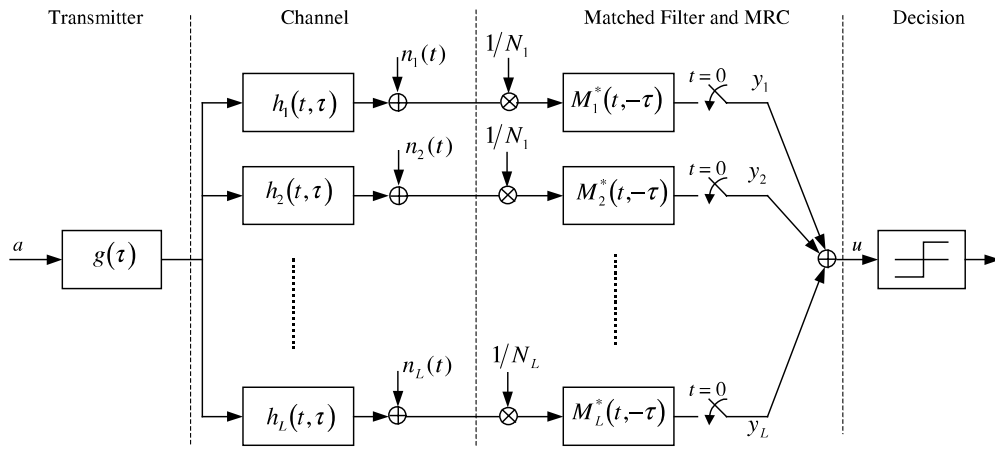


Figure 2.1: System model with L diversity branches.

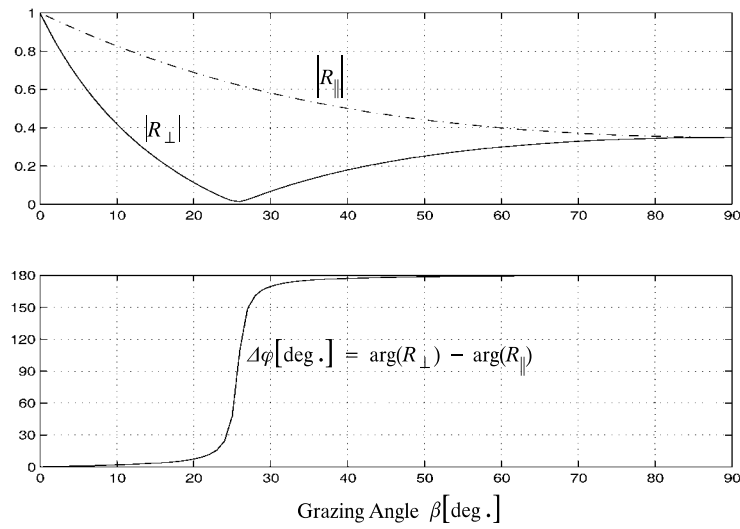


Figure 2.2: Fresnel coefficient for vertical and horizontal polarization for cement.

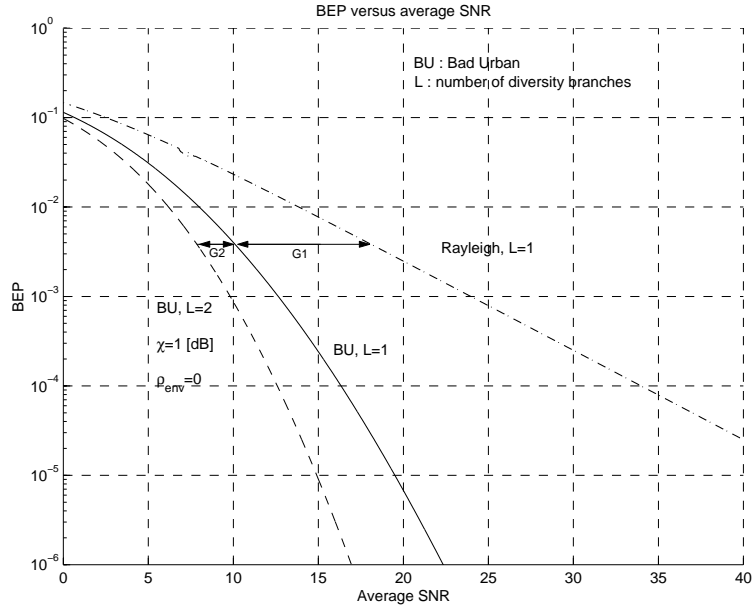


Figure 2.3: Multipath diversity gain and antenna diversity gain. Example of GSM system in Bad Urban Channel (BU) [36].

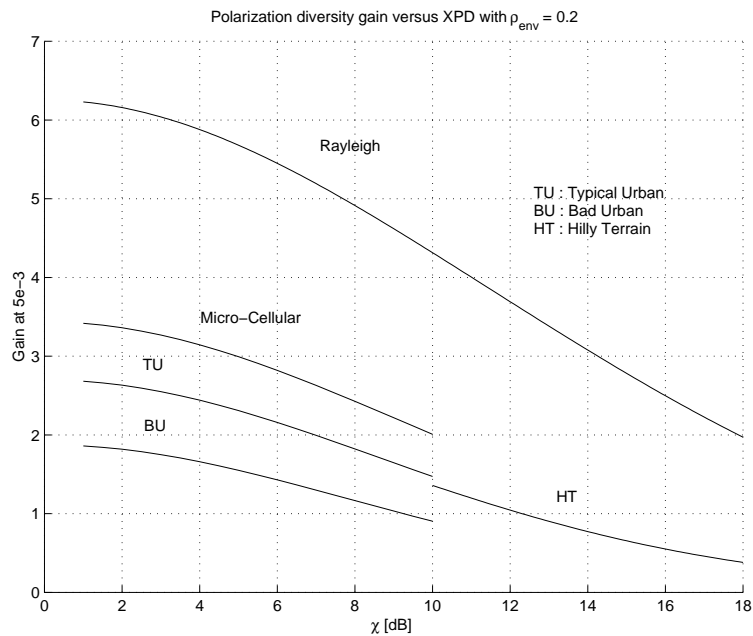


Figure 2.4: Polarization diversity gain vs. XPD χ (dB) in GSM for various channels [36].

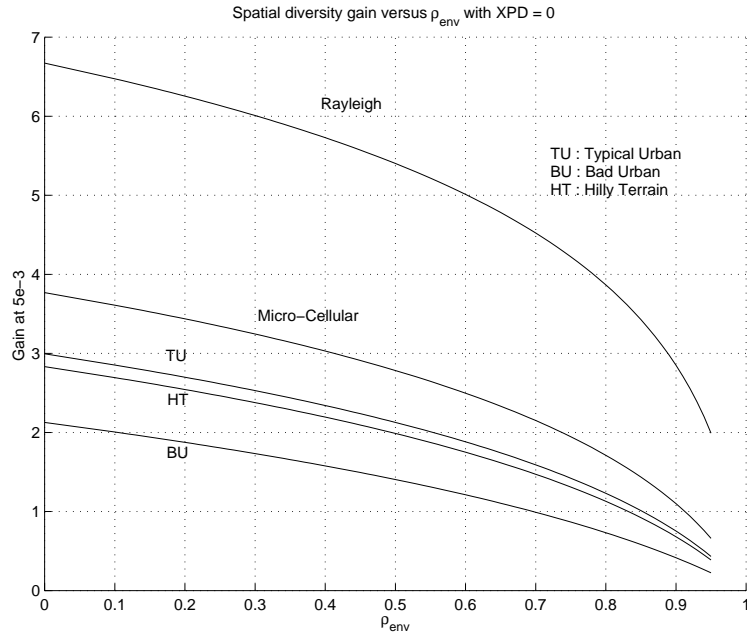


Figure 2.5: Spatial diversity gain vs. envelope correlation in GSM, for various channels [36].

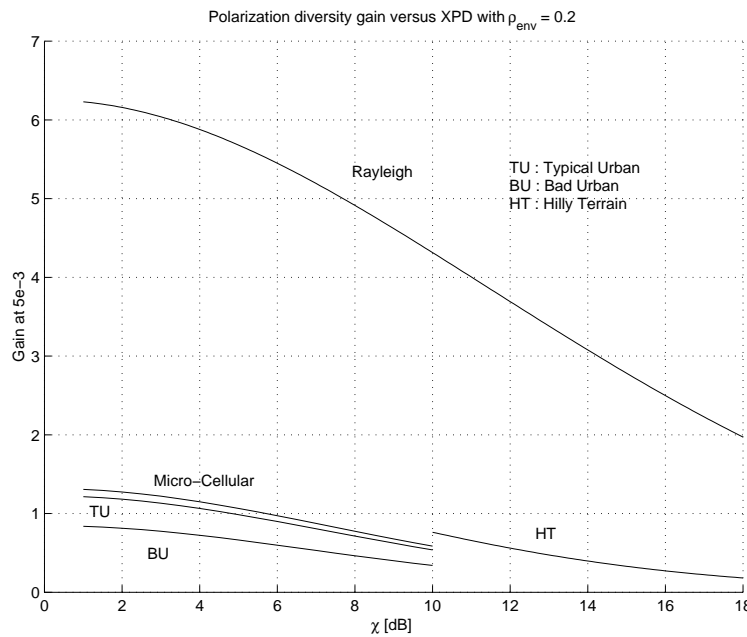


Figure 2.6: Polarization diversity gain vs. XPD χ (dB) in IS-95 for various channels [36], with an envelope correlation of 0.2.

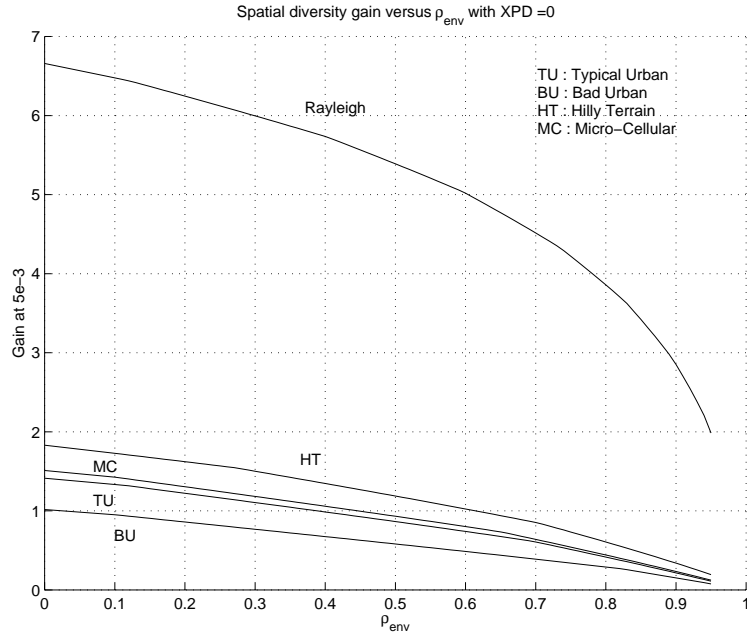


Figure 2.7: Spatial diversity gain vs. envelope correlation in IS-95 for various channels [36].

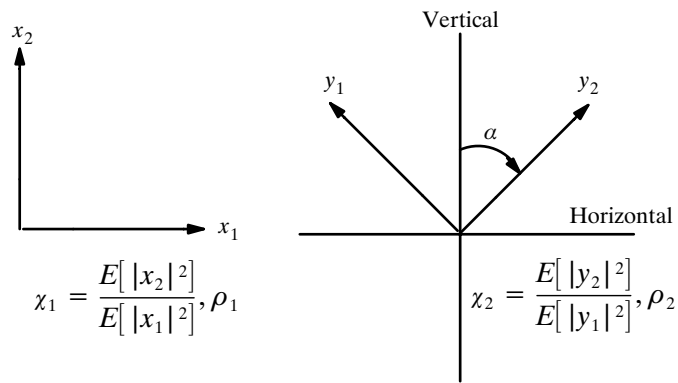


Figure 2.8: Antennas rotation of an angle α from the vertical for polarization diversity.

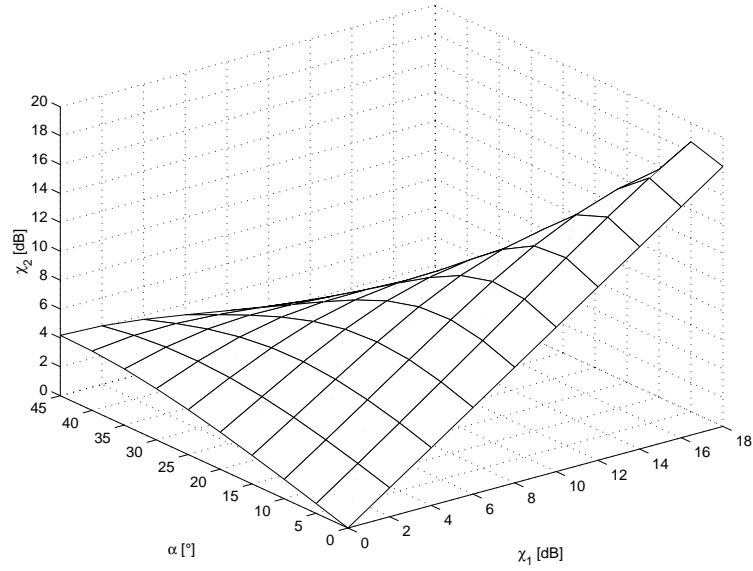


Figure 2.9: New XPD χ_2 (dB) as a function of the initial XPD χ_1 (dB) and the rotation angle α of the base station antennas with an initial envelope correlation coefficient of 0.2.

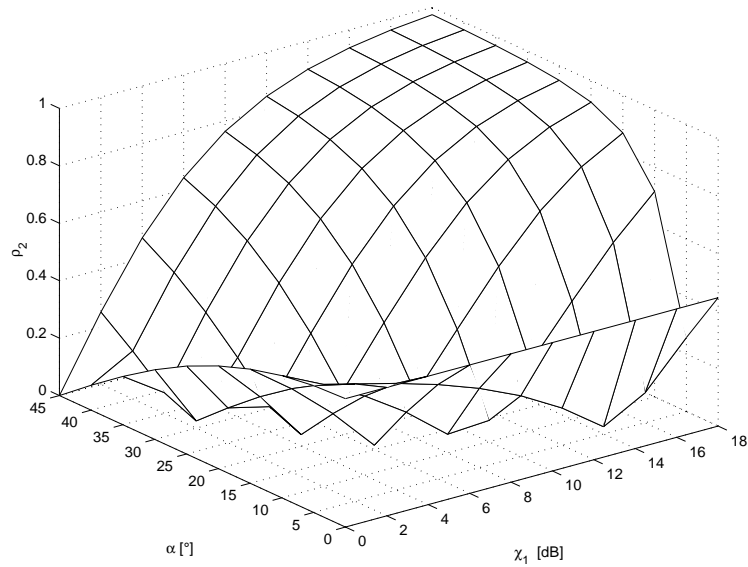


Figure 2.10: Correlation coefficient ρ_2 as a function of the initial XPD χ_1 (dB) and the rotation angle α of the base station antennas with an initial envelope correlation coefficient of 0.2.

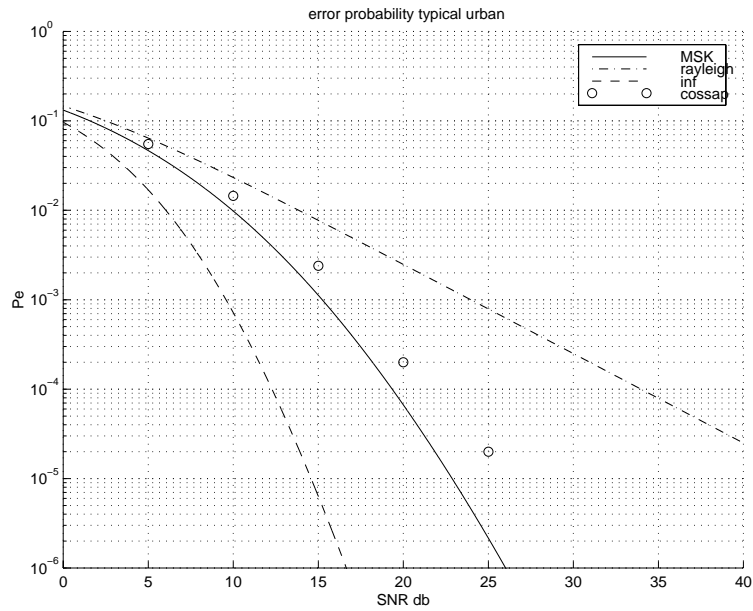


Figure 2.11: Comparison of the Matched Filter Bound to a Monte Carlo simulation: MSK represents the Matched Filter Bound for GMSK transmitted through TU [36] channel and COSSAP the Monte Carlo simulation of the same system with perfect channel estimation.

Chapter 3

Joint Equalization and decoding using the Generalized Viterbi for broadband wireless applications.

3.1 Introduction

The optimal way to decode trellis encoded signals transmitted on InterSymbol Interference (ISI) Channels is to use the Maximum Likelihood (ML) "supertrellis", a combination of ISI and error-control code trellises, whose state complexity is the product of both [34]. Unfortunately, for frequency selective radio channels, the number of states of the ISI trellis increases exponentially with the bit rate, which precludes this approach for broadband wireless radio interfaces. As a consequence, a lot of work has been done on sub-optimal receivers for Trellis Coded Modulation (TCM) in the presence of ISI [34], [126], [38], [44]. In [34], a systematic method is developed for lowering the state complexity of the supertrellis. An interesting case arises when the receiver trellis is reduced to the code trellis [34], [126], [38], [44], whose complexity does not depend on bit rate. The ISI due to the channel is not taken into account in the trellis states but in the edge metric, as done in a classical Decision Feedback Equalizer (DFE). It follows that such a receiver, commonly called Parallel Decision Feedback Decoding (PDFD), inherently suffers (as the DFE) from error propagation, especially in the case of non minimum phase channels. Therefore, PDFD receiver needs pre-filtering to turn the channel into minimum phase. This pre-filtering is cumbersome and increases the overall receiver complexity. Besides, error propagation still remains.

In parallel, many efforts have been devoted to improve sub-optimal equalization techniques for broadband wireless channels. Once again, the issue is the complexity of the ML ISI trellis. In [38], [61] a method is proposed to reduce the ML ISI trellis. In [61], it is shown that the GVA, which retains more than one survivor per state, is a very efficient algorithm

to fight against error propagation.

The proposed receiver combines the PDFD algorithm with the GVA. Simulations prove that the GVA makes the PDFD receiver very robust to error propagation (even in the case of non minimum phase channels) for a reasonable complexity increase. It is even shown that in most cases the ML optimal performance is attained with only four survivors per state. The paper is organized as follows. Section 3.2 describes in details the proposed algorithm for any error-control code trellis. In Section 3.3 some possible applications together with simulation results are presented for cyclic block codes, convolutional codes, for static and time-varying multipath Rayleigh channels. Notably, the algorithm was proved to perform well for simple convolutional codes, in the context of Broadband Radio mobile channels.

3.2 Proposed Algorithm

The discrete time equivalent structure of the proposed communication model is shown in Fig. 3.1. The data signals are transmitted in bursts containing N coded data symbols and a known training sequence (located at the beginning of the burst) used both for channel estimation and algorithm initialization. Let the estimated (symbol spaced) impulse response of the convolution of the transmitter filter, the receiver filter and the radio-mobile channel, be denoted

$$\{h_l\}_l, l \in [0, K - 1], \tag{3.1}$$

where K is the channel constraint length.

Note that the overall channel does not need to be minimum phase [29, page 78]. The receiver filter should ensure however that noise samples at the symbol rate R_s are uncorrelated at its output, which is the case for a squared-root raised cosine filter for example. The output of the received filter at timing instant t is given by

$$y_t = h_0 x_t + b_t + I_t, \tag{3.2}$$

where x_t is the current coded data symbol to be received, b_t is a Gaussian noise sample, and I_t is the ISI contribution term with

$$I_t = \sum_{l=1}^{K-1} h_l x_{t-l} \tag{3.3}$$

We define the error-correcting code C in a general sense, seeing it as a time-variant Markovian process. The coded symbols x_t are then related to the incoming binary sequence by a time-variant relationship of the form

$$x_t = \Psi(u_t, u_{t-1}, \dots, u_{t-L_t}), \tag{3.4}$$

taking into account encoding and bit mapping operations, where L_t is the instantaneous code constraint length at time t . In the general case, for both block and convolutional codes, the coded sequences produced by C can be described by an irregular trellis $T(V, E, \vartheta)$ of rank N where V and E respectively denote the vertex and edge spaces and ϑ the set of edge multivaluations. We also introduce V_t and E_t the vertex and edge subspaces at time index t of complexities $|V_t|$ and $|E_t|$. With those notations, we have

$$|V| = \sum_{t=1}^N |V_t| \quad |E| = \sum_{t=1}^N |E_t| \quad W = \max_{0 \leq t \leq N} |V_t|. \quad (3.5)$$

For time-invariant Markovian processes, such as convolutional codes, or linear cyclic block codes, the (regular) trellis can be brought back to a single section.

The PDFD evaluates the ML metric

$$\mu = \sum_{t=1}^N \left\| y_t - h_0 x_t - \widehat{I}_t \right\|^2, \quad (3.6)$$

on the full C trellis, where \widehat{I}_t is the estimated ISI evaluated, as in the DFE, by the use of a traceback array of size in $O(|V|)$ that saves the path leading to a given survivor [126] at every time $t < N$. A path is a succession of edges, each one carrying the input bit $\vartheta^{(1)} = u_t$, the output produced symbol $\vartheta^{(2)} = x_t$, and the departure and arrival vertices.

The novelty in the proposed algorithm consists in combining classical PDFD and GVA, thus keeping at each vertex the S best incoming paths instead of a single one, and storing them in a generalized traceback array Θ of size in $O(S \times |V|)$.

Let ν_i^t denote a vertex of label i , $0 \leq i \leq |V_t| - 1$, at time t , $0 \leq t \leq N$, and $e_{i \rightarrow j}^{t-1, t}$ the edge associated with transition $\nu_i^{t-1} \rightarrow \nu_j^t$. Let also $M_k(\nu_i^t)$ be the accumulated vertex metric (or path metric) at termination vertex ν_i^t of the survivor of rank k , $0 \leq k \leq S - 1$. We define

$$\mu_k(e_{i \rightarrow j}^{t-1, t}) = \left\| y_t - h_0 x_t - \widehat{I}_t^{(k)} \right\|^2 \quad (3.7)$$

the edge metric for the transition $e_{i \rightarrow j}^{t-1, t}$ associated with the k^{th} survivor stored at time $t - 1$.

The so-called Generalized Parallel Decision-Feedback Decoder (GPDFD) can be recursively described as follows

Generalized Joint Equalizer and Decoder (GPDFD)

- *Initialization step:* At time t_0 , initialize all the path metrics to infinity except $M_0(\nu_0^0)$ which is set at 0 (assuming the code C starts from all-zero state). The `trace_back Theta` array is empty.

- 1) *Path extension step*: Go through the trellis section at time t and compute, for all $S \times |E_t|$ possible extended paths, the new candidate path metrics

$$M_*(\nu_j^t) = M_k(\nu_i^{t-1}) + \mu_k(e_{i \rightarrow j}^{t-1,t}), \quad i \in V_{t-1}, j \in V_t, k \in [0, S-1], \quad (3.8)$$

using the generalized traceback array Θ .

- 2) *Path selection step*: Classify the candidate path metrics $M_*(\nu_j^t)$ at each vertex $j \in V_t$ and keep the S best ones. Simultaneously update the section $t-1$ of the generalized traceback array Θ .
- 3) *Final step*: Go up the best path from the final all-zero state using the complete fulfilled Θ . Read the input bits from the stored edges among the path.

It is to be underlined that the GPDFD comes down to the PDFD algorithm in the case of $S=1$. Simulation results, hereafter, always include that simple case in order to enable the comparison of this two algorithms.

3.3 Applications

3.3.1 Application 1: Cyclic block codes, joint equalization and decoding on various full code trellises

In this section, we show that the proposed receiver also works for block encoded signals. The TCM code trellis used by the GPDFD can be designed in several ways. The first way aims at optimizing the receiver decoding complexity, which is in $O(|E|)$. The problem consists in searching efficient time axis orderings, leading to reduced trellises. Optimal minimal Kschichang-Sorokine (KS) trellises have been found via simulated annealing based heuristic [70],[18]. The code is used in its systematic form for encoding step, but codewords are permuted according to optimal exhibited orderings, before BPSK mapping and transmission over ISI channel.

The second approach aims at introducing a natural QPSK mapping, as done in application 3.3.3. The receiver is then applied on sectionalized trellises. By sectionalization, we mean the choice of a symbol alphabet at each time index. For a given code of time axis τ , the sectionalization effectively shrinks τ at the expense of increasing the code alphabet and the trellis vertices out-degrees. For example, binary extended Hamming codes of length $n = 2n'$ can be thought as quaternary codes of length n' by grouping pairs of consecutive coded bits together. Such an operation substantially affect the edge and vertex complexities of the minimal code trellis. Optimal sectionalized trellises may be found by implementing the Vardy-Lafourcade algorithm described in [73].

A third approach would aim at establishing a connection between block and convolutional encoded signals by means of tail-biting trellises. Some results are presented in [32], where it is shown that unwrapping a tail-biting representation of a good block code, such as the extended Golay code, can produce a good convolutional code.

We finally focus on a fourth approach and investigate the performance of the GPDFD when applied on the regular trellis of any binary polynomial block code of generators

$$g(x) = \sum_{i=0}^{n-k} g_i x^i \quad (3.9)$$

Such a trellis is directly designed using the shift register which would perform the non-systematic polynomial encoding operation. As explained in [115], a systematic encoding must be realized for the purpose of optimizing the final BER on message bits. At reception, the GPDFD is applied onto the regular trellis associated with the non-systematic code version. A convolution between the non-systematic decoded message sequence $\hat{u}'(x)$ and $g(x)$ is performed for recovering the final decoded message $\hat{u}(x)$ which consists of the k last symbols of the produced codeword. By way of an illustration, Fig. 3.2 shows the performance in terms of BER of the GPDFD used for decoding a TCM made of an expurgated binary BCH code $(31, 25, d_{min} = 4)$ mapped onto a simple BPSK constellation and transmitted through the worst static 6-taps ISI channel [92]

$$H(z) = 0.23 + 0.42z^{-1} + 0.52z^{-2} + 0.52z^{-3} + 0.42z^{-4} + 0.23z^{-5} \quad (3.10)$$

whose ISI theoretical loss is 7 dB . The regular code trellis section has an overall state complexity of

$$w = 2^{31-25} = 64. \quad (3.11)$$

Considering the optimal MAP detection performance of uncoded BPSK signals as a reference, the TCM gain provided by this 1-error correcting code is weak compared to the gain provided by convolutional TCM presented in section 3.3.3. We also observe that error propagation is completely eliminated for $S=2$.

3.3.2 Application 2: cyclic block codes, joint equalization and decoding on reduced code trellises

In this second application, we employ the GPDFD to decode more powerful binary BCH codes. Even reduced by efficient time axis orderings, trellises of such codes are usually prohibitive in state complexity [18]. To thwart this problem, we investigate and compare several GVA-based algorithms employing polynomial block codes reduced-states trellises.

Algorithm 1:

This algorithm is inspired by a procedure, first described in [80]. Let C be an expurgated t -correcting binary BCH code of primitive length n , of designed distance $\delta = 2t + 2$ and generator polynome

$$g(x) = \underbrace{(1+x)m_\alpha(x)}_{\tilde{g}(x)} \underbrace{\left\{ \prod_{j=2}^t m_{\alpha^{i_j}}(x) \right\}}_{\bar{g}(x)} \quad (3.12)$$

where $m_\alpha(x)$ is the primitive minimal polynome corresponding to the primitive n^{th} root of unity α . Finally, we also introduce the check polynome of C

$$h(x) = \frac{(x^n - 1)}{g(x)} \quad (3.13)$$

Let T be the optimal minimal trellis of C . A father code \tilde{C} of C is a code which contains all codewords of C . Typically, expurgated Hamming codes are father codes of more powerful expurgated BCH codes of same length. Let \tilde{T} be the trellis of \tilde{C} directly constructed from the generator polynome $\tilde{g}(x)$. Such a trellis, even in its regular non-reduced form, is far smaller than T . At emission, we encode the message sequence $u(x)$ systematically using the generator polynome $g(x)$. Let

$$c(x) = r(x) + u(x)x^{n-k} = u'(x)g(x) \quad (3.14)$$

be the produced systematic codeword where $r(x)$ is equal to $u(x)x^{n-k}$ modulo $g(x)$. Given the received word, the GPDPD performs joint equalization and decoding, working on the regular trellis section \tilde{T} , and produces in parallel a list of the S best message sequences

$$\widehat{u}'_1(x), \widehat{u}'_2(x), \dots, \widehat{u}'_S(x), \quad (3.15)$$

which all are under the form

$$\widehat{u}'_i = \widehat{u}'_i(x)\tilde{g}(x), \quad (3.16)$$

and which would generate the best father codewords

$$\widehat{c}_1(x), \widehat{c}_2(x), \dots, \widehat{c}_S(x), \quad (3.17)$$

naturally classified with respect to an increasing path metric order. To explicitly obtain the list $\widehat{c}_1(x), \widehat{c}_2(x), \dots, \widehat{c}_S(x)$, each estimated message sequence \widehat{u}'_i is re-encoded by a simple convolution with $\tilde{g}(x)$. A simple syndrome computation is sequentially performed using the check polynome $h(x)$ on each of the candidate father codewords. The final decision delivered by algorithm 1 is the message sequence $\widehat{u}(x)$ corresponding to the first candidate codeword in the list, for which

$$\widehat{c}(x)h(x) = 0 \text{ mod } x^n - 1. \quad (3.18)$$

As an example, we have tested algorithm 1 for an expurgated BCH code $(31, 20, d_{min} = 6)$ decoded on the trellis of the father expurgated Hamming code $(31, 25, d_{min} = 4)$. Performance in terms of BER is shown on Fig. 3.3, considering a transmission over the worst static 6-taps ISI channel. When choosing $S = 8$, a slight degradation of 0,4 dB occurs compared to the optimal case.

Algorithm 2:

In this new scenario, the GPDFD is applied on a code sub-trellis, obtained by reducing the state space of the original polynomial code C . As illustrated on Fig. 10, only the $L - 1$ first input symbols of the full trellis states $\{u_{t-1}, u_{t-2}, \dots, u_{t-n+k}\}$ are retained for constituting trellis sub-states or labels. The label constraint length L usually satisfies inequality

$$L \ll n - k + 1. \quad (3.19)$$

Residual input symbols involved in edge metric computation are evaluated by per-survivor processing. Keeping a sufficient number of survivors per label prevents error propagation caused by overall trellis reduction (ISI and code states space), as shown by simulation results. Algorithm 2 has been tested on the same expurgated BCH code $(31, 20, d_{min} = 6)$. The GPDFD is applied on a 16-state sub-trellis, corresponding to a label constraint length $L = 5$. Performance in terms of BER is shown on Fig. 3.4, considering a transmission over the worst static 6-taps ISI channel.

3.3.3 Application 3: Convolutional encoded signals, joint equalization and decoding process for broadband wireless applications.

Although the proposed receiver works with any trellis (TCM, block code, etc...), rate 1/2 convolutional codes and QPSK mapping appear to be the best trade off between performance and complexity in the context of broadband wireless channels. For that reason, all simulations hereafter are based on the simple convolutional code used in GSM. We recall that the GSM convolutional code is a half-rate non-recursive non-systematic 16-state convolutional code with polynomial generators

$$g_1(D) = 1 + D + D^2 + D^4 \quad g_2(D) = 1 + D^3 + D^4. \quad (3.20)$$

The TCM reduces to coded bits attacking a gray QPSK mapping. The signal to noise ratio given in abscissa takes into account the code rate, the modulation and the training sequence (when involved).

For the case of time varying multipath Rayleigh channels (paragraph 3.3.3 and 3.3.3), the transmit and receive filters are root raised cosine filters with roll-off 0.22.

We take advantage of the Constant Amplitude Zero Autocorrelation (CAZAC) binary sequence properties to estimate the channel [128]. For sake of simplicity, we chose to place the training sequence at the beginning of the burst. The training sequence consist of $K - 1$ preamble and P midamble binary symbols. The P midamble are chosen as a CAZAC sequence, whereas the preamble sequence consists of the repetition of the last $K - 1$ symbols of the CAZAC sequence. The channel estimation is always linear and derived from the Least Square (LS) criteria . Thus, the given training sequence enables to estimate K channel coefficients (assuming symbol synchronization) whose variances are equal to the noise variance of b_t divided by P [67]. In all the simulations, the synchronization is assumed to be perfect, the K channel coefficients (derived from a training sequence consisting of $K - 1$ preamble symbols) are kept and fed to the equalizer. As a result of very high bit rate and low speed the quasi-static assumption (the channel is assumed to be stationary over the duration of each data packet) is supposed to be valid.

Static channel

The figure 3.5 shows the performance in terms of Bit Error Rate (BER) of the proposed receiver for the worst 6-tap static ISI channel (whose ISI theoretical loss is 7 dB [92]). It shows that, with S=4, the proposed receiver nearly reaches the optimal.

Typical Urban Wireless channel.

The figure 3.6 gives the performance in term of Frame Error Rate (FER) for a time varying and frequency selective GSM Typical Urban channel whose delay profile in microsecond and power profile in [dB] are respectively $[0.0, 0.2, 0.5, 1.6, 2.3, 5.0]\mu s$ and $[-3.0, 0.0, -2.0, -6.0, -8.0, -10.0]$ dB at low speed and at 2Mbit/s user bit rate. The (noisy) channel estimation is done with a BPSK-modulated training sequence of length 120 symbols, consisting of 20 preamble and 100 midamble symbols. The coded data part of the burst contains 800 QPSK symbols, which correspond to 796 uncoded data bits taking into account the tail bits (to close the code trellis into all zero state).

Of course any number of diversity can be used, for two branch diversity with Maximal Ratio Combining. the metric becomes [69]

$$\mu = \sum_{t=1}^N \left\| y_t^1 - h_0^1 x_t - \hat{I}_t \right\|^2 + \left\| y_t^2 - h_0^2 x_t - \hat{I}_t \right\|^2 \tag{3.21}$$

where y_t^α and $\{h_l^\alpha\}_l$ are respectively the received samples and channel coefficient of diversity branch $\alpha \in [1, 2]$. The curve Fig.3.7 corresponds to the same simulation assumptions as

curve Fig. 3.6 but with 2 diversity branches. Again, $S = 4$ seems to be a good trade off between performance and complexity.

Broadband Radio Access Network channels.

A set of indoor channel models which was defined, at Broadband Radio Access Network (BRAN) eight meeting, was to be used for High Performance Radio Local Area Network 2 (HIPERLAN/2) simulations. A tapped delay line type of model, which is basically described in [41], has been chosen. In order to reduce the number of taps needed, the time spacing is non uniform. For shorter delays, a more dense spacing is used. The average power decreases exponentially with time. Except for the first tap, which can have a Ricean factor of 10, all taps have Rayleigh fading statistics. A classical (Jake's) Doppler spectrum corresponding to a terminal speed of 3 m/s is assumed for all taps. Five models, A, B, C, D and E, have been compiled. Model A corresponds to a typical office environment. Model B corresponds to a typical large open space environment with NLOS conditions or an office environment with large delay spread. Models C and E correspond to typical large open space indoor and outdoor environments with large delay spread. Model D corresponds LOS conditions in a large open space indoor or an outdoor environment.

The goal (in order to select a radio interface, OFDM was finally retained) was a spectral efficiency of 1 bit/Hz/s, which is roughly the case for a QPSK modulation with rate 1/2 convolutional code (despite the training sequence and the transmitter filter that decreases slightly the spectral efficiency). The targeted Frame Error Rate (FER) for the Radio Link Control layer was 1% without transmission diversity or reception diversity.

We chose to present simulation results only for model C and model E that are the most difficult to equalize (i.e., where a simple PDFD algorithm performs very poorly). the delay profile given in nanosecond of model C and model E are respectively [0, 10, 20, 30, 50, 80, 110, 140, 180, 230, 280, 330, 400, 490, 600, 730, 880, 1050]ns and [0, 10, 20, 40, 70, 100, 140, 190, 240, 320, 430, 560, 710, 880, 1070, 1280, 1510, 1760]ns whereas the power profiles given in dB are respectively [-3.3, -3.6, -3.9, -4.2, 0.0, -0.9, -1.7, -2.6, -1.5, -3.0, -4.4, -5.9, -5.3, -7.9, -9.4, -13.2, -16.3, -21.2] dB and [-4.9, -5.1, -5.2, -0.8, -1.3, -1.9, -0.3, -1.2, -2.1, 0.0, -1.9, -2.8, -5.4, -7.3, -10.6, -13.4, -17.4 -20.9] dB.

The Performance hereafter are given in term of FER at 25Mbit/s user bit rate. The (noisy) channel estimation is done for model C, as before, with a BPSK-modulated training sequence of length 120 symbols, consisting of 20 preamble and 100 midamble symbols. The coded data part of the burst contains 800 QPSK symbols. The channel model E, due to a very long delay spread, needs a longer channel estimate (of 50 coefficients). To keep the same ratio between the number of data symbols and the number of training symbols, we chose a BPSK-modulated training sequence of length 149 symbols (consisting of 49 preamble and

100 midamble symbols) and coded data length of 1000 QPSK symbols. We checked that the quasi static assumption is valid for these system parameters (i.e data rate, speed and burst length). As before, $S = 4$ seems to be a good trade off between performance and complexity for the BRAN context.

3.4 Conclusions

In this chapter, we have described a new joint equalization and decoding process based on the GVA and we presented some broadband wireless applications. This receiver is suitable for severe ISI channels and does not need minimum phase pre-filtering. As shown by simulations, its performance is closed to the optimal ML one with a reasonable complexity increase. Besides, in the context of high bit rate packet wireless transmissions, granularity constraints do not allow interleaving on more than one cell. Since the proposed process does not require any kind of interleaving, it appears as a natural candidate technique for such applications.

This approach could appear as a competitor for turbo-detection[39], [8] where, on the contrary, coding and interleaving (time) diversity is fully exploited. However, it exists a possible bridge when considering serially concatenated TCM (SCTCM) over ISI channels. A classical serial concatenation of two error-control codes and an ISI channel is used as the simpler concatenation of two codes only; the outer error-control code and an inner code obtained from the combination of the second error-control code and the ISI channel. Our joint detection technique is a possible candidate for decoding the inner box in such serial concatenations [19].

A very interesting direction for 4G-TDMA systems seems to be the generalization of such an approach to Multiple Input Multiple Output channel for transmitted Multilayered Trellis Coded Modulations as described in chapter 7.

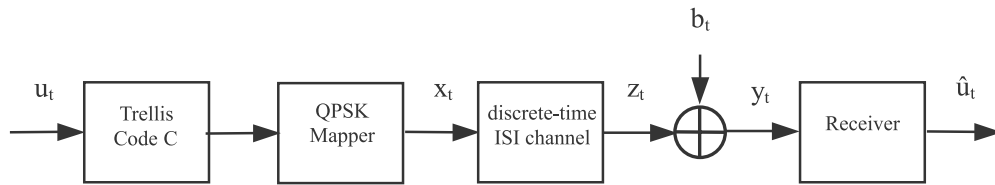


Figure 3.1: Structure of the discrete time equivalent communication system.

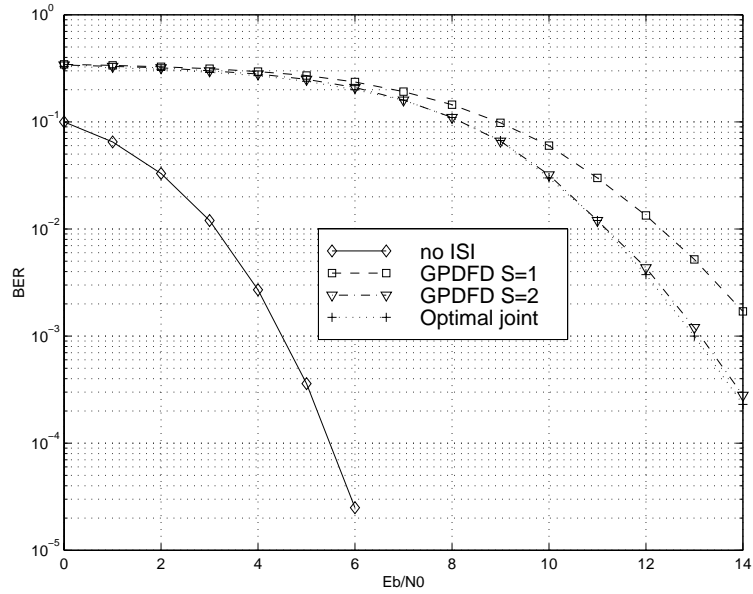


Figure 3.2: BER over the worst static 6-taps ISI channel, BCH (31,20, $d_{\min}=6$) code, BPSK mapping, algorithm 1.

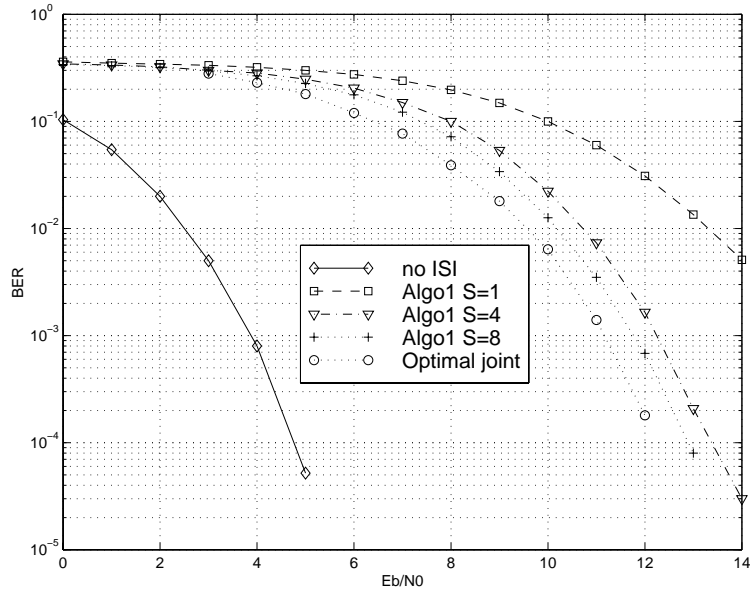


Figure 3.3: BER over the worst static 6-taps ISI channel, BCH (31,20, $d_{min}=6$) code, BPSK mapping, algorithm 1.

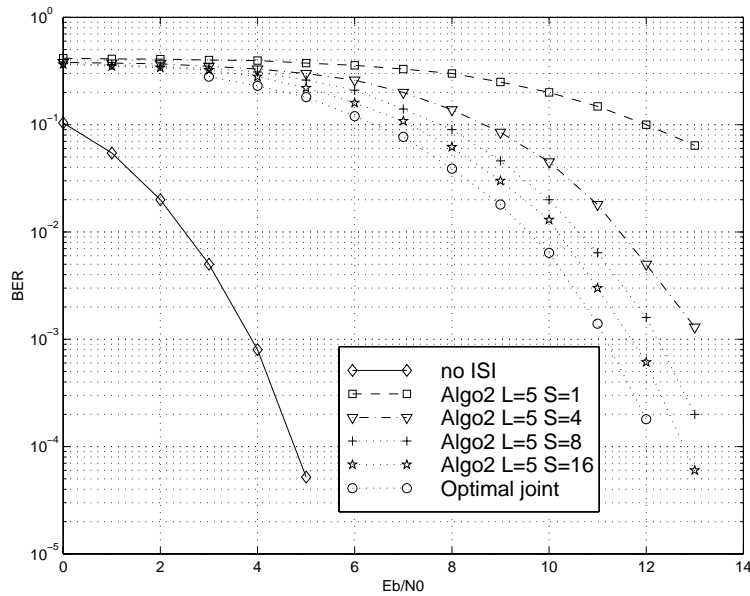


Figure 3.4: BER over the worst static 6-taps ISI channel, BCH (31,20, $d_{min}=6$) code, BPSK mapping, algorithm 2

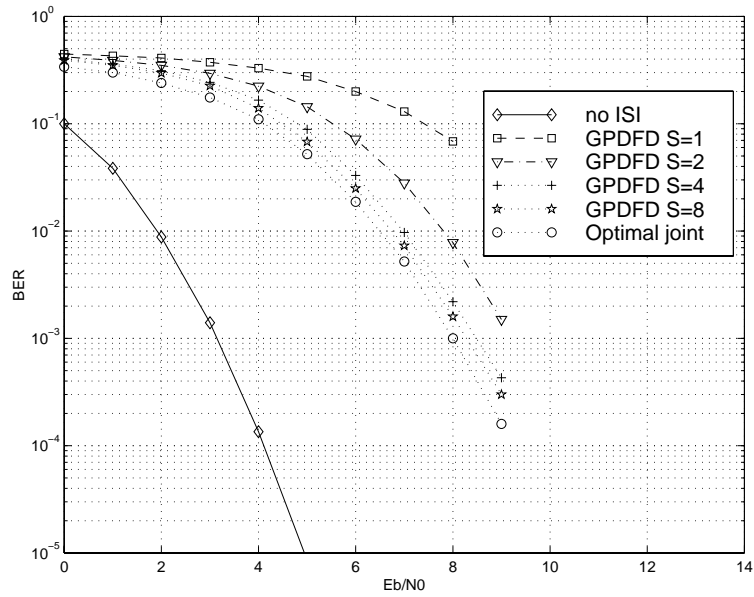


Figure 3.5: BER over the worst static 6-taps ISI channel, rate-1/2 16-state convolutional code, QPSK mapping.

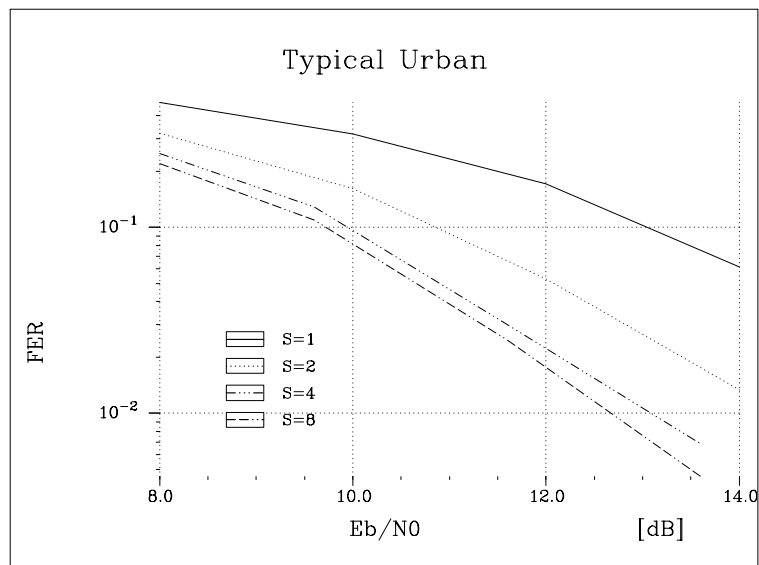


Figure 3.6: FER over Typical Urban channel, rate-1/2 16-state convolutional code, QPSK mapping.

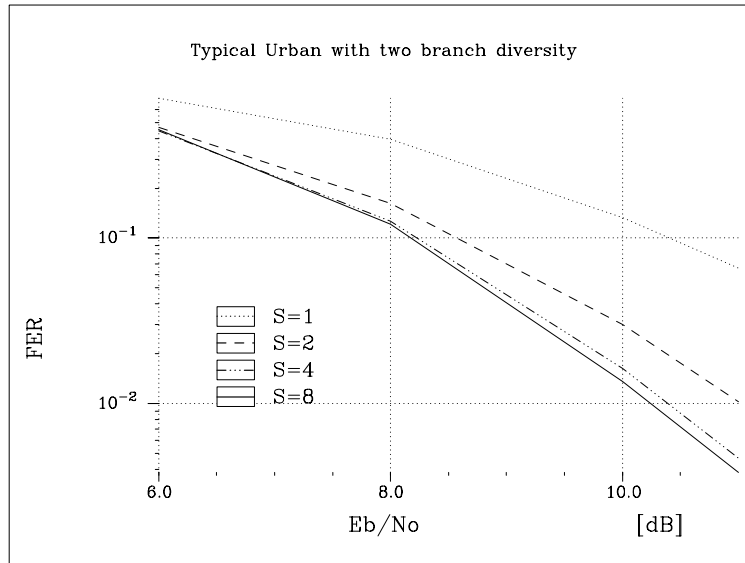


Figure 3.7: FER over Typical Urban channel with two-branch diversity, rate-1/2 16-state convolutional code, QPSK mapping.

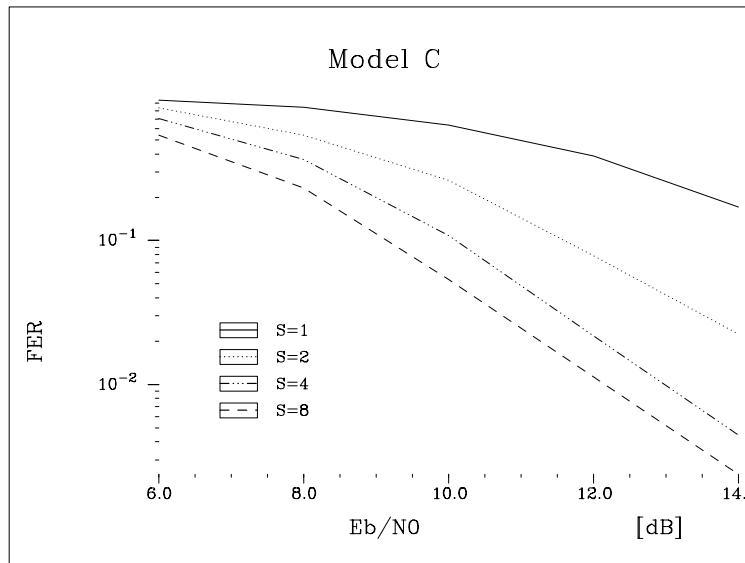


Figure 3.8: FER over channel model C, rate-1/2 16-state convolutional code, QPSK mapping.

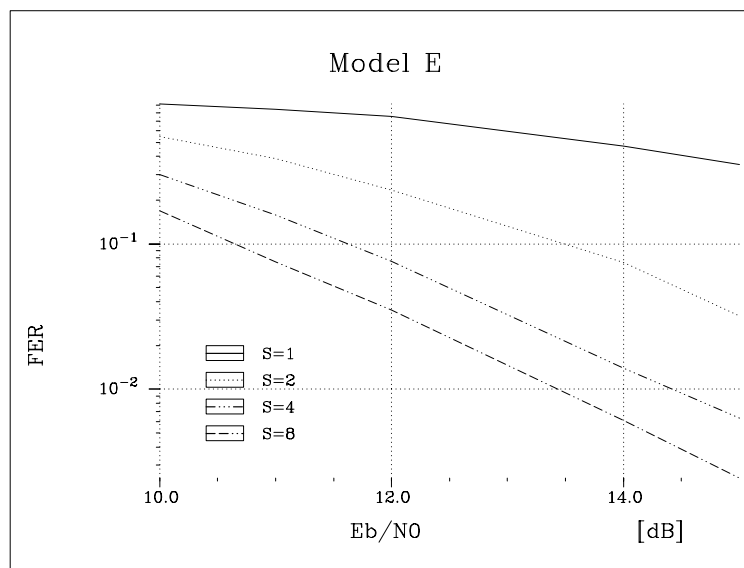


Figure 3.9: FER over channel model E, rate-1/2 16-state convolutional code, QPSK mapping.

Chapter 4

Iterative Equalization and Estimation for Advanced TDMA Systems

4.1 Introduction

A general problem of reliable data transmission over channels with intersymbol interference (ISI) includes joint estimation, detection and decoding, and as a whole it is non-tractable because of tremendous complexity involved. A suboptimal method to solve this problem is to split the processing into tractable sub-blocks, and then iteratively exchange locally processed information among sub-blocks. For example, decoding of celebrated turbo codes is based on iterative information update among relatively simple decoders [17]. The same principle applied to channel equalization leads to a turbo equalization scheme [39] that recently has gained a lot of interest [91], [53], [8], [9], [10], [51], [107], [54], [50], [21], [118], [22], [93]. This technique performs iterative ISI removal, where iterations proceed between a detector and a channel decoder relying on channel estimates that usually are obtained based on a known training sequence. On the other hand, in practice channel estimates may have rather poor quality that in turn deteriorates the efficiency of equalization. This fact motivated us to consider a decision-directed channel estimation similar to [102], [33]. The principle of turbo equalization applied to channel estimation leads to iterative (turbo) estimation schemes [99],[84],[108]. Following [85] in this chapter we extend this approach and include iterative channel estimation (ICE) into turbo detection loop. Furthermore, we show that iterative data processing applied for Incremental Redundancy (IR), the sophisticated retransmission scheme retains for EDGE, can favorably benefit from such a receiver.

In this chapter we propose a generic TDMA receiver that performs iterative equalization and estimation in a joint/iterative fashion. Although this receiver design can be used for any TDMA system, it is particularly interesting for high order modulation such as 8-PSK adopted in EDGE standard [52]. The maximum-likelihood (ML) detection of 8 PSK modulated

symbols in the presence of ISI is too complex for mobile communications, so to keep the overall receiver complexity low a sub-optimal equalizer has to be introduced. In particular, we introduce a low complexity suboptimal SISO equalizers based on the Decision Feedback Sequence Estimation (DFSE) [45],[38] that as such can be used in conventional receiver without iterative data processing. Next, we present its modifications suitable for turbo equalization, which as it is shown in [51], [22], [93] brings a substantial gain in EDGE environment. To keep the receiver complexity low we also suggest a simple method of updating channel estimate that includes the decoder outputs into the iteration process and also may be coupled with iterative detection.

To study receiver performance-complexity trade-off we consider different iterative estimation-equalization scenarios for GSM/EDGE packet data services. In particular, we consider General Packet Radio Service (GPRS) and Enhanced GPRS (EGPRS) where enhanced packet data services in GSM environment will be provided by 8PSK modulation used instead of binary GMSK modulation [52].

The chapter is organized as follows. In Section 2, we introduce notations and an overview of the conventional receivers. In Section 3, we discuss reduced complexity SISO equalizers. Notably, two different soft output computation methods are compared based on forward backward recursion and forward only recursion. Next, in Section 4, we consider turbo-detection for Q -ary modulation and propose a combined iterative estimation - equalization scheme. Application of turbo-equalization for retransmission schemes is addressed in the same section. Trade-off between performance gain and receiver complexity in (E)GPRS under different scenarios is addressed in Section 5, with conclusions following in Section 6.

4.2 System Model

4.2.1 Notation

Let us consider a digital communication system with a block diagram depicted in figure 4.1. A data sequence $\mathbf{u}_1^{\tau_0} = (\mathbf{u}_1, \dots, \mathbf{u}_{\tau_0})^\top$ of τ_0 symbols enters an encoder C_o which outputs a coded sequence $\mathbf{c}_1^{\tau_0} = (\mathbf{c}_1, \dots, \mathbf{c}_{\tau_0})^\top = \Xi \mathbf{u}_1^{\tau_0}$. Each data symbol $\mathbf{u}_n = (u_{n,1}, \dots, u_{n,k_0})^\top$ contains k_0 bits, whereas each coded symbol $\mathbf{c}_n = (c_{n,1}, \dots, c_{n,n_0})^\top$ contains n_0 bits. Coded bits are interleaved by an interleaver Π and punctured to match data rates to a transmitted format. Resulting bits are grouped into Q -ary symbols and then are allocated into N bursts. Each burst consists of τ symbols $\mathbf{a}_1^\tau = (\mathbf{a}_1, \dots, \mathbf{a}_\tau)^\top$, and it includes known symbols for channel estimation and synchronization purposes together with tail and guard symbols. Let \mathbf{m} denote a training sequence consisting of L preamble and P midamble symbols. The resulting data burst \mathbf{a}_1^τ of length τ is formed by sub-blocks, $\mathbf{a}_1^\tau = (\mathbf{d}_1^\top, \mathbf{m}^\top, \mathbf{d}_2^\top)^\top$, where $\mathbf{d}_1 = \mathbf{a}_1^{\tau_0/2}$, $\mathbf{m} = \mathbf{a}_{\tau_0/2+1}^{\tau_0/2+L+P}$, $\mathbf{d}_2 = \mathbf{a}_{\tau_0/2+L+P}^\tau$. To each symbol $\mathbf{a}_n = (a_{n,1}, \dots, a_{n,q})^\top$, a $Q = 2^q$ -

ary signal mapper Ψ associates a complex-valued symbol z_n . The transmitter produces the complex base-band waveform:

$$w_x(t) = \sum_n z_n h_x(t - nT) \quad (4.1)$$

where $h_x(t)$ denotes the base-band complex impulse response of the low-pass equivalent transmitter filter and $\frac{1}{T}$ is the symbol rate. At reception, the received base-band signal is given by:

$$w_r(t) = \sum_n z_n g(t - nT) + \epsilon'(t) \quad (4.2)$$

where the complex impulse response $g(t)$ takes into account the transmitter and receiver filters, together with the dispersive channel. $\epsilon'(t)$ denotes the convolution of the complex zero-mean Gaussian noise $\epsilon(t)$ (of single-sided power spectral density N_0) with the receiver filter $h_r(t)$. The signal is then sampled at rate $\frac{1}{T}$ to yield the non-quantized sequence $\mathbf{y}_1^\tau = (y_1, \dots, y_\tau)^\top = \mathbf{y}$.

4.2.2 The equivalent discrete-time channel model

The equivalent discrete-time channel model is made of an encoder C_o with associated puncturing schemes, an interleaver Π , a signal mapper Ψ , and a transversal filter with $\nu_c + 1$ complex coefficient vector $\mathbf{h} = (h_0, h_1, \dots, h_{\nu_c})^\top$, see figure 4.2. At the output of the equivalent discrete-time channel (including transmit and receive filters), received samples are given by:

$$y_n = h_0 z_n + \sum_{k=1}^{\nu_c} h_k z_{n-k} + w_n \quad (4.3)$$

or in the matrix form

$$\mathbf{y} = \mathbf{Z}\mathbf{h} + \mathbf{w} \quad (1)$$

where $\sum_{k=1}^{\nu_c} h_k z_{n-k}$ corresponds to the ISI introduced by the channel and w_n is a circularly symmetric complex Gaussian variable of variance $2\sigma^2$ (i.e., its real and imaginary parts are uncorrelated and of same power $\sigma^2 = N_0/2$). Beside, we considered that the noise samples w_n are independent identically distributed (iid) in the following (even if the receive filter does not comply with the Nyquist criterion, the performance degradation involved by such an approximation is rather small in practice). Here and below capital bold letters are used both for vectors and matrices.

For AWGN the autocorrelation matrix \mathbf{R} of the noise vector \mathbf{w} is considered $\mathbf{R} = 2\sigma^2\mathbf{I}$ with \mathbf{I} being the $(\tau \times \tau)$ dimensional unit matrix.

As well known, the equivalent discrete-time ISI channel can be regarded as a non-recursive non-systematic rate-1 convolutional code with memory ν_c , whose single complex-valued generator polynomial may vary in time. The time progression of the states, as well as the

possible transitions can be presented by a regular trellis diagram. We denote by \mathbf{S}_n and \mathbf{B}_n state and branch spaces at trellis section n , respectively. Due to time-invariant property, the state and the branch space complexities satisfy:

$$|\mathbf{S}_n| = Q^{\nu_c}, \forall n \in [0, \tau] \text{ and } |\mathbf{B}_n| = Q^{\nu_c+1}, \forall n \in [1, \tau] \quad (2)$$

The ML symbol by symbol detection may be performed by the BCJR algorithm [3],[8], which operates on the full ISI channel trellis with complexity $O(|\mathbf{B}|)$.

4.2.3 Conventional receiver

We define $y_1^{N\tau}$ as the received samples of N consecutively transmitted bursts $\mathbf{a}_1^{N\tau}$, and \mathbf{h}_1^N as the set of channel coefficient vectors corresponding to N bursts. For the sake of simplicity, we use thereafter the simplified notations \mathbf{u} for $\mathbf{u}_1^{\tau_0}$ and \mathbf{c} for $\mathbf{c}_1^{\tau_0}$.

According to the ML criteria applied to minimize block error rate for data block \mathbf{u} , the optimal receiver is to find

$$\hat{\mathbf{u}} = \arg \max_{\mathbf{h}_1^N, \mathbf{u}} \Pr(y_1^{N\tau} | \mathbf{h}_1^N, \mathbf{a}_1^{N\tau}) = \arg \max_{\mathbf{h}_1^N, \mathbf{u}} \Pr(y_1^{N\tau} | \mathbf{h}_1^N, \mathbf{m}_1^N, \Xi \mathbf{u}, \Pi) \quad (3)$$

The optimal solution of (3) is prohibitively complex, and in practice (3) is split into several problems, which are then considered separately. Separating channel equalization (detection) and decoding, and taking into account that the training sequence is known, a suboptimal solution for (3) may be presented as

$$\hat{\mathbf{a}}_1^{N\tau} = \arg \max_{\mathbf{h}_1^N, \mathbf{a}_1^{N\tau}} \Pr(y_1^{N\tau} | \mathbf{h}_1^N, \mathbf{a}_1^{N\tau}) \implies \hat{\mathbf{c}} = \arg \max_{\mathbf{h}_1^N, \mathbf{c}} \Pr(y_1^{N\tau} | \mathbf{h}_1^N, \mathbf{c}) \quad (4)$$

$$\hat{\mathbf{u}} = \arg \max_{\mathbf{u}} \Pr(\hat{\mathbf{c}} | \mathbf{u}) \quad (5)$$

The optimal solution requires a search over all possible \mathbf{c} and \mathbf{h}_1^N that is impractical for realistic values of τ_0, N, ν_c . A typical suboptimal solution of (4) is to separate channel estimation and equalization and perform them burst by burst, i.e.

$$\hat{\mathbf{h}} = \arg \max_{\mathbf{h}} \Pr(y_1^\tau | \mathbf{m}, \mathbf{h}) \quad (6)$$

$$\hat{\mathbf{a}}_1^\tau = \arg \max_{\mathbf{a}_1^\tau} \Pr(y_1^\tau | \hat{\mathbf{h}}, \mathbf{a}_1^\tau) \quad (7)$$

In particular, assuming a linear channel with time-invariant CIR during a transmitted block, a received block can be presented as

$$\mathbf{y} = \mathbf{Z}\mathbf{h} + \mathbf{w} = [\mathbf{y}_1^\top \mathbf{y}_m^\top \mathbf{y}_2^\top]^\top$$

where \mathbf{Z} is $\tau \times (L+1)$ block matrix formed by data $\mathbf{d}_1, \mathbf{d}_2$ and training sequence \mathbf{m} mapped into Q -ary symbols; $\mathbf{Z} = [\mathbf{Z}_1^\top \mathbf{M}^\top \mathbf{Z}_2^\top]^\top$.

In a conventional receiver the channel estimation is made based on received symbols $\mathbf{y}_m = \mathbf{M}\mathbf{h} + \mathbf{w}$, and the ML channel estimate [67]

$$\hat{\mathbf{h}}_{ML} = \arg \max_{\mathbf{h}} \Pr(\mathbf{y}_m | \mathbf{M}, \mathbf{h}) = \mathbf{C}(\hat{\mathbf{h}}_{ML}) \mathbf{R}^{-1} \mathbf{M}^H \mathbf{y}_m \quad (8)$$

where $\mathbf{C}(\hat{\mathbf{h}}_{ML}) = (\mathbf{M}^H \mathbf{R}^{-1} \mathbf{M})^{-1}$ is a covariance matrix of the estimate.

Given $\hat{\mathbf{h}}$, one of equalization algorithms is applied to remove ISI and obtain $\hat{\mathbf{c}}$. Finally, a decoder recovers transmitted information $\hat{\mathbf{u}}$.

4.3 Low Complexity Q -ary SISO Equalizer

4.3.1 Decision Feedback Soft-In Soft-Out (DF-SISO) equalizer

Depending on the optimization criteria, the detection (7) may be implemented by BCJR algorithm [3] or Viterbi algorithm (VA) for max *a posteriori* (APP) or MLSE criteria, respectively. Both algorithms operate on the full ISI channel trellis with complexity of $O(|\mathbf{B}|)$. For 8-PSK modulation adopted in EDGE and a typical GSM channels the optimal equalizer currently seems unacceptable for complexity reasons.

To reduce the equalizer complexity a number of suboptimal schemes have been proposed. Among the set of trellis-based Reduced-States Sequence Estimators (RSSE) [45], the Decision Feedback Sequence Estimators (DFSE) [38] seem to be the most suitable candidate providing acceptable performance at moderate complexity [54]. To provide soft decision outputs that are necessary for the decoding different methods may be applied. In particular, a soft output equalizer based on MMSE [107], and the DFSE where soft decisions are formed using neural networks approach [55] are recently introduced. In this chapter we consider the trellis-based equalizers and present the DFSE modifications of different complexity to provide soft decision outputs.

The main idea of RSSE [45] and DFSE [38] is to operate on a reduced complexity trellis Γ , where only ν_r symbols (related to ν_r channel taps) form the trellis state space S , and the other $\nu_c - \nu_r$ symbols are used through the embedded decision-feedback structure.

Let's define S_n and B_n as state and branch spaces at n^{th} section (time instant) of a reduced trellis Γ . For a positive integer ν_r , we say that a trellis input sequence \mathbf{a}_1^n ends at a sub-state $s \in S_n$ if \mathbf{a}_1^n terminates with the substring $s = \mathbf{a}_{n-\nu_r+1}^n$. At any trellis depth n , the sub-state space S_n coincides with the full BCJR trellis state space if $\nu_r = \nu_c$. In a case where $\nu_r < \nu_c$, the state space S is reduced to a subset made of all possible sub-states s derived from full states trellis, so that:

$$|S_n| = Q^{\nu_r}, \forall n \in [0, \tau] \quad \text{and} \quad |B_n| = Q^{\nu_r+1}, \forall n \in [1, \tau] \quad (9)$$

Any trellis branch $b_n \in B_n$ at depth n of a sub-trellis Γ is characterized by three fields, $b_n = \{s_{n-1}, s_n, \mathcal{A}_n\}$:

- a starting state $s_{n-1} \in S_{n-1}$;
- an arrival state $s_n \in S_n$;
- a label \mathcal{A}_n representing an input symbol \mathbf{a}_n , where $\mathcal{A}_n = \{\mathcal{A}_{n,1}, \mathcal{A}_{n,2}, \dots, \mathcal{A}_{n,q}\}$ is the binary presentation of \mathbf{a}_n

The above formalism defines a reduced trellis $\Gamma(S, B)$ on which the DFSE algorithm proceeds. Each trellis path is a set of edges $\{b_1, b_2, \dots, b_\tau\}$ starting from state δ at time $n = 0$ and terminating at state η at time $n = \tau$. At each trellis section $n \in [1, \tau]$ and for all bit indices $j \in [1, q]$, an optimal symbol by symbol algorithm is to compute the log *a posteriori* ratio (LAPPR):

$$\lambda(a_{n,j}) = \ln \frac{\Pr(a_{n,j} = 1 \mid y_1^\tau, \hat{\mathbf{h}})}{\Pr(a_{n,j} = 0 \mid y_1^\tau, \hat{\mathbf{h}})} \quad (10)$$

It is assumed that channel taps $\hat{\mathbf{h}}$ are estimated by some channel estimator using the training sequence \mathbf{m} before the equalization process. In the following derivation the conditioning by $\hat{\mathbf{h}}$ is implicit and omitted for the ease of expressions.

Equation (10) can be rewritten as follows:

$$\lambda(a_{n,j}) = \ln \frac{\sum_{\mathbf{a}_1^\tau, a_{n,j}=1} p(\mathbf{a}_1^\tau, y_1^\tau)}{\sum_{\mathbf{a}_1^\tau, a_{n,j}=0} p(\mathbf{a}_1^\tau, y_1^\tau)} \quad (11)$$

where $p(\mathbf{a}_1^\tau, y_1^\tau) = p(y_1^\tau \mid \mathbf{a}_1^\tau) \Pr(\mathbf{a}_1^\tau)$.

Based on the approximation

$$\ln \left(\sum_i \exp(\Delta_i) \right) \approx \max_i \Delta_i, \quad (12)$$

the approximated soft decision output is defined as:

$$\lambda_{eq}(a_{n,j}) = \max_{\mathbf{a}_1^\tau, a_{n,j}=1} \{\ln p(\mathbf{a}_1^\tau, y_1^\tau)\} - \max_{\mathbf{a}_1^\tau, a_{n,j}=0} \{\ln p(\mathbf{a}_1^\tau, y_1^\tau)\} \quad (13)$$

or equivalently:

$$\lambda_{eq}(a_{n,j}) = \min_{\mathbf{a}_1^\tau, a_{n,j}=0} \{-\ln p(\mathbf{a}_1^\tau, y_1^\tau)\} - \min_{\mathbf{a}_1^\tau, a_{n,j}=1} \{-\ln p(\mathbf{a}_1^\tau, y_1^\tau)\} \quad (14)$$

where $\{-\ln p(\mathbf{a}_1^\tau, y_1^\tau)\}$ corresponds to the trellis path metric associated with symbol sequence \mathbf{a}_1^τ . In trellis terminology, $\lambda_{eq}(a_{n,j})$ is the algebraic difference at time instant n between the path metric associated with the best trellis path that decodes a bit 0 at position j and the path metric associated with the best trellis path that decodes a bit 1 at position j .

Let $\mu^{\leftrightarrow}(b_n)$ be the accumulated metric of the best path starting from state $s_0 = \delta$, terminating at state $s_\tau = \eta$, and passing by transition $b_n = \{s_{n-1}, s_n, \mathcal{A}_n\}$ at trellis section n . The DF-SISO equalizer soft output can be equivalently rewritten as:

$$\lambda_{eq}(a_{n,j}) = \min_{b_n \in B_n, \mathcal{A}_{n,j}=0} \mu^{\leftrightarrow}(b_n) - \min_{b_n \in B_n, \mathcal{A}_{n,j}=1} \mu^{\leftrightarrow}(b_n); \quad (15)$$

where $\mu^{\leftrightarrow}(b_n)$ may be presented in the form

$$\mu^{\leftrightarrow}(b_n) = \mu^{\rightarrow}(s_{n-1}) + \gamma(b_n) + \mu^{\leftarrow}(s_n); \quad (16)$$

- $\mu^{\rightarrow}(s_{n-1})$ is the accumulated metric of the best subpath starting from state $s_0 = \delta$ and terminating at state s_{n-1} ;
- $\mu^{\leftarrow}(s_n)$ is the accumulated metric of the best subpath starting from state s_n and terminating at state $s_\tau = \eta$;
- $\gamma(b_n)$ is the (approximated) edge metric associated with b_n . For any state $s_n \in S_n$ at time n the metric $\mu^{\rightarrow}(s_n)$ can be recursively computed using the forward recursion similar to [3]:

$$\mu^{\rightarrow}(s_n) = \min_{b_n \in B_n} \{\mu^{\rightarrow}(s_{n-1}) + \gamma(b_n)\} \quad (17)$$

with a boundary conditions $\mu^{\rightarrow}(s_0 = \delta) = 0$ and $\mu^{\rightarrow}(s_0 \neq \delta) = \infty$ at time $n = 0$.

At each section (time instant n) of the trellis Γ and for all transitions, the edge metric computation involves a convolution of discrete-time CIR with a sequence of ν_c already estimated symbols. The first ν_r estimated symbols of that sequence are derived based on the current trellis branch b_n of the sub-trellis Γ . The remaining part is evaluated by per-survivor processing [38]. In particular, for the existing transitions the edge metric expression used in the DF-SISO is

$$\gamma(b_n) = \frac{1}{2\sigma^2} \left\| r_n - \hat{h}_0 z_n - I_n^{(1)} - \hat{I}_n^{(2)} \right\|^2 \quad (18)$$

where:

- $I_n^{(1)}$ is the first part of ISI contribution term

$$I_n^{(1)} = \sum_{k=1}^{\nu_r} \hat{h}_k \Psi(\mathbf{a}_{n-k}); \quad (19)$$

which involves the sequence $\hat{\mathbf{a}}_{n-\nu_r}^{n-1}$ of Q -ary symbols contained in the trellis state s_{n-1} ;

- $\widehat{I}_n^{(2)}$ is the second part of ISI contribution term

$$\widehat{I}_n^{(2)} = \sum_{k=\nu_r+1}^{\nu_c} \widehat{h}_k \Psi(\widehat{\mathbf{a}}_{n-k}^{s_{n-1}}); \quad (20)$$

which involves the sequence $a_{n-\nu_c}^{n-\nu_r-1}$ of Q -ary symbols estimated by reading off the survivor path terminating at s_{n-1} .

Similarly, for any state $s_n \in S_n$ at time n the metric $\mu^\leftarrow(s_n)$ can be recursively computed using the backward recursion:

$$\mu^\leftarrow(s_n) = \min_{b_{n+1} \in B_{n+1}} \{\mu^\leftarrow(s_{n+1}) + \gamma(b_{n+1})\} \quad (21)$$

with boundary condition $\mu^\leftarrow(s_\tau = \eta) = 0$ and $\mu^\leftarrow(s_\tau \neq \eta) = \infty$ at time, $n = \tau$.

Since only the first ν_r channel taps form the trellis structure, it is beneficial for decision feedback equalizers to have the minimum phase CIR [125]. To meet this requirement the usual practice is to put a pre-filter before the equalizer. That pre-filter provides the minimum phase CIR for the forward recursion, while it is not true for the backward recursion. To avoid this problem it is suggested to perform first the forward recursion and to keep all associated edge metrics $\gamma(b_n)$ calculated according to (18). Then the stored edge metrics are used for the backward recursion (21).

Finally, the LAPPR on bit $a_{n,j}$ at the DF-SISO equalizer output

$$\lambda_{eq}(a_{n,j}) = \min_{b_n \in B_n, \mathcal{A}_{n,j}=0} \{\mu^\rightarrow(s_{n-1}) + \gamma(b_n) + \mu^\leftarrow(s_n)\} - \min_{b_n \in B_n, \mathcal{A}_{n,j}=1} \{\mu^\rightarrow(s_{n-1}) + \gamma(b_n) + \mu^\leftarrow(s_n)\} \quad (22)$$

It must be emphasized that the above minimization operation, as well as the metric expressions are exact if and only if $\nu_r = \nu_c$. In that case, the DF-SISO becomes formally equivalent to the max-log-MAP algorithm applied for the full ISI channel trellis. For the reduced-state trellis the estimated sequences taken from the path history and involved in edge metric derivations inevitably introduce a degradation in performance due to a possible error propagation effect.

4.3.2 DF-SISO equalizer with forward recursion

Described above DF-SISO performs the forward-backward recursions to provide bit-wise soft decisions. To reduce the equalizer complexity we can exclude the backward recursion which results to the original DFSE performing VA with only forward recursion. Recall that VA provides MLSE solution (i.e. only hard decisions), and to form bit-wise soft decisions for the DFSE one may follow the SOVA approach [60] [6]. Soft values in SOVA are obtained by comparing only two of the most likely sequences with different bits at a particular time

instant. According to SOVA the soft decisions are calculated via recursive updating of soft values within the VA decision delay window D (typically $D=5v_c$). Further complexity reduction may be provided by soft-output Viterbi equalizer (SOVE) [68], where only a few operations are added to the VA to form soft decisions. The simplification is obtained by omitting recursive update and shortening the VA decision delay ($D = v_c$) that results in a small degradation (0.2 dB) compared to the SOVA [95]. This degradation may be practically eliminated by expanding the decision delay $D = v_c + 2$ [83].

Specifically, soft decisions in SOVE may be obtained if we set $\mu^{\leftarrow}(s_n) = 0$ in (16), skip the backward recursion (21) and perform only the forward recursion according to (17)-(22). Finally, the LAPPR on bit $a_{n-D,j}$ at time instant n delivered by DF-SISO with forward-only recursion is:

$$\lambda_{eq}(a_{n-D,j}) = \min_{b_n \in B_n, \mathcal{A}_{n-D,j}=0} \{\mu^{\rightarrow}(s_{n-1}) + \gamma(b_n)\} - \min_{b_n \in B_n, \mathcal{A}_{n-D,j}=1} \{\mu^{\rightarrow}(s_{n-1}) + \gamma(b_n)\} \quad (23)$$

On the other hand, the original forward-only SOVA [60][6] may be easily modified to approach performance of max-log-MAP with only minor increase of complexity [49]. Hence, the forward only approach provides a number of low complexity solutions to approach max-log MAP performance.

To compare the forward-backward and the forward-only DF-SISO equalizers we considered their performance in static channels without prefiltering and with ideal channel estimates (see figure 4.3). We found that for the static channel $\text{CIR}_1 = \{0.5, 0.71, 0.5\}$ the performance of the two considered DF-SISO equalizers with $v_c=2$ is very close when comparing their hard decision outputs. To evaluate the quality of soft decisions for both algorithms we include the strongest EGPRS coding scheme MCS5 which is based on a rate 1/3 convolutional code with constraint length 7. Simulation results presented in figure 4.3 show that DF-SISO with forward-backward recursions provides some gain (0.3 dB at $\text{BER}=10^{-3}$) compared to the forward-only DF-SISO equalizer. On the other hand, this gain is not as visible (0.1 dB at $\text{BER}=10^{-3}$) for a minimum phase channel with $\text{CIR}_2 = \{0.77, 0.55, 0.33\}$. We consider below only the DF-SISO equalizer with forward-backward recursion.

4.3.3 Minimum-phase pre-filtering

If the main part of the ISI is contained in the last $\nu_c - \nu_r$ taps, the degradation in performance might be important compared to the Min-Log-BCJR ISI decoder. This happens when some roots of the equivalent discrete-time filter $H(z)$ are outside the unit circle. To assure an average error rate close to optimal performance, a correcting-phase pre-filtering must be fitted just before the SISO-DDFSE. This pre-filter turns the discrete-time channel impulse response into minimum phase, concentrating energy in the first taps, and thus, improving the accuracy of DDFSE branch metrics dramatically. Many algorithms exist to practically

construct the minimum-phase filter, the most straightforward being based on root finding. Because of its prohibitive complexity however, the CEPSTRE principle has been preferred here for an efficient calculation [125]. A low-complexity turbo detector is depicted on figure 4.5.

4.4 Iterative Receiver for EDGE

4.4.1 Turbo detection principle

One of the solutions related to DFSE is the method of turbo equalization [39]. This method is based on iterations between detection and decoding stages and attempts to find ML solution $\hat{\mathbf{u}}$ over a combined trellis formed by a multipath channel and encoder, i.e.

$$\hat{\mathbf{u}} = \arg \max_{\mathbf{u}} \Pr(y_1^{N\tau} | \hat{\mathbf{h}}_1^N, \mathbf{m}_1^N, \Xi \mathbf{u}, \Pi) \quad (24)$$

An iterative receiver with turbo equalization is outlined in figure 4.4. The SISO equalizer delivers bit-wise LAPPR on bits $a_{n,j}$ that can be split into two (called intrinsic and extrinsic) parts

$$\lambda_{eq}(a_{n,j}) = \lambda^a(a_{n,j}) + \lambda_{eq}^{ext}(a_{n,j}). \quad (25)$$

After de-interleaving Π^{-1} , the sequence of extrinsic LAPPR, $\lambda_{eq}^{ext}(\mathbf{a}_1^{N\tau})$, becomes a sequence of log *a priori* probability ratios $\lambda^a(\mathbf{c})$ on coded bits for the decoder. Similarly at the output of the SISO decoder, the LAPPR on coded bit $\lambda_d(c_{n,j})$ can be split into an intrinsic and an extrinsic parts. The latter can be computed by bit-wise subtraction of the *a priori* information $\lambda^a(c_{n,j})$ at the input of the decoder from the corresponding LAPPR $\lambda_d(c_{n,j})$ at the output,

$$\lambda_d^{ext}(c_{n,j}) = \lambda_d(c_{n,j}) - \lambda^a(c_{n,j}). \quad (26)$$

Sequence of extrinsic LAPPRs on coded bits $\lambda_d^{ext}(\mathbf{c})$ is re-interleaved by Π and passed to the SISO detector as a new sequence of log *a priori* probability ratios $\lambda^a(\mathbf{a}_1^\tau)$ for the next detection attempt.

4.4.2 Q-ary turbo-detection with DF-SISO equalizers

The transition metric in the presence of independent *a priori* information on the transmitted symbol, $\Pr(\mathbf{a}_n = \mathcal{A}_n)$, for DF-SISO equalizers is given by

$$\gamma^a(b_n) = \frac{1}{2\sigma^2} \left\| r_n - \hat{h}_0 z_n - I_n^{(1)} - \hat{I}_n^{(2)} \right\|^2 - \ln \Pr(\mathbf{a}_n = \mathcal{A}_n) \quad (27)$$

Assuming perfect decorrelation between symbols bits $\{a_{n,j}\}$, $j \in [1, q]$, $n \in [1, \tau]$ after re-interleaving Π of the encoded sequence c :

$$\Pr(\mathbf{a}_n = \mathcal{A}_n) = \prod_{j=1}^q \Pr(a_{n,j} = \mathcal{A}_{n,j}) \quad (28)$$

Since it is always possible to write:

$$\prod_{j=1}^q \Pr(a_{n,j} = \mathcal{A}_{n,j}) = \Pr(a_{n,j} = \mathcal{A}_{n,j}) \prod_{\substack{l=1 \\ l \neq j}}^q \Pr(a_{n,l} = \mathcal{A}_{n,l}) \quad (29)$$

then $\Pr(a_{n,j} = \varepsilon | y_1^\tau)$, $\varepsilon \in \{0, 1\}$ at the equalizer output can be presented as

$$\begin{aligned} -\ln \Pr(a_{n,j} = \varepsilon | y_1^\tau) &= \min_{b_n \in B_n^{L-1}, \mathcal{A}_{n,j} = \varepsilon} \{\mu^\rightarrow(s_{n-1}) + \gamma^a(b_n) + \mu^\leftarrow(s_n)\} \\ &= \min_{b_n \in B_n^{L-1}, \mathcal{A}_{n,j} = \varepsilon} \{\mu^\rightarrow(s_{n-1}) + \gamma^{ext}(b_n) + \mu^\leftarrow(s_n)\} - \ln \Pr(a_{n,j} = \varepsilon) \end{aligned} \quad (30)$$

where:

$$\gamma^{ext}(b_n) = \frac{1}{2\sigma^2} \left\| r_n - \hat{h}_0 z_n - I_n^{(1)} - \hat{I}_n^{(2)} \right\|^2 - \sum_{\substack{l=1 \\ l \neq j}}^q \ln \Pr(a_{n,l} = \mathcal{A}_{n,l}) \quad (31)$$

Finally, the LAPP on the bit $a_{n,j}$, $\lambda_{eq}(a_{n,j})$, at the output of Q -ary SISO equalizer

$$\lambda_{eq}(a_{n,j}) = \ln \frac{\Pr(a_{n,j} = 1 | y_1^\tau)}{\Pr(a_{n,j} = 0 | y_1^\tau)} = \lambda^a(a_{n,j}) + \lambda_{eq}^{ext}(a_{n,j}) \quad (32)$$

where $\lambda^a(a_{n,j})$ is the log *a priori* probability ratio on the bit $a_{n,j}$ provided by SISO decoder

$$\lambda^a(a_{n,j}) = \ln \frac{\Pr(a_{n,j} = 1)}{\Pr(a_{n,j} = 0)}; \quad (33)$$

and the incremental knowledge on bit $a_{n,j}$ brought by detection process (the extrinsic information) is

$$\begin{aligned} \lambda_{eq}^{ext}(a_{n,j}) &= \min_{b_n \in B_n, \mathcal{A}_{n,j}=0} \{\mu^\rightarrow(s_{n-1}) + \gamma^{ext}(b_n) + \mu^\leftarrow(s_n)\} \\ &\quad - \min_{b_n \in B_n, \mathcal{A}_{n,j}=1} \{\mu^\rightarrow(s_{n-1}) + \gamma^{ext}(b_n) + \mu^\leftarrow(s_n)\} \end{aligned} \quad (34)$$

In the similar way, the extrinsic information for forward-only DF-SISO equalizer is formed as

$$\lambda_{eq}^{ext}(a_{n-D,j}) = \min_{b_n \in B_n, \mathcal{A}_{n-D,j}=0} \{\mu^{\rightarrow}(s_{n-1}) + \gamma^{ext}(b_n)\} - \min_{b_n \in B_n, \mathcal{A}_{n-D,j}=1} \{\mu^{\rightarrow}(s_{n-1}) + \gamma^{ext}(b_n)\} \quad (35)$$

Note that the effect of *a priori* information $\Pr(\mathbf{a}_n = \mathcal{A}_n)$ on Q -ary turbo-detection is twofold. First, it is accumulated during forward-backward recursions in $\mu^{\rightarrow}(s_n)$ and $\mu^{\leftarrow}(s_n)$ due to the usage of $\gamma^a(b_n)$ instead of $\gamma(b_n)$ in (17),(21). Second, it explicitly presents in (31),(34) as $\sum_{\substack{l=1 \\ l \neq j}}^q \ln \Pr(a_{n,l} = \mathcal{A}_{n,j})$. In case of binary modulation (e.g., GMSK, $q=1$) the second term is not present. Hence, turbo-equalization is expected to provide more gain for schemes with high level modulation. Simulation results presented below confirm this conjecture.

4.4.3 Iterative (turbo) channel estimation

In the turbo detection scheme (24) the iteration proceeds only between the signal detector and channel decoder assuming a known channel state $\hat{\mathbf{h}}$ during iterations. Given a known training sequence \mathbf{m} , the channel estimate may be obtained by (8) based on the data \mathbf{y}_m . However, in many cases the accuracy of channel estimate, which is based only on a relatively short training sequence \mathbf{m} , may be rather low. That in turn may cause a significant performance degradation at the receiver that cannot be fully compensated by the turbo detection. This fact motivated us to use a decision-directed adaptive channel estimation method during the iteration process similar to [102],[33]. The idea is to feed back the decoded symbols to the channel estimator and update previous channel estimates assuming that the whole burst is now known by the receiver (figure 4.7) [99], [84], [85], [108]. Hence, the receiver relies on the hard decoded data symbols $\check{\mathbf{c}}_1^{\tau_0}$ and the known training sequence \mathbf{m} to form a new channel estimate. In other words, the receiver iteratively updates the channel estimate based on an "extended" training sequence. In particular, after decoding procedure the data $\hat{\mathbf{u}}$ are re-encoded as $\check{\mathbf{c}} = \Xi \hat{\mathbf{u}}$ interleaved and then combined with the training sequence \mathbf{m} , forming a new "extended" training sequence $\check{\mathbf{a}}_1^{\tau}$ of length τ . If we would use all available data \mathbf{a}_1^{τ} as the known training sequence, then the ML channel estimate in AWGN channel is

$$\hat{\mathbf{h}}^{extend} = C(\hat{\mathbf{h}}^{extend}) \mathbf{Z}^H \mathbf{y} \quad (36)$$

where the covariance matrix of the new "extended" estimate is

$$C(\hat{\mathbf{h}}^{extend}) = (\mathbf{Z}^H \mathbf{Z})^{-1} = (\mathbf{Z}_1^H \mathbf{Z}_1 + \mathbf{M}^H \mathbf{M} + \mathbf{Z}_2^H \mathbf{Z}_2)^{-1} \quad (37)$$

and matrix \mathbf{Z} is formed by all data \mathbf{a}_1^{τ} [84].

The variance of the "extended" estimate \hat{h}^{extend} may be bounded by Cramer-Rao lower bound (CRLB) [67] (see appendix A)

$$\text{var}(\hat{\underline{h}}_i^{extend}) \geq \frac{\sigma^2}{P + \frac{(\tau - L - P)\sigma^2}{4p - 4p^2 + \sigma^2}} \quad (38)$$

where p is bit error probability for bits $\check{\mathbf{c}}$ forming the extension of the training sequence \mathbf{m} .

As an illustration the bounds (A.1),(A.5) are visualized at figure 4.6 for parameters $P=20$ and $N_d=58$ accepted in GSM.

As can be seen from (38), in case of minimum variance unbiased channel estimator the variance of the "extended" estimate is always lower than one calculated only from the training sequence, i.e. $\text{var}(\hat{\underline{h}}_i^{extend}) \leq \text{var}(\hat{h}_i^{extend}) < \text{var}(\hat{h}_i)$ for $p > 0$. It can be explained by an observation that by extending training sequence even with unreliable symbols, in average we make covariance matrix (37) more diagonal dominant, and that finally improves the channel estimate. Another point to mention is that the gain from the "extended" training sequence is mainly visible at low signal/noise ratios (SNR) and practically disappears at high SNR where the initial estimate is already rather accurate.

As it follows from (36)-(37), the channel re-estimation includes the inverse of matrix built for every transmitted block. To avoid heavy computation of the matrix inverse a suboptimal methods based on Toeplitz presentation is proposed in [99]. However, this method seems still rather complex, and in this chapter we suggest an adaptive algorithm to update the estimate. In particular, we applied stochastic adaptation of the estimate [85] based on the LMS algorithm [67]

$$\hat{\mathbf{h}}^{(k+1)} = \hat{\mathbf{h}}^{(k)} - \alpha(\hat{\mathbf{Z}}^{(k)})^H(\hat{\mathbf{Z}}^{(k)}\hat{\mathbf{h}}^{(k)} - \mathbf{y}) \quad (39)$$

where $\hat{\mathbf{h}}^{(k)}$ is a vector of channel coefficients estimated at k^{th} iteration, $\hat{\mathbf{Z}}^{(k)}$ is an estimated data matrix containing all (data+training) symbols known at k^{th} iteration, \mathbf{y} is the received vector and α is a step size of the iterative algorithm. At the initial round the channel estimate could be based on some conventional method, e.g., one-shot ML estimate (8) which exploits only the known training sequence.

4.4.4 Combined iterative estimation-equalization

Iteratively updating channel estimate and decoded symbols (turbo-estimation) on one hand, and detected and decoded symbols (turbo-equalization) on the other hand, we actually attempt to find a solution to the general problem (3). The block diagram of the suggested iterative receiver is presented at figure 4.7. The proposed algorithm may be described as follows [85]:

Initialization (conventional receiver):

1. Make an initial channel estimate based on the known training sequence. The initial channel estimate could be based on some conventional method, e.g. one-shot estimate,

$$\hat{\mathbf{h}}_a^{(0)} = (\mathbf{M}^H \mathbf{M})^{-1} \mathbf{M}^H \mathbf{y}_m$$

2. Calculate the prefilter coefficients and the resulting minimum phase channel $\hat{\mathbf{h}}^{(0)}$, based on channel estimate $\hat{\mathbf{h}}_a^{(0)}$.

3. Given a channel estimate $\hat{\mathbf{h}}^{(0)}$, detect a sequence $\hat{\mathbf{c}}^{(0)}$

$$\hat{\mathbf{c}}^{(0)} = \arg \max_{\mathbf{c}} \Pr(y_1^{N\tau} | \hat{\mathbf{h}}^{(0)}, \mathbf{c})$$

Reliability for detected bits may be calculated according to (22) or (23).

4. Decode detected symbols

$$\hat{\mathbf{u}}^{(0)} = \arg \min_{\mathbf{u}} \|\hat{\mathbf{c}}^{(0)} - \Xi \mathbf{u}\|^2 = \Omega(\hat{\mathbf{c}}^{(0)})$$

In case of turbo-equalization a SISO decoder should be used.

Iterations (iterative receiver)

5. Based on decoded symbols make re-encoding operation, $\check{\mathbf{c}}^{(k)} = \Xi \hat{\mathbf{u}}^{(k)} = \Xi \Omega(\hat{\mathbf{c}}^{(k)})$ for the k^{th} iteration.

6. Rebuild the matrix $\hat{\mathbf{Z}}^{(k)}$ based on the updated $\check{\mathbf{c}}^{(k)}$ ($\hat{\mathbf{c}}^{(k)}$ for uncoded data).

7. Update channel estimate using some adaptation rule, e.g. the LMS:

$$\hat{\mathbf{h}}_a^{(k+1)} = \hat{\mathbf{h}}_a^{(k)} - \mu (\hat{\mathbf{Z}}^{(k)})^H (\hat{\mathbf{Z}}^{(k)} \hat{\mathbf{h}}_a^{(k)} - \mathbf{y})$$

8. Recalculate the prefilter coefficients and the resulting minimum phase channel $\hat{\mathbf{h}}^{(k+1)}$, based on channel estimate $\hat{\mathbf{h}}_a^{(k+1)}$.

9. Given channel estimate $\hat{\mathbf{h}}^{(k+1)}$, update detected sequence $\hat{\mathbf{c}}^{(k+1)}$ and its bit-wise likelihoods $\lambda_{eq}(a_{n,j})$ (e.g., according to (22),(23)). In case of turbo-equalization the extrinsic information from the decoder $\lambda_d^{ext}(\check{\mathbf{c}}_n)$ is to be interleaved, $\lambda^a(\mathbf{a}_n) = \Pi \lambda_d^{ext}(\check{\mathbf{c}}_n)$, and then to be used as *a priori* information at the detection stage (27).

10. Update decoded symbols $\hat{\mathbf{u}}^{(k+1)} = \Omega(\hat{\mathbf{c}}^{(k+1)})$. In case of turbo-equalization a SISO decoder is to provide the soft outputs $\lambda_d(\check{\mathbf{c}}_n)$.

11. Iterate between steps 5-10 (ICE) or/and between steps 9-10 (turbo-equalization) as needed.

The France Telecom receiver including turbo estimation and turbo detection is depicted figure 4.7.

4.4.5 Turbo equalization for retransmission schemes

Efficiency of iterative data processing in schemes presented above clearly depends on the used channel coding scheme (CS). In modulation-coding schemes (MCS) where the coding rate is one (e.g., the coding rates for CS4/GPRS and MCS9/EGPRS [42]) a gain from turbo-equalization is not expected (in reality, the presence of a coded packet header brings some gain). To meet quality of service (QoS) requirements the (E)GPRS relies on retransmissions. This mechanism can be favorably exploited by an iterative receiver even in the case of

uncoded transmission. A simple way to couple the turbo-equalization/turbo-estimation with retransmissions is presented below.

Let $\mathbf{c}^{(k)}$ denotes the k^{th} re-transmitted coded block. Retransmitted blocks may be repeated (e.g., GPRS) or differ in applied puncturing patterns (e.g., EGPRS). Let λ_{eq}^{ext,k,n_k} be a sequence of extrinsic probability ratios (LEPR) on a coded block $\mathbf{c}^{(k)}$ at the output of the equalizer, n_k is a number of turbo-equalization/estimation iterations performed for the k^{th} retransmitted block. If puncturing is applied then zeros are inserted instead of punctured bits. The proposed algorithm is the following:

```

k=0
while QoS not satisfied
  k=k+1
  Request (re-)transmission
  for  $i = 1..n_k$ 
    Perform channel (re-)estimation
    Perform SISO detection
    Update LEPR for decoder (bitwise sum)
     $\lambda_{det}^{ext,k,i} \leftarrow \lambda_{det}^{ext,k,i} + \lambda_{det}^{ext,k-1,n_{k-1}}$ 
    Perform SISO decoding
  end for
  Store  $\lambda_{det}^{ext,k,n_k}$ 
  Test QoS
end while

```

4.5 Simulation Results

4.5.1 Turbo detection without channel re-estimation

Figures 4.8 and 4.9 show simulation results for a time-varying and frequency-selective GSM Typical Urban (TU) channel at low speed (the channel is assumed to be stationary over the duration of each radio burst defined as in [42]) and ideal frequency hopping (the channel is independent from burst to burst). The equalizer is fed with perfect channel estimate. The structure of the communication chain is given figure 4.1 and the turbo-detector is based on figure 4.4 (channel re-estimation is not included in the iterative loop). The channel coding is based on a RSC code of rate $\frac{1}{2}$ and generator polynomials $\left(1, \frac{1+D^2}{1+D+D^2}\right)$. We use 6-taps LS estimator (8) (the LMS adaptation rule (39) gives the same results), the DF-SISO equalizer ($v_r=2$) with the forward-backward recursion (23) and max-log-MAP decoder to provide soft

decision outputs. Figure 4.8 is for 8-PSK with interleaving depth of 2784 bits and 64-state SISO-DDFSE ($\nu_r = 2$), the transmitter filter being the linearized GMSK pulse shape and the receiver filter a root raise cosine filter with roll-off 0.5. Figure 4.9 is for GMSK with interleaving depth of 928 bits and 32-state MLSE ($\nu_r = 5$), the receiver filter being a 6-pole butterworth with $BT = 0.6$. In chapter 1, we already pointed out that the uncoded MFB was reached for GSM systems in Urban environment, to finally conclude that the distribution of the minimum distance associated to each channel outcome, has a large peak at the Gaussian distance (no ISI). Turbo detection is of interest to fight the ISI degradation thanks to the interleaving scheme and the decoder, but is powerless against the channel fadings. Hence, it is no surprise that figure 4.9 exhibits very poor gains at each iteration.

4.5.2 Turbo detection and LS-based channel re-estimation

Same assumptions as before, except that real channel estimates, obtained (at first iteration) from the 26-symbol CAZAC training sequence of the GSM burst[42], are fed to the equalizer. Subsequently, LS-based channel re-estimation is included into the iterative loop.

The full turbo-detector is based on figure 4.7. Figure 4.10 is for 8-PSK and figure 4.11 is for GMSK. The relative gain due to Turbo-detection and Turbo-estimation are compared in [86]. It is shown moreover that, for the Modulation scheme MCS5 of EGPRS and a high number of iterations, channel re-estimation accelerates the convergence of turbo detection more than it improves its gain .

Our approach, on the contrary, was to consider that channel re-estimation added into the turbo detection loop did not bring much complexity to the receiver.

To validate our approach another channel re-estimation method based on the Expectation Maximization (EM) algorithm described in [21] should have been compared to the scheme presented here. This is for further study.

However, we are convinced that the proposed architecture is a good trade-off between complexity and performance for TDMA packet-switched transmission (we shared that view with another team).

4.5.3 application of the Turbo equalization to GSM EDGE Radio Access Network

From the simulations shown above, iterative Equalization and estimation for Advanced TDMA Systems, seems to be of great interest. However, gains remains to be assessed for existing standard. We proposed here after to evaluate the potential gain of a full turbo receiver as described in 4.7 both for GPRS and all the more for the 8-PSK coding scheme of EDGE standard.

As a practical testbed we consider performance of iterative receivers for (E)GPRS in typical mobile radio channels. In particular, we present results for schemes with the strongest channel coding CS1/GPRS and MCS5/EGPRS that employ a 1/2-rate and a 1/3-rate convolutional codes [42], respectively. Rectangular interleaving over 4 bursts is used in all cases. We use 6-taps LS estimator (8) (the LMS adaptation rule (39) gives the same results) , the DF-SISO equalizer ($v_r=2$) with the forward-backward recursion (23) and max-log-MAP decoder to provide soft decision outputs. Quality of service in packet data transmission is characterized by block error rate (BLER).

As expected, turbo detection on top of channel re-estimation brings few gain for GPRS, this is due to the GSM modulation as previously discussed, see figure 4.12 .

However, for the Modulation and Coding Scheme based on 8-PSK of the EGPRS standard, the gain of turbo detection worth the added complexity of SISO decoder. Figures 4.13-4.17 shows the potential gain of adopting such a receiver for that standard. As expected, the gain decreases as the coding rate increases. Table 4.1 is a recapitulating table of the gain obtained at a BLER of 10% for MCS59.

Coding scheme	MCS5	MCS6	MCS7	MCS8	MCS9
Code rate	0.37	0.49	0.76	0.92	1.0
TE gain 2iter (4iter)	2.2 (3.2)	2.1 (3.1)	1.9 (2.4)	0.9 (1.7)	0.7 (1.4)

Table 4.1: EGPRS: Turbo-equalization (TE) gain in [dB] for MCS5-9 at BLER= 10^{-1}

The EGPRS standard defines a sophisticated re-transmission scheme known as Incremental Redundancy (IR) [42]. According to the IR scheme each MCS has three disjoint puncturing patterns which are taken cyclically for retransmissions. Simulation results for MCS9/EGPRS are shown at 4.18 for first, second and third re-transmissions with number of iterations: $(n_1 = 1, n_2 = 0, n_3 = 0)$, $(n_1 = 1, n_2 = 1, n_3 = 0)$, $(n_1 = 1, n_2 = 1, n_3 = 1)$, $(n_1 = 1, n_2 = 2, n_3 = 1)$ and finally $(n_1 = 1, n_2 = 2, n_3 = 2)$. As one can see the proposed scheme provides 1.8dB gain at BLER 10^{-2} if we compare retransmissions without $(n_1 = 1, n_2 = 1, n_3 = 1)$ and with $(n_1 = 1, n_2 = 2, n_3 = 2)$ turbo-equalization.

4.6 Conclusions

In this chapter a receiver concept that includes channel estimation, detection and channel decoding into a common iterative process is presented. In order to keep the receiver complexity low (which is especially important for high level modulation) suboptimal DF-SISO equalizers and its modifications suitable for turbo equalization are derived. It is shown that turbo-equalization provides more gain for high level modulation schemes such as 8-PSK.

To further improve the radio-link performance we include decoder into the ICE procedure and suggest a simple method to update channel estimates. We also propose a simple way to embed the iterative detection into retransmission schemes. Evaluation of the combined iterative receiver in the context of GSM EDGE Radio Access Network (GERAN) third generation TDMA system shows that the suggested approach provides a significant performance improvement.

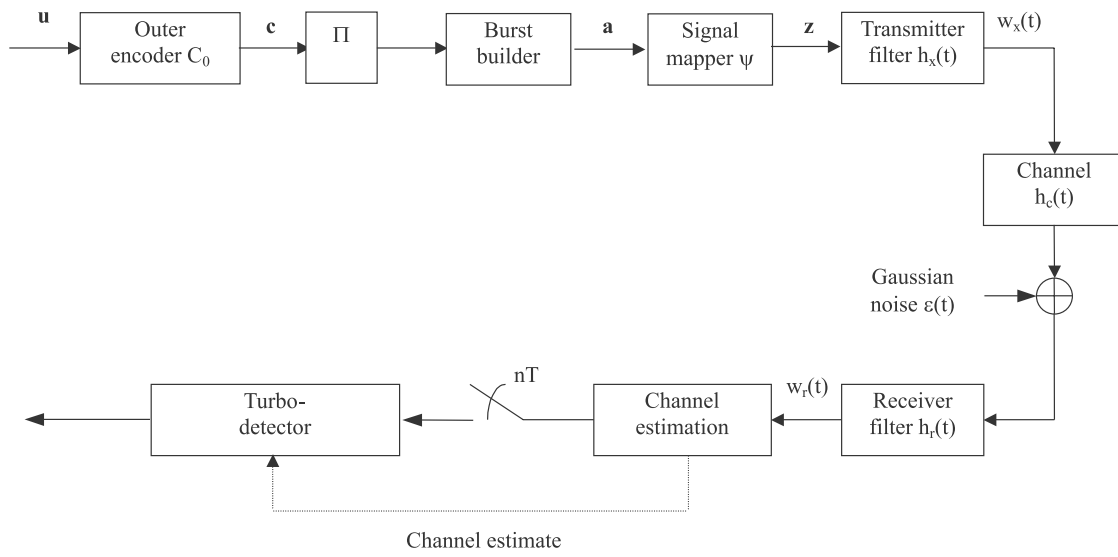


Figure 4.1: Block diagram of communication system

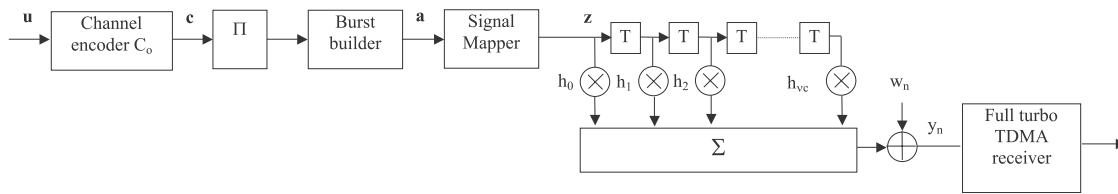


Figure 4.2: Equivalent discrete-time model.

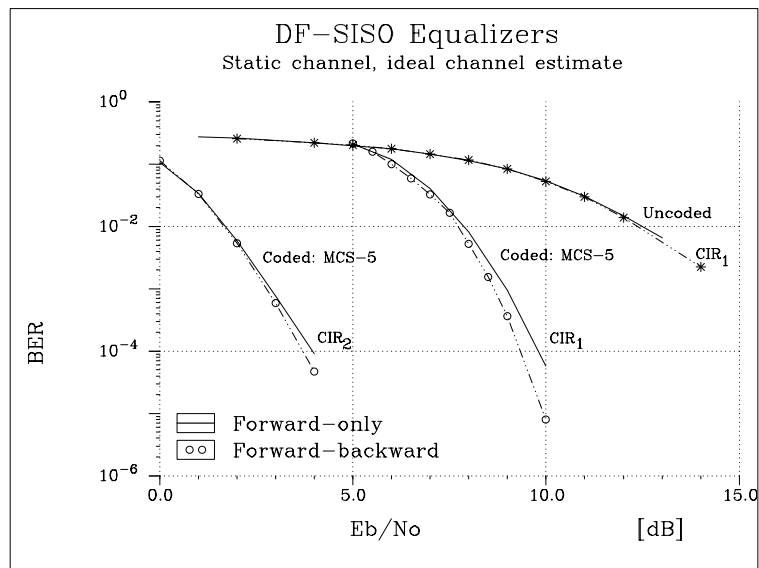


Figure 4.3: DF-SISO performance in static channels with $CIR_1 = \{0.5, 0.71, 0.5\}$, $CIR_2 = \{0.77, 0.55, 0.33\}$.

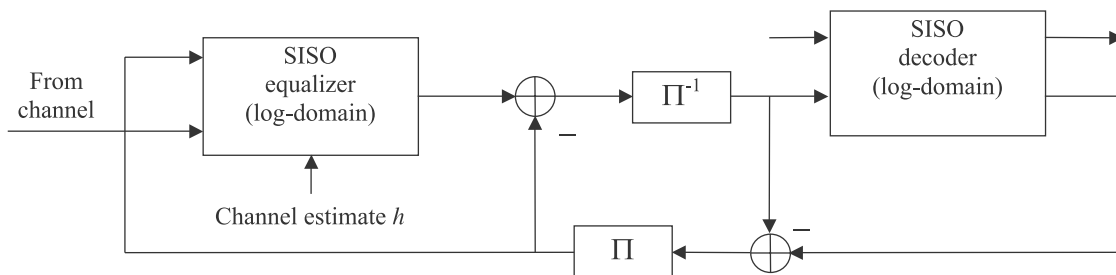


Figure 4.4: Block diagram of iterative receiver

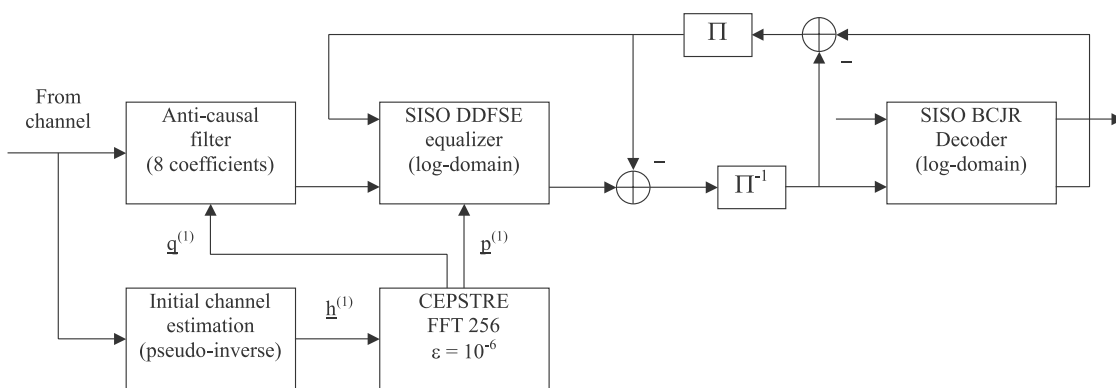


Figure 4.5: Block diagram of iterative receiver

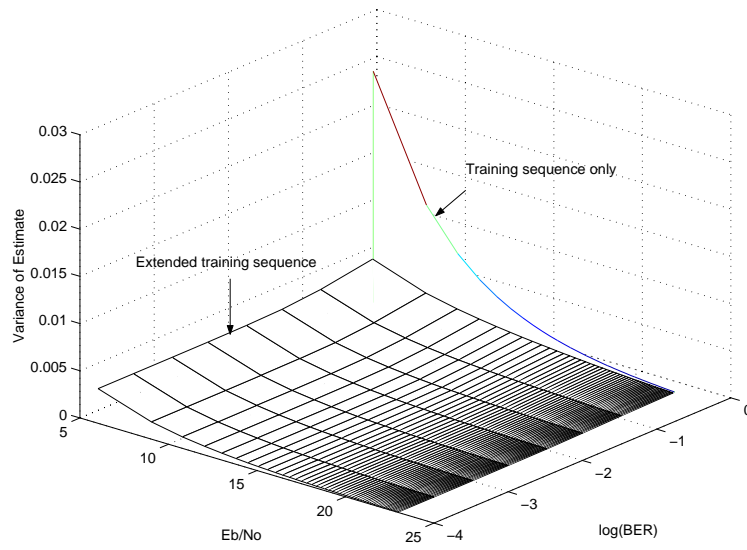


Figure 4.6: Variance of estimate (simulation from nokia)

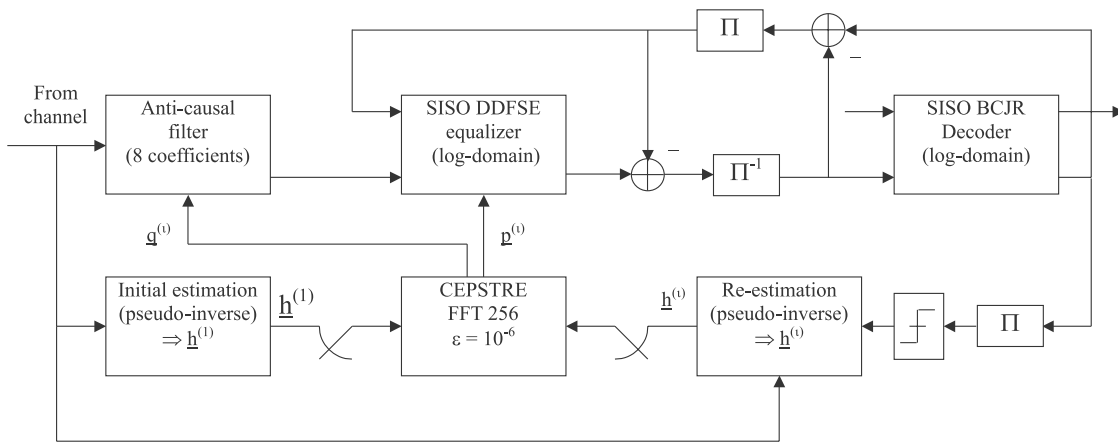


Figure 4.7: Full Turbo receiver (with Bootstrap channel re-estimation).

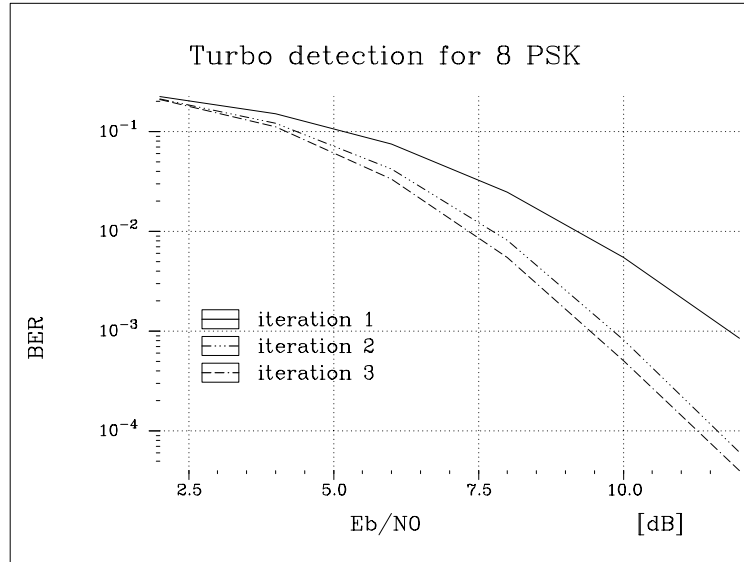


Figure 4.8: Low-complexity turbo-detector (rate 1/2 16-state RSC outer code, 8-PSK, TU channel profile) with SISO-DDFSE ($\nu_r = 2$).

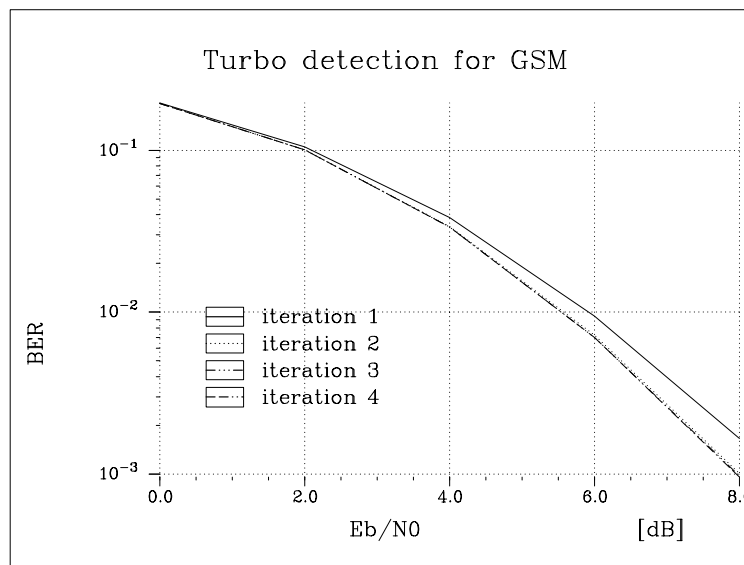


Figure 4.9: turbo-detector (rate 1/2 16-state RSC outer code, GMSK, TU channel profile) with SISO-MLSE.

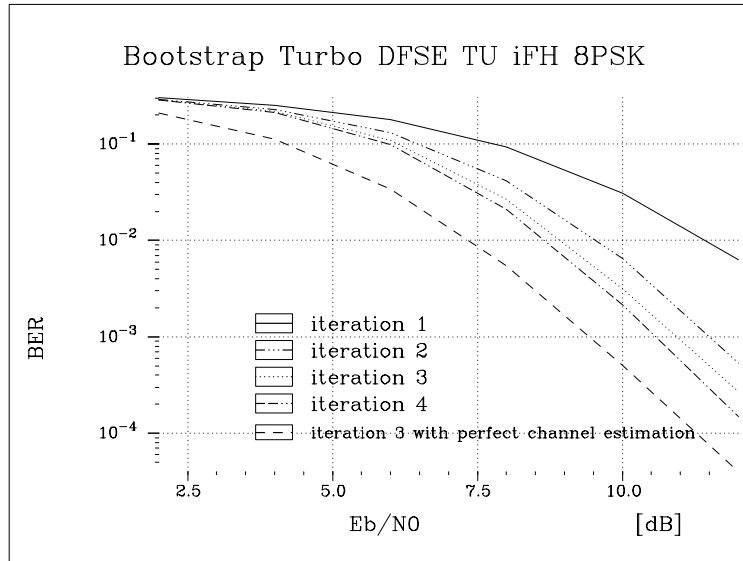


Figure 4.10: Low-complexity full turbo-detector (rate 1/2 16-state RSC outer code, 8-PSK, TU channel profile) with SISO-DDFSE ($\nu_r = 2$) and Bootstrap channel re-estimation.

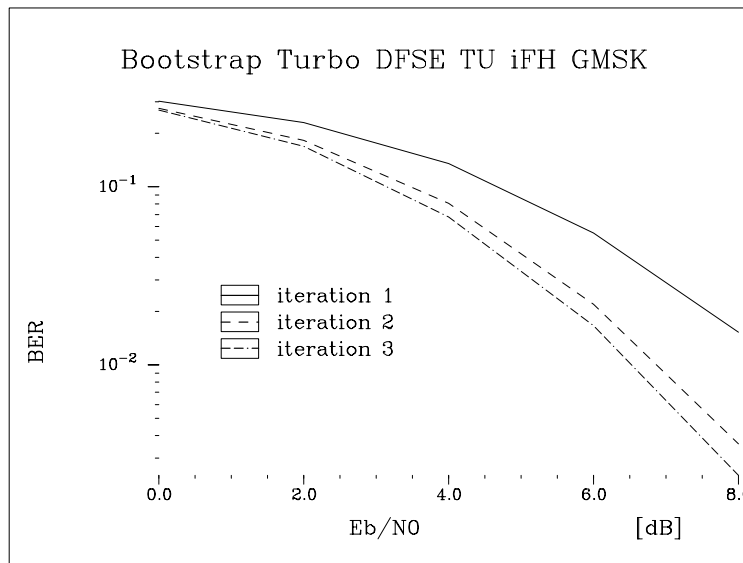


Figure 4.11: Low-complexity full turbo-detector (rate 1/2 16-state RSC outer code, GMSK, TU channel profile) with SISO-DDFSE ($\nu_r = 5$) and Bootstrap channel re-estimation.

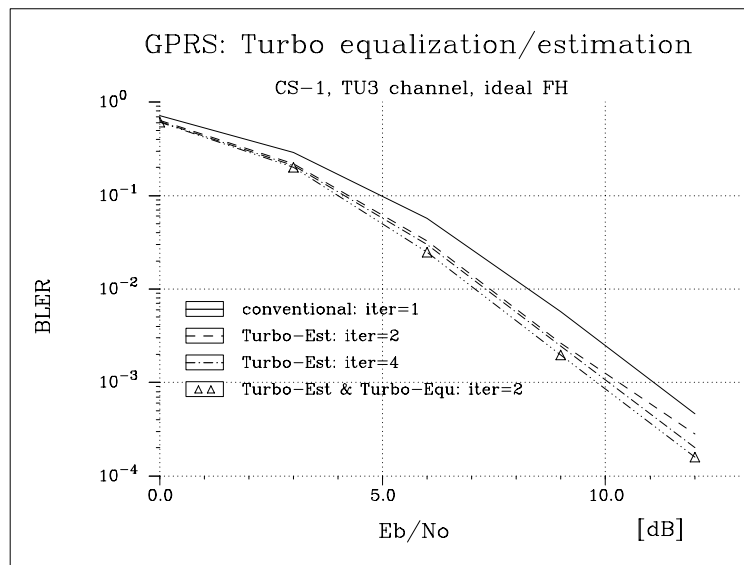


Figure 4.12: Performance of GPRS iterative receiver (simulation from Nokia)

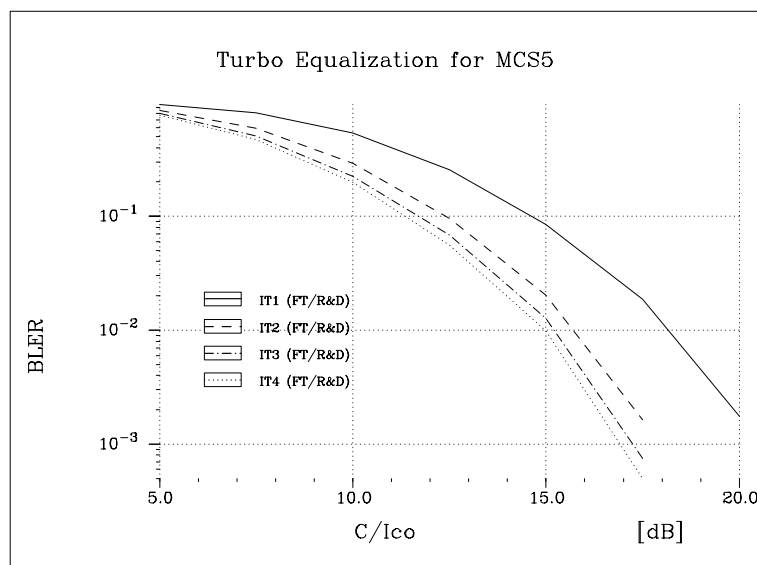


Figure 4.13: EGPRS: Performance of turbo-equalization for MCS-5; TU3 channel, iFH.

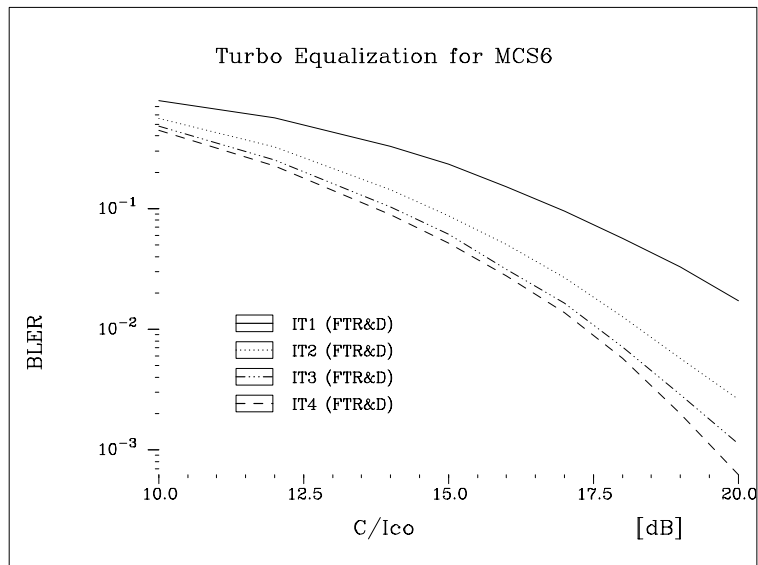


Figure 4.14: EGPRS: Performance of turbo-equalization for MCS-6; TU3 channel, iFH.

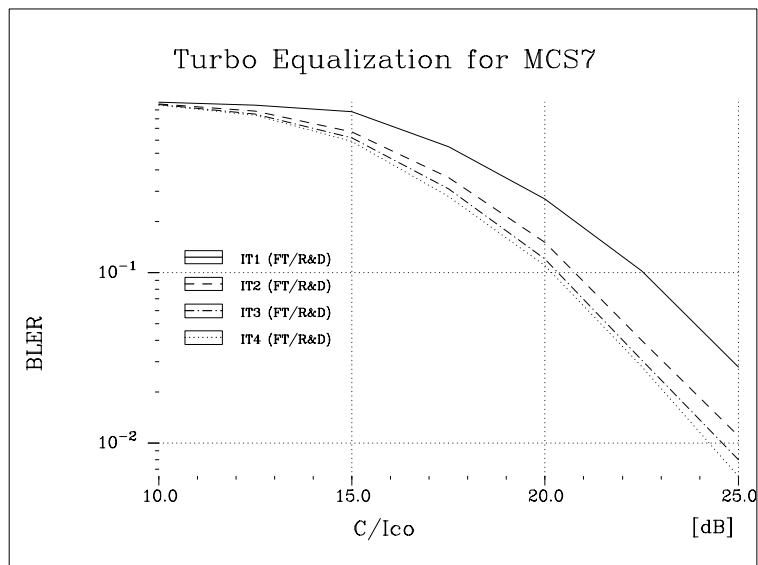


Figure 4.15: EGPRS: Performance of turbo-equalization for MCS-7; TU3 channel, iFH.

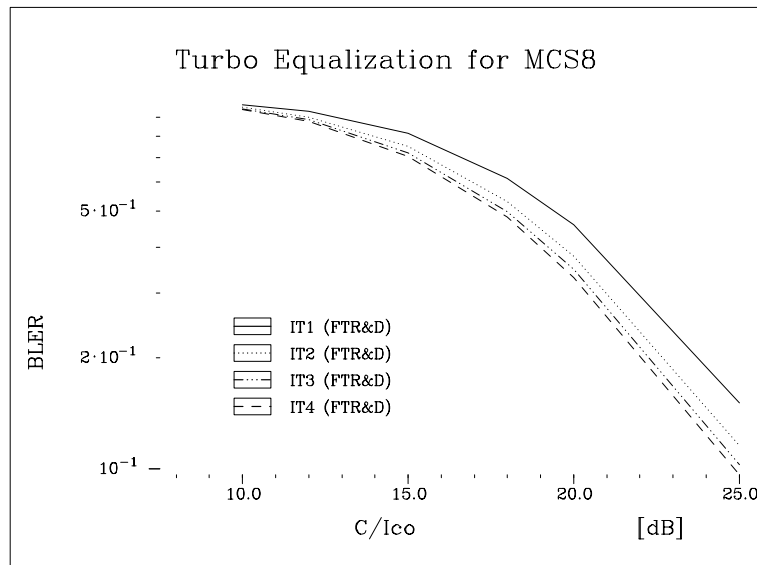


Figure 4.16: EGPRS: Performance of turbo-equalization for MCS-8; iFH.

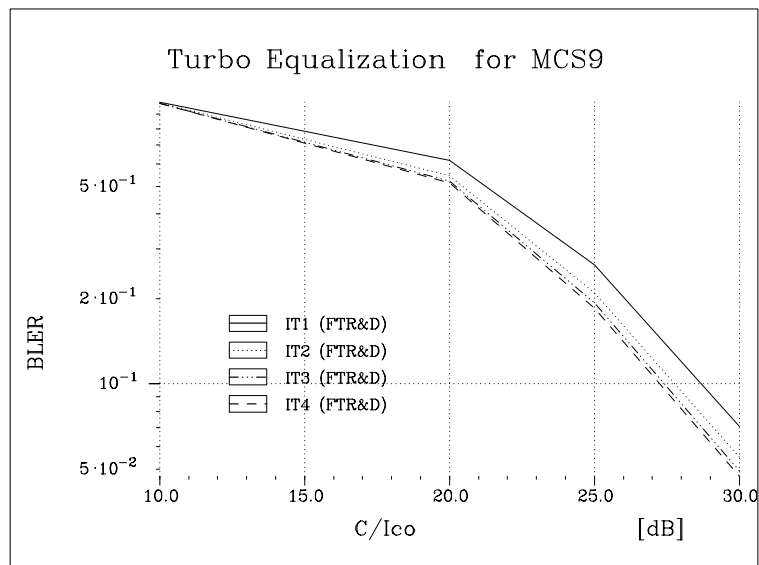


Figure 4.17: EGPRS: Performance of turbo-equalization for MCS-9; iFH.

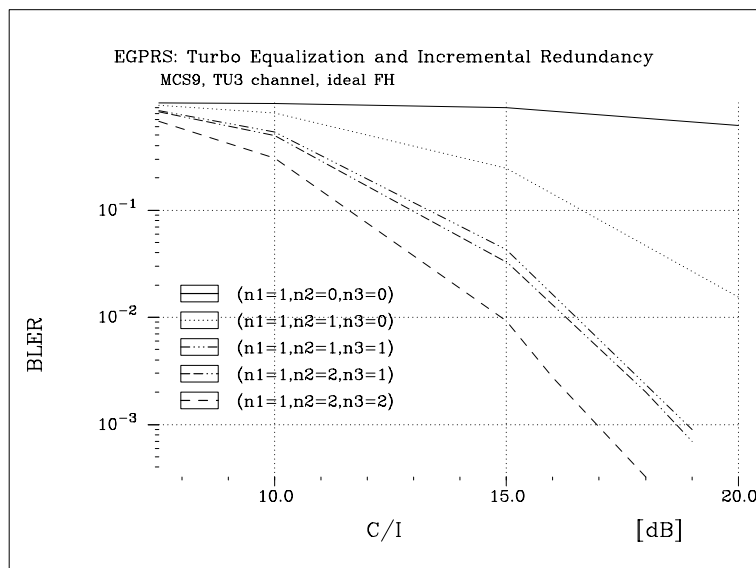


Figure 4.18: Performance of turbo-equalization combined with incremental redundancy.

Chapter 5

Iterative Low-Complexity Receiver for High Bit Rate CDMA

5.1 Introduction

In the UMTS specifications [58], the transmitted data rate is increased by using small spreading factors. For such services, the spreading sequences have bad autocorrelation properties causing the appearance of InterSymbol Interference (ISI). The study of the Rake receiver performance degradation due to ISI was developed in [28]. This study showed that some equalization techniques must be used when the spreading factor is smaller than 16.

ISI reduction was studied only for the downlink since the uplink suffers more from the MultiUser Interference (MUI) due to the Near-Far problem and also because high data rate services are expected to be asymmetric towards the downlink. Most of the conventional equalization techniques, used in TDMA systems, were adapted to the UMTS downlink. Two interesting solutions were previously proposed. The use of a Linear Minimum Mean Square Error (LMMSE) chip equalizer was introduced [56] [62] in order to reduce both the ISI and the MUI. Note that in the downlink, the MUI is due to the multipath channels since the spreading sequences between different users are orthogonal (spatially white). This solution showed a very interesting MUI reduction compared to the Rake receiver. However, this approach does not reduce much of the ISI because of the linear characteristic of the equalizer. It is well known that a close to optimal approach (optimal for sequence detection) for ISI reduction is the Maximum likelihood Sequence Estimation (MLSE). The use of this kind of equalizer following the classical rake receiver was recently proposed in [109], the whole receiver structure was called Rake-MLSE receiver. The performance obtained in the case of perfect channel knowledge was very near to the Matched Filter Bound (MFB). However, the complexity of this approach increases exponentially with the channel delay spread, and the constellation size. Furthermore, the performance degradation due to mis-

match channel estimation as well as channel coding was not taken into account. The use of higher constellation cardinality than the actual one (MDP4) is subject to recent study in the UMTS working groups [57]. A new mode called High Speed Downlink Packet Access (HSDPA) characterized by the giving up of closed loop power control, link adaptation using variable constellations (QPSK,MAQ16,MAQ64), and low spreading factor is ongoing standardization. The Rake-MLSE would be too complex to implement for that particular mode.

In this chapter, we use a Decision Feedback Sequence Estimator (DFSE) equalizer [7] at the Rake receiver output (Rake-DFSE). This approach consists in reducing the trellis state complexity thanks to the so-called Per Survivor Technique (see Chapter 4). For TDMA systems this approach suffers from error propagation that entails the use of a pre-filter beforehand to turn the equivalent discrete time channel into minimum phase. In the CDMA context, such an approach is impossible as the equivalent channel model at the RAKE output varies from symbol to symbol. Fortunately, we witness that in most cases equivalent channels originating from a Rake receiver output do not involve too much of error propagation in the DFSE. This holds for a spreading factor as low as 4 and a trellis state complexity reduced up to the studied constellation cardinality.

Mobile radio interfaces include channel coding and their performance should be assessed after the decoding. It is also well known that the performance of the decoder are improved if fed with soft value. Therefore, we extend our receiver to deliver *a posteriori* probability (APP) ratios on coded bits to the decoder (Rake Soft-In Soft-Out DFSE) [121]. Moreover, some sub-optimality results from performing equalization and decoding separately. A way to recover from that sub-optimality is to perform equalization and decoding iteratively [121]. An iterative Receiver based on the Rake Soft-In Soft-Out (SISO) DFSE equalizer is also introduced.

We then focus on alleviating the mismatched channel estimation impairment. First, we noticed that conventional channel estimates suffer from ISI so that the performance of the equalizer degrades significantly. Hence, we propose to use the knowledge of the structure of the ISI in order to construct a Minimum Mean Square Error (MMSE) channel estimate. Moreover, when the number of pilot symbols is not sufficient, we also propose to insert in the turbo-detection loop a data aided channel estimation process known also as bootstrap [28]. This iterative process consists in making a first decoding based on channel estimates obtained from the pilot symbols. Then, we use the estimated data, at the output of the channel decoder, to reduce channel estimation noise for the next iteration. It is to be stressed that the re-estimated channel coefficients are used both by the Rake and the DFSE via the equivalent channel model

This chapter is organized as follows. The next section describes the system model. Section

5.3 describes the equivalent channel model at the Rake receiver output. In section 5.4 the structure of the proposed low complexity iterative receiver is described. For conveniences, we called it turbo Rake SISO DFSE. Note that this structure includes the Rake-MLSE receiver. Section 5.5, proposes a new channel estimator as well as a data aided approach for re-estimation. Section 5.6, gives some simulation results. Finally, section 5.7 concludes.

5.2 System model

The transmitted signal is depicted in Fig. 5.1. A data sequence $\mathbf{u}_1^{\tau_0} = (\mathbf{u}_1, \dots, \mathbf{u}_{\tau_0})^\top$ of τ_0 symbols enters an encoder C_o which outputs a coded sequence $\mathbf{c}_1^{\tau_0} = (\mathbf{c}_1, \dots, \mathbf{c}_{\tau_0})^\top$. Each data symbol $\mathbf{u}_n = (u_{n,1}, \dots, u_{n,k_0})^\top$ contains k_0 bits, whereas each coded symbol $\mathbf{c}_n = (c_{n,1}, \dots, c_{n,n_0})^\top$ contains n_0 bits. Coded bits are interleaved by an interleaver Π and punctured to match data rates to a transmitted format (i.e., frames of length τ including pilot symbols for channel estimation) Resulting bits are grouped into $Q = 2^q$ -ary symbols $\mathbf{a}_k = (a_{k,1}, \dots, a_{k,q})^\top$ containing q bits. Each symbol \mathbf{a}_k finally pilots a $Q = 2^q$ -ary modulator that transmit the corresponding modulated symbol $s(k)$.

In the presence of multipath propagation, the received signal at the input of a spread spectrum receiver at time t can be written as

$$r(t) = \sum_{l=1}^L f_l(t) \sum_k s(k) e_k(t - kT_s - \tau_l(t)) + w(t), \quad (5.1)$$

where $e_k(t) = \sum_{q=0}^{N-1} e_{kN+q} g(t - qT_c)$ is the spreading waveform for the $Q - ary$ modulated symbol $s(k)$, e_q is the spreading sequence, N is the spreading factor, T_c and T_s are respectively the chip and symbol periods, $g(t)$ is a square root raised cosine filter with roll-off 0.22, L is the number of paths, $f_l(t)$ and $\tau_l(t)$ are respectively the complex amplitude and the delay of the l -th path and $w(t)$ is a white Gaussian noise with one-sided power spectral density N_0 .

5.3 Equivalent channel Model at the Rake receiver output

The despread signal over the j -th finger and the k -th symbol can be written as

$$z_k(\tau_j) = s_k f_j + \sum_{i \neq j} f_i \sum_{n=kN}^{(k+1)N-1} e_n^* d_{n+\tau_{ji}} + w_k(\tau_j). \quad (5.2)$$

where d_k is the product of the spreading sequence by the transmitted symbols and $\tau_{ji} = (\tau_j - \tau_i)/T_c$.

By using the results of [28], we can easily show that the output of the Rake receiver \hat{o}_k can be written as

$$\hat{o}_k = \sum_{j=1}^L f_j^* z_k(\tau_j) = \sum_{l=-L'}^{L'} g_l(k) s_{k-l} + w_k, \quad (5.3)$$

where

$$w_k = \sum_{j=1}^L f_j^* w_k(\tau_j), \quad (5.4)$$

$g_l(k)$ is the l -th amplitude of the equivalent model of the Rake receiver output, $(2L' + 1)$ is the number of taps in the equivalent model.

If we suppose that path delays are separated by a multiple of the chip period, the parameters of this equivalent model are given by

$$L' = 1 + \max \left\{ \left\lfloor \frac{\tau_{ij}}{N} \right\rfloor \right\}, \quad (5.5)$$

$$g_0(k) = \sum_{j=1}^L |f_j|^2 + \sum_{-1 < \frac{\tau_{ji}}{N} < 1} f_j^* f_i \sum_{n=\varepsilon_{ij}^-(k)}^{\varepsilon_{ij}^+(k)} e_n^* e_{n+\tau_{ji}}, \quad (5.6)$$

$$g_l(k) = \sum_{l-1 < \frac{\tau_{ji}}{N} \leq l} f_j^* f_i \sum_{n=kN}^{kN - \tau_{ji} - 1 - (l-1)N} e_n^* e_{n+\tau_{ji}} \quad (5.7)$$

$$+ \sum_{l < \frac{\tau_{ji}}{N} < l+1} f_j^* f_i \sum_{n=kN - \tau_{ji} - lN}^{(k+1)N - 1} e_n^* e_{n+\tau_{ji}}, \quad \forall 1 \leq l \leq L, \quad (5.8)$$

$$g_{-l}(k) = \sum_{-l \leq \frac{\tau_{ji}}{N} < -(l-1)} f_j^* f_i \sum_{n=(k+1)N - \tau_{ji} + (l-1)N}^{(k+1)N - 1} e_n^* e_{n+\tau_{ji}} \quad (5.9)$$

$$+ \sum_{-l-1 < \frac{\tau_{ji}}{N} < -l} f_j^* f_i \sum_{n=kN}^{(k+1)N - \tau_{ji} + lN} e_n^* e_{n+\tau_{ji}}, \quad \forall 1 \leq l \leq L, \quad (5.10)$$

$$\varepsilon_{ij}^-(k) = \max(kN - \tau_{ji}, kN), \quad (5.11)$$

and

$$\varepsilon_{ij}^+(k) = \min((k+1)N - \tau_{ji}, (k+1)N). \quad (5.12)$$

5.4 Low-complexity iterative Receiver

5.4.1 Turbo Rake SISO DFSE receiver

A delay is introduced after the Rake receiver in order to make the equivalent channel model causal. Let y_k be the delayed samples

$$y_k = z^{-L'} \hat{o}_k = \sum_{l=0}^{2L'} h_l(k) s_{k-l} + w_k \quad (5.13)$$

where $h_l(k) = g_{l-L'}(k - L')$.

The output of the Rake receiver being modeled as a simple convolution of the emitted symbol with an equivalent channel that varies from symbol to symbol, a SISO DFSE equalizer (as described in chapter 4) can be used for ISI removal with the modified metric:

$$\gamma^a(b_n) = \frac{1}{2\sigma^2} \left\| y_n - \hat{h}_0(n) s_n - \sum_{k=1}^{\nu_r} \hat{h}_k(n) s_{n-k} - \sum_{k=\nu_r+1}^{2L'} \hat{h}_k(n) \hat{s}_{n-k} \right\|^2 - \sum_{l=1}^q \ln \Pr(a_{n,l} = b_l^\vee)$$

This gives rise in its iterative extension to the receiver depicted in fig. 5.2. As we already pointed out in chapter 4, Per Survivor Processing (PSP) technique used by the DFSE equalizer can introduce a degradation in performance, due to error propagation. However, as noted in the introduction, it appears that equivalent channels at the Rake output does not induce significant error propagation into the DFSE structure for spreading factor as low as 4. As a result, the choice of $\nu_r = 1$ seems to be sufficient in most cases.

5.5 Channel estimation improvement

5.5.1 MMSE channel estimates

The performance of the conventional channel estimates, which are obtained by correlating and averaging over pilot symbols, degrades at low spreading factors because of the ISI. In this section, we propose to improve channel estimation quality by using the knowledge of the ISI structure. If we suppose that path delays are separated by a multiple of the chip period and that the delay spread is less than the symbol period, the conventional channel estimates are given by

$$\hat{\mathbf{f}} = \left(\hat{f}_1, \dots, \hat{f}_L \right)^T = \mathbf{M}\mathbf{f} + \mathbf{n}, \quad (5.14)$$

where

$$\mathbf{M} = [M_{ji}]_{0 \leq j, i \leq L-1}, \quad (5.15)$$

$$M_{ii} = 1, \quad 0 \leq i \leq L-1, \quad (5.16)$$

$$M_{ji} = \sum_{p=0}^{P-1} \frac{s_p^*}{|s_p|^2} \left[\begin{array}{c} (p+1)N-1-\tau_{ji}+N \lfloor \frac{\tau_{ji}}{N} \rfloor \\ s_{p+\lfloor \frac{\tau_{ji}}{N} \rfloor} \quad \sum_{n=pN}^{(p+1)N-1-\tau_{ji}+N \lfloor \frac{\tau_{ji}}{N} \rfloor} e_n^* e_{n+\tau_{ji}} \end{array} \right] \quad (5.17)$$

$$+ s_{p+\lfloor \frac{\tau_{ji}}{N} \rfloor+1} \sum_{n=(P+1)N-\tau_{ji}+N \lfloor \frac{\tau_{ji}}{N} \rfloor}^{(p+1)N-1} e_n^* e_{n+\tau_{ji}}, \quad \text{if } \tau_j > \tau_i \quad (5.18)$$

$$M_{ji} = \sum_{p=0}^{P-1} \frac{s_p^*}{|s_p|^2} \left[\begin{array}{c} (p+1)N-1 \\ s_{p+\lfloor \frac{\tau_{ji}}{N} \rfloor+1} \quad \sum_{n=pN-\tau_{ji}+N \lfloor \frac{\tau_{ji}}{N} \rfloor}^{(p+1)N-1} e_n^* e_{n+\tau_{ji}} \end{array} \right] \quad (5.19)$$

$$+ s_{p+\lfloor \frac{\tau_{ji}}{N} \rfloor} \sum_{n=pN}^{pN-1-\tau_{ji}+N \lfloor \frac{\tau_{ji}}{N} \rfloor} e_n^* e_{n+\tau_{ji}}, \quad \text{if } \tau_j < \tau_i \quad (5.20)$$

P is the number of pilot symbols, $\mathbf{f} = (f_1, \dots, f_L)^T$ being the perfect channel coefficients (without noise), \mathbf{n} is the channel estimation noise which is assumed to have a variance equal to N_0/E_{pilot} and E_{pilot} is the energy of the pilot symbols. MMSE channel estimates are given by

$$\hat{\mathbf{f}}^{MMSE} = \mathbf{L}^H \hat{\mathbf{f}}, \quad (5.21)$$

where

$$\mathbf{L} = \underset{\mathbf{L}}{\operatorname{argmin}} \left\| \hat{\mathbf{f}}^{MMSE} - \mathbf{f} \right\|. \quad (5.22)$$

By using (5.14), we deduce

$$\hat{\mathbf{f}}^{MMSE} = \mathbf{M}^H \left(\mathbf{M}\mathbf{M}^H + \frac{N_0}{E_{pilot}} \mathbf{I}_L \right)^{-1} \hat{\mathbf{f}}. \quad (5.23)$$

A Least Square estimate can also be used, which is

$$\hat{\mathbf{f}}^{LS} = (\mathbf{M}^H \mathbf{M})^{-1} \mathbf{M}^H \hat{\mathbf{f}}. \quad (5.24)$$

The LS estimate does not take into account the noise power and thus gives slightly worse performance at low signal to noise ratio than the MMSE estimate. However, simulation will show that a classical channel estimate only based on correlation with pilot symbols gives bad performance with low spreading factor. The structure of the ISI must be taken into account thanks to the LS or MMSE estimator presented above.

5.5.2 iterative (turbo) channel estimation

Once an iterative receiver has been built for joint equalization and decoding, it is very tempting to add in the turbo detection loop channel re-estimation. This iterative channel estimation consists in making a first decoding based on channel estimates obtained from the pilot symbols. Then, we use the estimated data, from the channel decoder, to reduce channel estimation noise for the next iteration. The full turbo receiver including channel re-estimation and turbo detection is described in figure 5.3. This very simple approach is inspired by the well-known bootstrap technique. Instead of considering estimated data symbols after the Rake SISO DFSE, however, decisions are taken after re-interleaving of soft-output sequence on \mathbf{c}_1^{70} . Thus, the so-called bootstrap re-estimation benefits from time diversity brought by interleaving and from channel decoding efficiency.

5.6 Simulation results

Simulations were performed for a spreading factor of four and EQ-4 wireless channel which consists of four taps of equal power separated by the chip period. The spreading sequence results from the superposition of a Walsh sequence and a gold sequence as defined in the UMTS standard [58]. Each tap is a circularly complex Gaussian variable, i.e. follows a Rayleigh fading. We suppose that the channel is constant during a burst but varies independently from slot to slot (quasi-static assumption). The outer code is a 16-state Recursive systematic code of rate 1/2 and generator polynomials $(1, \frac{1+D^3+D^4}{1+D+D^4})$ generating a pre-encoded sequence \mathbf{c} of size $15 \times 636 \times 2 = 19080$ bits (including tail). The outer encoded sequence \mathbf{c} is sent to a pseudo-random interleaver Π and divided into 15 slots of length 640 QPSK symbols including four pilot symbols at their start. The state complexity of the DFSE trellis is only of 4 states.

Fig. 5.4 considers an uncoded transmission and perfect channel estimation at the receiver. It shows that the Rake SISO DFSE (with four states) outperforms by far the LMMSE approach [62] and keeps close to the Rake SISO MLSE.

Fig. 5.5 gives simulation results based on the receiver of Fig. 5.2. It shows that the soft output of the Rake-DFSE is as good as the one the Rake SISO MLSE. Indeed, the performance of the Rake SISO DFSE are close to the ones of Rake SIOS MLSE with max-log MAP soft algorithm. Unfortunately, for the simulation parameter chosen, iteratively equalizing and decoding does not bring substantial gain. This quite understandable as at the first iteration the Rake SISO DFSE and Rake-MLSE are very close to the coded Matched filter (MF). Nonetheless, we do think that turbo-detection in other context (higher modulation, more selective wireless channel) would bring substantial gain as witnessed in TDMA for the EDGE standard [121].

Finally, fig. 5.6 shows that for the simulation parameters chosen iterative channel estimation brings substantial gain i.e. more than 1 dB. Moreover, the proposed channel estimate taking into account the ISI structure is of paramount importance for the first iteration performance.

5.7 Conclusion

In this chapter, a low complexity iterative receiver for high bit rate CDMA is derived. Adding a SISO DFSE equalizer at the Rake receiver output for spreading factor as low as 4 is shown to give close to optimal performance with reasonable complexity.

The use of a low spreading factor not only degrades the Rake receiver performance but also the conventional channel estimator one. This is understandable as both the Rake receiver and the conventional channel estimator rely heavily on spreading sequence correlation properties. Hence a new channel estimator is also proposed that takes into account the residual ISI structure .

Finally, the so-called "turbo principle" was transposed to that context using the algorithms and approaches of chapter 4 with mitigated success. For the chosen Monte Carlo simulation parameters (QPSK modulation, spreading factor of four and EQ-4 channel) only the turbo channel estimation brings substantial gains, on the other hand performing iteratively equalization and decoding was proved to be useless. This is not surprising since the system performance (for that given set of parameters) with perfect channel estimation is very close to the coded Matched Filter Bound at first iteration.

Nevertheless, the overall receiver structure is foreseen as very attractive for the High Speed Downlink Packet Access (HSDPA) mode of UMTS release 5.

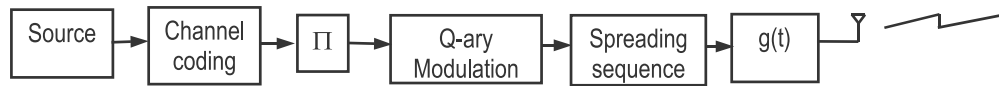


Figure 5.1: transmitted signal.

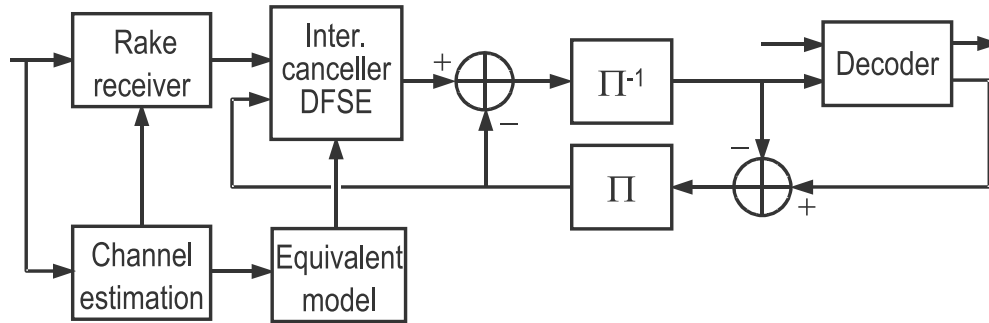


Figure 5.2: Turbo-Detection using a SISO Rake-DFSE for low spreading factor CDMA.

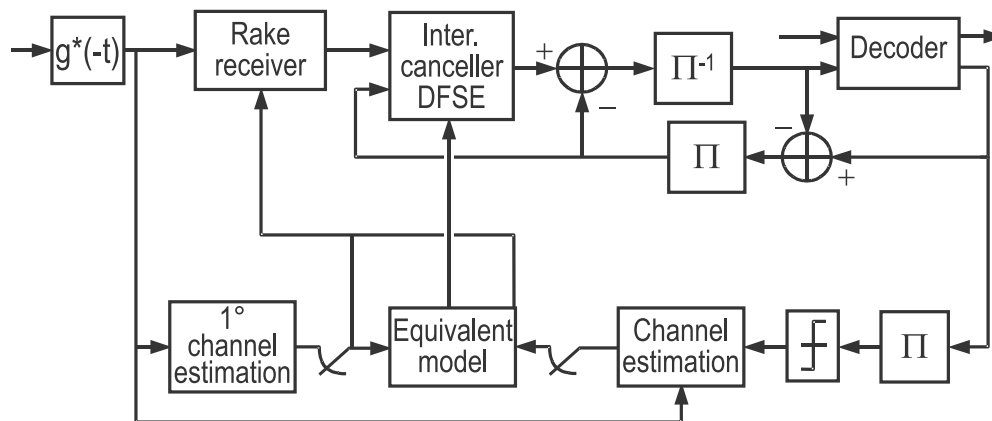


Figure 5.3: full turbo receiver for low spreading factor CDMA.

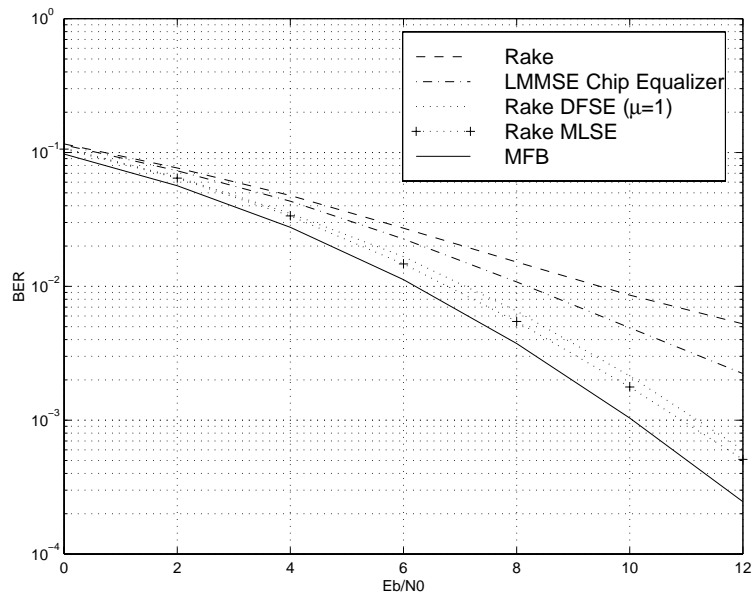


Figure 5.4: Performance at the equalizer output.

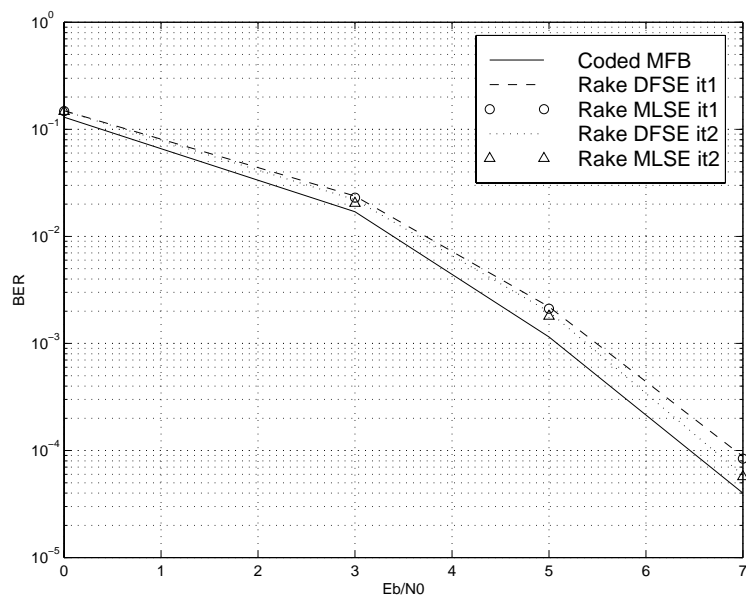


Figure 5.5: Channel decoder output : perfect channel estimation.

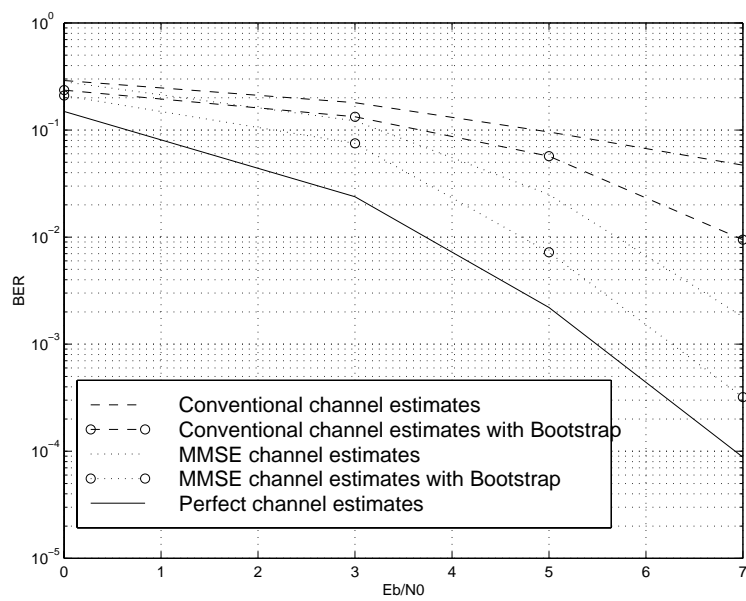


Figure 5.6: Improvement of Channel estimation.

Chapter 6

Iterative Receivers for Bit-Interleaved Coded Modulation over Wireless Frequency-Selective Channels

6.1 Introduction and motivations

Based on Ungerboeck's paradigm of jointly adapting coding with bitwise set partitioning requirements, Trellis Coded Modulation (TCM) was considered for a long time as the most efficient way of combining modulation and channel coding operations. Thanks to an exhaustive maximization of the minimum Euclidean distance between produced coded signals, Ungerboeck succeeded in exhibiting powerful TCM for the Gaussian channel [116]. Later, because of a growing interest in mobile-radio applications, TCM was naturally transposed on flat Rayleigh fading channels, and a symbol-based interleaving of depth greater than the channel coherence time was introduced to exploit the intrinsic time-diversity of the fading process [26] [65]. The code diversity order was proved to be the smallest number of different *channel symbols* between any two possible coded sequences.

Ten years after Ungerboeck's TCM breakthrough, Zehavi demonstrated that the code diversity order over a flat Rayleigh fading channel could be improved up to the Hamming distance by replacing the conventional symbol interleaving at the encoder output with an interleaver operating on the *bit level*, and by using an appropriate bitwise soft-decision metric as an input to the Maximum A Posteriori (MAP) decoder [130]. Recognizing Zehavi's idea, referred to as Bit-Interleaved Coded Modulation (BICM), comes down to admitting that breaking the Ungerboeck's fundamental concept of modulation and coding coupling can lead to much better results for transmissions over time-varying wireless channels. Potential gain of BICM over TCM as well as information-theoretical background have been recently expounded in [31]. It is also interesting to note that BICM, treating coding and modulation

as two serially concatenated entities, lends itself to iterative decoding. The corresponding Soft-in Soft-out (SISO) demodulation and decoding modules can be distinguished and activated sequentially at the receiver side. An iterative exchange of bitwise soft information between them alleviates part of the sub-optimality which would normally result from their separation.

In parallel, promising performance of radio interfaces based on Multiple-Input Multiple-Output (MIMO) wireless channel has motivated a huge amount of both theoretical and practical implementation studies. In particular, it has been proved that the so-called outage capacity of a MIMO channel increases linearly with the number of transmit antennas provided that the number of receive antennas remain greater or equal [113] [47]. On frequency selective channels however, an increasing channel memory leads to a roughly logarithmic growth of the channel capacity [12].

Since, for single-antenna systems, BICM was proved to be very robust to the wireless channel, an attractive idea consists in investigating how it behaves in an equivalent, but MIMO context [27]. Several attempts have already been realized on that topic. In [105], a binary encoder is concatenated with N memoryless modulators with various constellation sizes, through a bit-interleaver. The produced coded modulated streams are sent onto *static block flat Rayleigh fading* channels. It is clearly demonstrated that BICM involving simple time turbo-encoders performs significantly better than best found space-time trellis codes [110] even for short (equivalent) block lengths. Conserving a similar communication model, [74] describes an improved *iterative* strategy for decoding BICM. In addition, the problem of mismatched channel estimation was treated using the Expectation-Maximization (EM) algorithm embedded in the iterative structure (see also reference [30]). The successful results that have been obtained in those aforementioned contributions strongly encourage us to pursue that direction.

Still, the most recent space-time layered coding structures [112], [111], [105], [74], have been essentially designed for a flat fading process, i.e., considering a delay spread small compared to the symbol period. When the delay spread becomes too large on the channel link connecting any two elements of the considered antenna network, a severe degradation in terms of performance is observed, entailing the need for multilayer (coded) data detection. This issue was first treated in [13] for space-time trellis codes, using a MAP multilayer data detector, whose complexity becomes quickly prohibitive for more than two transmit antennas and channel memory greater than 1.

This chapter is organized as follows. In section 6.2, we present a generic model for BICM over wireless frequency selective MIMO channel, that basically extends the system model described in [105], [74] to the presence of InterSymbol Interference (ISI). A reduced-complexity trellis-based receiver performing iteratively channel estimation, multilayer data

detection and channel decoding is derived in both sections 6.3 and 6.4. Section 6.3 details the low-complexity SISO multilayer data detector with perfect channel knowledge. Section 6.4 suggests a simple algorithm for channel estimation and re-estimation purpose. Finally, section 6.5 shows by Monte-Carlo simulations that our approach can dramatically improve the downlink performance of existing Time Division Multiple Access (TDMA) systems using high order modulation, keeping a reasonable complexity at the receiver side.

6.2 Communication model

The transmitted signal is depicted on Fig. 6.1. An outer binary data sequence $\mathbf{d} = \{d_1, \dots, d_{K_o}\}$ is encoded by a channel encoder C_o , made of one single constituent trellis code (punctured or not), or, more generally, of a trellis code combination. The outer coded stream $\mathbf{c} = \{c_1, \dots, c_{N_o}\}$ enters a pseudo-random interleaver Π operating on bit level. The interleaved binary stream is then scattered onto N_T different transmit layers (each layer being connected to one single transmit antenna in this model). Transmit antennas are separated by more than a wavelength for channel decorrelation purpose.

On layer $t \in [1, N_T]$, each frame is itself split into \mathfrak{B} bursts $\{\mathbf{a}_1^t, \dots, \mathbf{a}_\tau^t\}$ of τ bit-labeled symbols $\mathbf{a}_n^t = \{a_{n,1}^t, \dots, a_{n,q_t}^t\}$ (including tail, training sequence, and guard time). Note that the training sequence is preferably placed in the middle of the burst to guarantee a channel estimation more robust to time variation. Each burst enters a Q_t -ary modulator ($Q_t = 2^{q_t}$) which associates, to any input symbol \mathbf{a}_n^t a complex valued symbol $z_n^t = \Psi_t(\mathbf{a}_n^t)$. Although the mapping function Ψ_t could be of any type, the Gray mapping provides good performance. In practice, the same signal mapping rule is used for each layer. However, this degree of freedom could be used favorably for introducing Unequal Error Protection (UEP) between data streams.

Due to multipath propagation and mobility, a time-varying frequency selective wireless channel links the transmit antenna of any layer $t \in [1, N_T]$ to any receive antenna $r \in [1, N_R]$. For Monte Carlo simulations, these radio channels are modeled as multipath Rayleigh fading channels with classical Doppler profile as defined in [36]. The independence between the radio channels seen by any receive antenna is ensured by a sufficient separation of the transmit antennas. This is of tremendous importance for joint multilayer coded data detection. On the other hand, the independence between the channels seen by different receive antennas is preferable of course, in order to maximize the overall diversity order [120], but not necessary. After synchronization and channel estimation the convolution of the transmit and receive filter, together with the radio channel linking transmit antenna t with receive antenna r gives rise to an equivalent base-band discrete-time channel impulse response $\mathbf{h}^{t,r} = [h_0^{t,r}, \dots, h_\nu^{t,r}]^T$ where ν denotes the channel memory and $[\cdot]^T$ the transpose operator. All channels $\mathbf{h}^{t,r}$

$\forall t \in [1, N_T]$, $r \in [1, N_R]$ are supposed to have the same memory. As mentioned in [13], this assumption is reasonable because the number of individual multipath components is predominantly dictated by large structures and reflecting objects.

At the input of the receiver, after synchronization and channel estimation, received samples for antenna r are given by:

$$y_n^r = \sum_{t=1}^{N_T} \sum_{i=0}^{\nu} h_i^{t,r} z_{n-i}^t + \zeta_n^r \tag{6.1}$$

where ζ_n^r represents the (considered uncorrelated) zero-mean complex Gaussian noise samples of variance $2\sigma^2$. ζ_n^r is a circularly symmetric complex Gaussian variable (i.e., its real and imaginary parts are uncorrelated and of same power σ^2).

6.3 Iterative multilayer data detection and channel decoding

One of the main idea of the proposed receiver consists in iteratively performing joint multilayer coded data detection and outer channel decoding. Indeed, the iterative structure enables the multilayer detector to exploit both time and space diversities of the radio channels via the *prior* knowledge on bits of coded data symbols that the decoder feeds back.

6.3.1 SISO joint multilayer data detection

For the purpose of iterative decoding, we aim at computing log A Posterior Probability (APP) ratios on each bit of each coded data symbol \mathbf{a}_n^t at any time $n \in [1, \tau]$ and for each layer $t \in [1, N_T]$. This can be optimally accomplished (in sense of Maximum A Posterior (MAP) criterion) by applying the well-known BCJR algorithm [3] on the full multilayer combined ISI trellis made of the cartesian product of all compound ISI trellises. The computation and storage requirements of such an optimum algorithm is roughly linear in the trellis edge complexity of the whole multilayer structure, so that this approach becomes quickly prohibitive in complexity and has to be discarded. One possible way to alleviate the complexity burden consists in restricting all full elementary combined trellises to sub-trellises, by truncating the effective overall channel memory ν to an arbitrary value μ_t in $[0, \nu]$ (which could vary from one layer to another) and recovering the resulting sub-optimality thanks to Per Survivor Processing (PSP) [38], [94]. Since reduction factors on state complexities of elementary combined trellises multiply, the resulting state complexity of the multilayer combined ISI trellis can be considerably lowered by such a truncating process.

6.3.2 A generalized reduced-state SOVA-like algorithm

As well known the reduction of trellis complexity by PSP induces error propagation. We witnessed that Generalized Per Survivor Processing (GPSP), which basically consists in keeping more than one survivor per state, was a very efficient method to fight back that impairment even in the case of non-minimum phase channels (see [61], [119] and references therein). It is all the more important in the MIMO context as a pre-filter turning every single channel into minimum phase does not exist [13]. The GPSP is well adapted to forward-only recursion for soft computation. Hence, we chose to extend the Soft-Output Viterbi Algorithm (SOVA) [60][6] [23] to GPSP. In the following derivation, we employ α , γ letters to mimic BCJR formalism [3], $\bar{\alpha}$, $\bar{\gamma}$ notations referring to logarithmic approximated probability density functions. Let us assume that, at any time section $n \in [1, \tau]$, to each departure sub-state s' are attached:

- an ordered list $\{\bar{\alpha}_{n-1,\omega}(s'), \omega \in [1, \Omega]\}$ of the Ω best forward accumulated sub-state metrics;
- an ordered list $\{\hat{\mathbf{a}}_{i=n-\theta-1}^{n-1, s'} = \{\hat{\mathbf{a}}_{n-\theta-1}^{s'}, \hat{\mathbf{a}}_{n-\theta}^{s'}, \dots, \hat{\mathbf{a}}_{n-1}^{s'}\}, \omega \in [1, \Omega]\}$ of the Ω corresponding survivor paths (of length θ) terminating in s . Note that $\hat{\mathbf{a}}_n^{s'}$ denotes the estimate of $\hat{\mathbf{a}}_n$ associated with the departure sub-state s' and rank ω .
- an ordered list $\{\mathbf{L}_{i=n-\theta-1}^{n-1, s'} = \{\mathbf{L}_{n-\theta-1}^{s'}, \mathbf{L}_{n-\theta}^{s'}, \dots, \mathbf{L}_{n-1}^{s'}\}, \omega \in [1, \Omega]\}$ of the Ω bitwise unsigned soft sequences (of length θ) associated with survivors.

The one-way generalized SOVA-like algorithm performs a forward recursion. It computes at depth n , for each termination sub-state s , and for all transitions b terminating at s , and for all ranks $\omega \in [1, \Omega]$, the new accumulated sub-state metrics:

$$\bar{\alpha}_{n,\omega}(s) = \bar{\alpha}_{n-1,\omega}(s') + \bar{\gamma}_{n,\omega}(b) . \quad (6.2)$$

The transition metric $\bar{\gamma}_{n,\omega}(b)$ is expressed as:

$$\bar{\gamma}_{n,\omega}(b) = \frac{1}{2\sigma^2} \sum_{r=1}^{N_R} \left\| \mathbf{y}_n^r - \sum_{t=1}^{N_T} \left\{ \sum_{i=0}^{\mu} h_i^{t,r} z_{n-i}^t{}^b + \sum_{i=\mu+1}^{\nu} h_i^{t,r} \hat{z}_{n-i}^t{}^b \right\} \right\|^2 - \sum_{(t,j)} \ln \Pr(a_{n,j}^t) \quad (6.3)$$

where $\hat{z}_n^t{}^b$ denotes the estimate of the transmitted symbol z_n^t that has been recovered by GPSP using the path survivor of rank ω which terminates in sub-state s' of branch b at section n . Also, $a_{n,j}^t$ stands for the j^{th} bit of the t^{th} estimated coded data sequence at time n .

Those metrics are then classified by increasing order (the smallest has first rank). This recursion is carried out with respect to the boundary conditions:

$$\bar{\alpha}_{0,1}(0) = 0 \quad \bar{\alpha}_{0,\omega}(0) = \infty \text{ for } \omega > 1, \quad (6.4)$$

$$\bar{\alpha}_{0,\omega}(s) = \infty, \quad \forall s \neq 0, \quad \omega \in [1, \Omega]. \quad (6.5)$$

Only the Ω best ones will be stored at sub-state s for next section step.

Simultaneously, the past survivor paths are extended according to existing transitions. The new potential survivor paths are temporarily stored and sorted in compliance with the rank of their associated metrics, but only the Ω best ones (in metric sense) will be actually used for next section step. Similarly to path survivors, the past bitwise unsigned soft sequences $\mathbf{L}_{i=n-\theta-1}^{n-1} \omega^{s'}$, $\omega \in [1, \Omega]$, are first extended according to existing transitions. The new potential unsigned soft sequences are temporarily stored and sorted in compliance with the rank of the corresponding path metrics. For each layer $t \in [1, N_T]$ and for each input bit $j \in [1, q_t]$, estimated unsigned soft values are initialized in accordance with:

$$L_{n,j}^t \omega^s = \infty. \quad (6.6)$$

Again, only the Ω best unsigned soft sequences need to be stored for next section step. Now comes the soft-deciding updating part of the algorithm.

For each sub-state s , for each layer $t \in [1, N_T]$, for each input bit $j \in [1, q_t]$, and for each rank $\omega \in [1, \Omega]$, bitwise unsigned soft sequences $\mathbf{L}_{i=n-\theta}^n \omega^s$ are updated from depth $i = n - 1$ down to depth $i = n - \delta$ according to:

$$L_{i,j}^t \omega^s = f(L_{i,j}^t \omega^s, \Delta_{n,j}^t \omega^s) \quad (6.7)$$

where $f(\cdot)$ is an updating function, and where:

$$\Delta_{n,j}^m \omega^s = \bar{\alpha}_{n,\tilde{\omega}_{i,j}^t}(s) - \bar{\alpha}_{n,\omega}(s), \quad (6.8)$$

with:

$$\tilde{\omega}_{i,j}^t = \min \{ \varsigma \geq \Omega + 1, \hat{a}_{i,j}^t \omega^s \neq \hat{a}_{i,j}^t \omega^s \}. \quad (6.9)$$

Following [60][6], the updating function $f(\cdot)$ in (6.7) is defined as:

$$f(L_{i,j}^t \omega^s, \Delta_{n,j}^t \omega^s) = \ln \frac{1 + \exp(L_{i,j}^t \omega^s + \Delta_{n,j}^t \omega^s)}{\exp(L_{i,j}^t \omega^s) + \exp(\Delta_{n,j}^t \omega^s)} \quad (6.10)$$

and may be approximated by:

$$f(L_{i,j}^t \omega^s, \Delta_{n,j}^t \omega^s) \approx \min \{ L_{i,j}^t \omega^s, \Delta_{n,j}^t \omega^s \}. \quad (6.11)$$

If $n \geq \theta$, the algorithm delivers bitwise signed soft decisions on $\mathbf{a}_{n-\theta}^t$. Those signed bitwise soft values:

$$\lambda_a(a_{n-\theta,j}^t) = (2 \times \widehat{a}_{n-\theta,j}^t \mathbb{1}_1^{s_{best}} - 1) \times L_{n-\theta,j}^t \mathbb{1}_1^{s_{best}} \quad (6.12)$$

are calculated for $t \in [1, N_T]$, $j \in [1, q_t]$ using the first rank survivor path $\widehat{\mathbf{a}}_{i=n-\theta}^n \mathbb{1}_1^{s_{best}}$ and the corresponding bitwise unsigned soft sequence $\mathbf{L}_{i=n-\theta}^n \mathbb{1}_1^{s_{best}}$, which both terminate, at section n , into the sub-state s_{best} defined as:

$$s_{best} = \arg \min_s \{\overline{\alpha}_{n,1}(s)\} . \quad (6.13)$$

Finally, useful approximated log extrinsic probability ratios on bits $a_{n-\theta,j}^t$ are computed by bitwise subtracting log prior probability ratios $\lambda_p(a_{n-\theta,j}^t)$ coming from the outer channel decoder to produce signed soft values:

$$\lambda_\varepsilon(a_{n-\theta,j}^t) = \lambda(a_{n-\theta,j}^t) - \lambda_p(a_{n-\theta,j}^t) \quad (6.14)$$

as described in Fig. 6.2. For convenience, let us call this algorithm Multilayer Generalized Soft Viterbi Equalizer (MGSVE).

6.4 Iterative channel estimation

Until now, the multilayer turbo-detector has been presented assuming that the channel coefficients were perfectly known. Here, a simple algorithm for practical channel (re)estimation is introduced. It is applied both for the initial (mismatched) channel estimation using training sequences and for subsequent channel re-estimations which take benefit from the log APP on coded bits delivered by the outer channel decoder.

6.4.1 Initial channel estimation

This section presents a simple Least Square (LS) estimator for channel estimation. Classically, the first channel estimation relies on the training sequences embedded in the transmitted data streams. A common approach to training sequence design based on a Minimum Mean Squared Error (MMSE) criterion, is also presented and finally used to derive 3 sequences of 26-symbol length.

Assuming N_T transmit antennas and training sequences consisting of p preamble and m midamble symbols ($p \geq \nu$ and the preamble being the repetition of the p last symbols of the midamble), then the vector of received samples at the r^{th} receive antenna, denoted by \mathbf{y}^r , can be written as:

$$\mathbf{y}^r = \mathbf{S}\mathbf{h}^r + \zeta^r \quad (6.15)$$

where $\mathbf{h}^r = [h_0^{1,r} \dots h_\nu^{1,r} \dots h_0^{N_T,r} \dots h_\nu^{N_T,r}]^T$ is the stacked vector of channel impulse responses assuming channel memory ν , $\zeta_r = [\zeta_p^r \dots \zeta_{m+p-1}^r]^T$ is a noise vector assumed to represent white Gaussian noise and \mathbf{S} is an $m \times N_T(\nu + 1)$ block-toeplitz matrix consisting of the training symbols. The definition of the block-matrix \mathbf{S} can be given in terms of N_T correlation matrices of dimension $m \times (\nu + 1)$:

$$\mathbf{S} = [\mathbf{S}^1 \quad \mathbf{S}^2 \quad \dots \quad \mathbf{S}^{N_T}] \quad (6.16)$$

where $\mathbf{S}^t(i, j) = \mathbf{s}^t(p + (i - j) \bmod m)$, $\forall t \in [1, N_T]$, $\forall i \in [0, m - 1]$, $\forall j \in [0, \nu]$ with mod the modulo operator and \mathbf{s}^t the t^{th} training sequence.

The Least Square (LS) channel estimate is then given by:

$$\hat{\mathbf{h}}^r = \arg \min_{\mathbf{h}^r} \|\mathbf{y}^r - \mathbf{S}\mathbf{h}^r\|^2 = (\mathbf{S}^\dagger \mathbf{S})^{-1} \mathbf{S}^\dagger \mathbf{y}^r \quad (6.17)$$

where \dagger denotes the transpose conjugate operator. Optimal training sequences can be searched for which minimize the MSE:

$$\min \left\{ E \left[\mathbf{h}^r - \hat{\mathbf{h}}_{LS}^r \right] \right\} \quad (6.18)$$

where $E[\cdot]$ denotes the expectation operator. It can be shown that the MMSE criterion (6.18) can be achieved by choosing training sequences that minimize:

$$\frac{m}{N_T(\nu + 1)} \text{tr} \left[(\mathbf{S}^\dagger \mathbf{S})^{-1} \right] \quad (6.19)$$

where the operator $\text{tr}[\cdot]$ denotes the trace of a matrix. In fact, the average degradation in [dB] compare to ideal sequences, perfectly white and spatially uncorrelated, amounts to $10 \log \left\{ \frac{m}{N_T(\nu + 1)} \text{tr} \left[(\mathbf{S}^\dagger \mathbf{S})^{-1} \right] \right\}$. Using (6.19) and restricting ourselves to Binary Shift Keying (BPSK) modulation (0 correspond to BPSK symbol -1.0 and 1 to 1.0), we found by exhaustive search that the following three sequences of length 26 symbols ($p = 6$ preamble and $m = 20$ midamble symbols respectively) were close to optimal in order to estimate 18 channel coefficients. The degradation compared to ideal sequences is only of 0.427 dB in average :

$$\begin{aligned} s_1 &= [01001100000001100101010011], \\ s_2 &= [00000001100101010011000000], \\ s_3 &= [01100101010011000000011001]. \end{aligned}$$

Note that those three sequences are actually derived from a single one [00000001100101010011]. The building of N_T sequences from a single one in order to estimate $N_T(\nu + 1)$ coefficients is well described in [106] and allows to reduce drastically the range of the exhaustive search. All simulations presented hereafter are for the case of $N_T = 3$ and use these three sequences for initial channel estimation.

6.4.2 LS-based turbo channel estimation

This very simple approach is inspired by the well-known bootstrap technique. Instead of considering the estimated symbols after the multilayer coded data detector, however, decisions are taken at the output of the channel decoder. The turbo channel estimation thus benefits from additional time and spatial diversities brought by channel pre-coding and interleaving operations.

We now describe the sequencing:

1. Hard decisions on bits of the codeword \mathbf{c} are derived from the log APP ratios available at the output of the decoder. The estimated codeword $\hat{\mathbf{c}}$ is then re-interleaved and the produced binary stream split into N_T sub-streams corresponding to the N_T transmit layers. From those sub-streams, emitted bursts are reconstituted, so that estimates of all complex-valued emitted symbols are available (tail symbols, guard symbols, and symbols of the three training sequences are known *a priori*).
2. The matrix system is formed:

$$\mathbf{y}^r = \mathbf{A}_\ell \mathbf{h}^r + \zeta^r \quad (6.20)$$

where \mathbf{y}^r is the vector of observed symbols, \mathbf{h}^r is the unknown stacked vector of channel coefficients, and $\mathbf{A}_\ell = [\mathbf{A}_\ell^1 \quad \mathbf{A}_\ell^2 \quad \cdots \quad \mathbf{A}_\ell^{N_T}]$ is a block-Toeplitz matrix whose complex coefficients are made of estimated symbols of $\hat{z}_{\ell,n}^t$ at iteration ℓ . More precisely, assuming that ν guard symbols are inserted at the end of the burst, the $\tau \times (\nu + 1)$ matrices \mathbf{A}_ℓ^t are defined as $\mathbf{A}_\ell^t(i, j) = \hat{z}_{\ell, (i-j) \bmod \tau}^t$, $\forall t \in [1, N_T]$, $\forall i \in [0, \tau[$, $\forall j \in [0, \nu]$.

3. A solution minimizing the error probability (or, equivalently, the Euclidean distance, ζ^r being a circularly complex Gaussian random vector with identity covariance matrix) correspond to the LS estimate already described in section 6.4.1:

$$\hat{\mathbf{h}}_\ell^r = (\mathbf{A}_\ell^\dagger \mathbf{A}_\ell)^{-1} \mathbf{A}_\ell^\dagger \mathbf{y}^r. \quad (6.21)$$

Matrix system (6.21) can be solved by a Choleski decomposition. An adaptive algorithm to update the estimate can be chosen to avoid the Choleski decomposition as described in [86].

A summary diagram is shown on Fig. 6.2 for the turbo-MGSVE receiver incorporating the LS-based turbo channel estimator.

6.5 Performance analysis

Although a generic model has been derived for any number of transmit and receive antennas, Monte-Carlo simulations have been realized for $N_T = 3$ and $N_R = 1$. Of course, adding diversity branches at the receiver improves performance. However, it is difficult for a mobile handset to carry more than one antenna. Noticing the equivalence in terms of data rate between a 2^{N_T} -order modulation and N_T BPSK transmitted in parallel, we aim at demonstrating that our approach can be used to improve the downlink radio performance of existing TDMA systems, notably Enhanced GPRS (EGPRS) [52], without significantly increasing the complexity of the receiver.

6.5.1 Optimal receiver

Figs. 6.3, 6.4 and 6.5 show the Bit Error Rate (BER) performance of an optimal (BCJR-based) receiver in the context of a time-varying EQ-3 MIMO ISI channel. Each basic EQ-3 ISI channel is made of 3 coefficients that are circularly complex Gaussian variables of equal power, separated by the symbol period. All channels are spatially independent, constant during the burst duration, and change independently from burst to burst (quasi-static assumption). The channel code is a 16-state recursive systematic convolutional code of rate 1/2 and generator polynomials (23, 35) generating a pre-encoded sequence \mathbf{c} of size $N_o = 1536$ bits (including tail). The outer encoded sequence \mathbf{c} is sent to a pseudo-random interleaver Π . The interleaved bit stream is scattered onto 3 distinct streams of size 512 bits, corresponding to $N_T = 3$ distinct transmit layers (or transmit antennas). On each layer $t \in [1, 3]$, the binary stream is segmented into $\mathfrak{B} = 4$ bursts, which all include the training sequence s_t defined in 6.4.1. Bursts enter a BPSK modulator before transmission over the time-varying EQ-3 MIMO ISI channel. Fig. 6.3 shows the performance of the described system when perfect channel knowledge is available. On the contrary, Fig. 6.4 illustrates the 2.4 dB of degradation due to a practical channel estimation based on the training sequences derived in section 6.4.1. As depicted on Fig. 6.5, the proposed LS-based turbo channel estimation enables to recover about 1 dB from that loss at third iteration.

6.5.2 Reduced-complexity multilayer data detector

As a second step, we now evaluate the hard-output quality of the reduced-state SOVA-like multilayer data detector. On each layer $t \in [1, 3]$, a burst of 128 bits enters a BPSK modulator before transmission over the time-varying EQ-3 MIMO ISI channel. Fig. 6.6 depicts the BER performance of the MGSVE. Simulations are carried out with parameters $N_T = 3$, $N_R = 1$, $\mu_t = 1$, $\forall t \in [1, N_T]$ (8-state multilayer ISI trellis), $\theta = \delta = 20$, and various Ω . For comparison purpose, the performance of the BCJR algorithm processing on the full

512-state multilayer combined trellis is also plotted. We observe that the MGSVE is less than 0.5 dB away from the optimal receiver with $\Omega = 4$.

6.5.3 Reduced-complexity receiver and its application to GERAN

The GSM EDGE Radio Access Network (GERAN) is ongoing standardization effort, and aims at evolving the GSM and IS-136 system towards 3G in their respective allocated frequency bands. The EGPRS will supply the GERAN radio bearers for Non Real Time services. It defines 9 Modulation and Coding Schemes [52]. The MCS from 5 to 9 are based on a new introduced modulation, namely the 8-Phase Shift Keying (8-PSK). This new modulation precludes an optimal receiver, and thus some low complexity receivers and their turbo extension has been recently suggested [86][121].

Here, we propose to replace the 8-PSK modulation of the EGPRS standard by three BPSK modulations in parallel keeping all the other system parameters unchanged. In order to point out the advantages of such an approach, we introduced below the two different schemes A and B that have roughly the same complexity. Scheme A is exhaustively described in [86][121], the coding and modulation as well as the transmit filter follow closely the fifth Modulation and Coding Scheme (MCS5) detailed in the EGPRS standard. The receive filter is a Root Raised Cosine (RRC) with roll-off 0.5 and bandwidth 180 kHz. The radio channel is Typical Urban at 3 km/h (TU3) [36], ideal frequency hopping is assumed (iFH). The receive filter is matched to the transmit filter. The channel estimation and sample synchronisation (prior symbol synchronization is assumed) is based on LS estimator (using the 26-symbol training sequence placed in each burst) that feeds the turbo-detector 6 channel coefficients. The receiver (excluding first channel estimation and synchronization) is a turbo-DFSE detector with bootstrap channel re-estimation [121]. The equalizer is composed of a pre-filter to turn the channel into minimum phase followed by a 64-state trellis DFSE. The outer coding of scheme B is inherited from MCS5 of the EGPRS standard, but the encoded sequence (derived from a punctured NRNSC code of rate 1/3) instead of being 8-PSK modulated is demultiplexed into three streams. Each stream has its own allocated training sequence chosen from the three proposed in section 6.4.1 and is divided into four GSM bursts. Each burst is then modulated in BPSK, oversampled (an oversampling factor of 8 was chosen) and filtered by a RRC filter with roll-off 0.22. Each modulated stream is then sent from a different antenna, all three antennas are supposed to be separated enough to ensure perfect decorrelation of the radio channels at the receiver. The radio channel model is MIMO TU3 [36] with iFH. The receive filter is matched to the transmit filter. The channel estimation and sample synchronization (prior symbol synchronization is assumed) is based on a LS estimator described in 6.4.1 that feeds to the multilayer data detector 18 channel coefficients (each channel has a constraint length of 6). The receiver (excluding first

channel estimation and synchronization) is a reduced-complexity multilayer turbo-detector with LS-based channel turbo estimation. We use the MGSVE as multilayer data detector with parameters $\mu_t = 1, \forall t \in [1, N_T]$ (8-state multilayer ISI trellis), $\Omega = 2$ (two survivors per state) and $\theta = \delta = 20$.

Fig. 6.7, related to scheme B, confirms that the choice of a 8-state reduced trellis, and $\Omega = 2$ survivors per state for the MGSVE is a good trade off between BER performance versus co-channel interference and computational complexity. Fig. 6.8 compares scheme A to scheme B in terms of BER performance versus co-channel interference. It shows that scheme B outperforms scheme A by more than 4 dB at fourth iteration for BER 10^{-2} . It also shows that the degradation due to mismatched channel estimation (with bootstrap channel re-estimation) is around 2 dB compare to perfect channel estimation for scheme B at third iteration (Scheme B, #3 perf). Figs. 6.9, 6.10 looks into Block Error Rate (BLER) performance. Again, scheme B outperforms scheme A of nearly 5 dB at fourth iteration and BLER 10^{-2} with a complexity that is somehow similar. Those impressive results can be explained by the fact that scheme B uses a much more robust modulation and has a diversity order 3 times higher than scheme A. It is also worth noting that the sophisticated re-transmission scheme retained for EGPRS (i.e, Incremental Redundancy) can favourably benefit from such iterative receivers as described in [86] [121].

6.6 Conclusion

In this chapter, a generic model of BICM over multipath Rayleigh fading MIMO channel was derived. A practical low complexity trellis-based receiver realizing iteratively channel estimation, multilayer coded data detection and channel decoding was introduced. Our approach, which employs an efficient reduced-state trellis-search algorithm to perform multilayer data detection, presents two-fold advantages. It enables to cope with severe MIMO channel ISI and allows to use more transmit antennas than receive antennas. Focusing on the case of N_T transmit antennas and one receive antenna, the equivalence in terms of data rate and receiver complexity between one 2^{N_T} -order modulation and N_T BPSK transmitted in parallel was pointed out. Providing that the N_T channels are independent (i.e., transmit antennas separated by more than the wavelength), the latter scheme seems to be more interesting as it uses more robust modulation and its diversity order is intrinsically N_T times higher. This was assessed for $N_T = 3$ in the context of third generation TDMA system GERAN for existing channel coding.

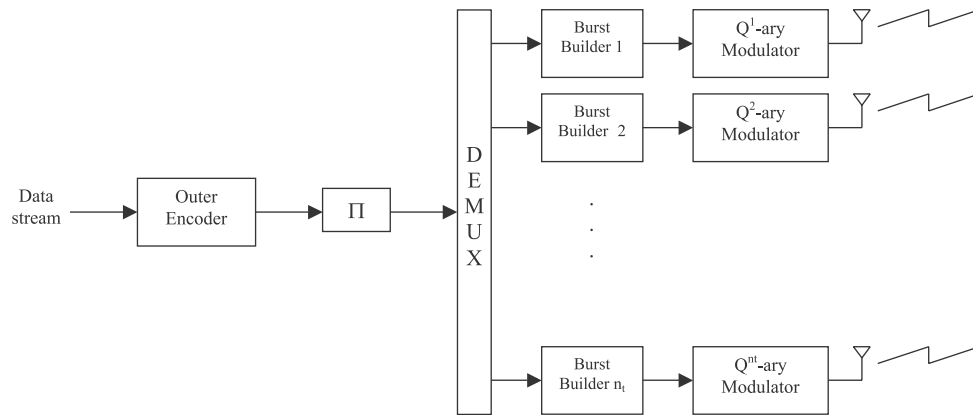


Figure 6.1: Transmitter.

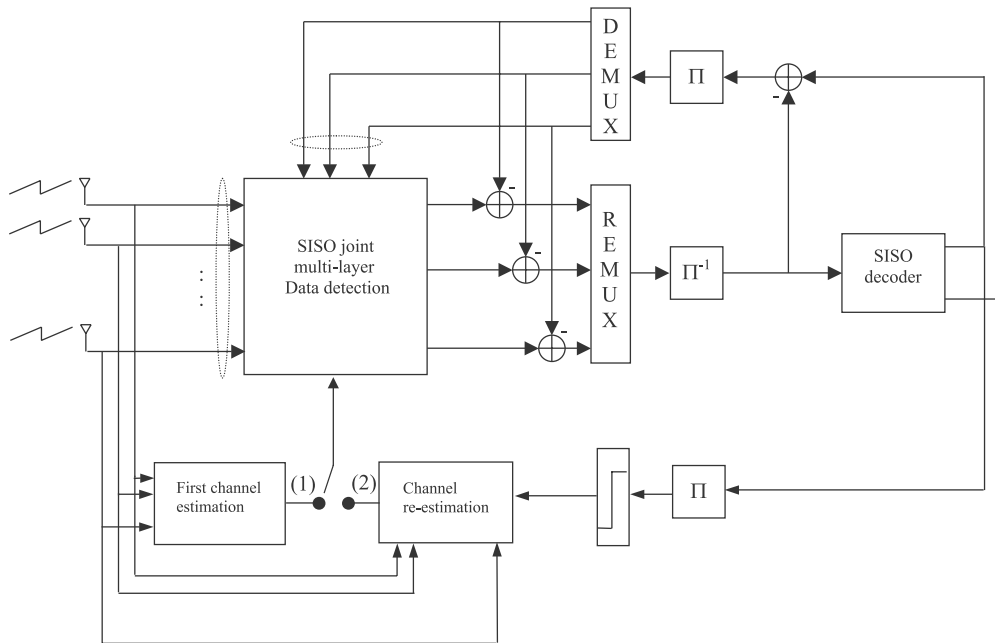


Figure 6.2: Iterative multilayer coded data detector with LS-based turbo channel estimation.

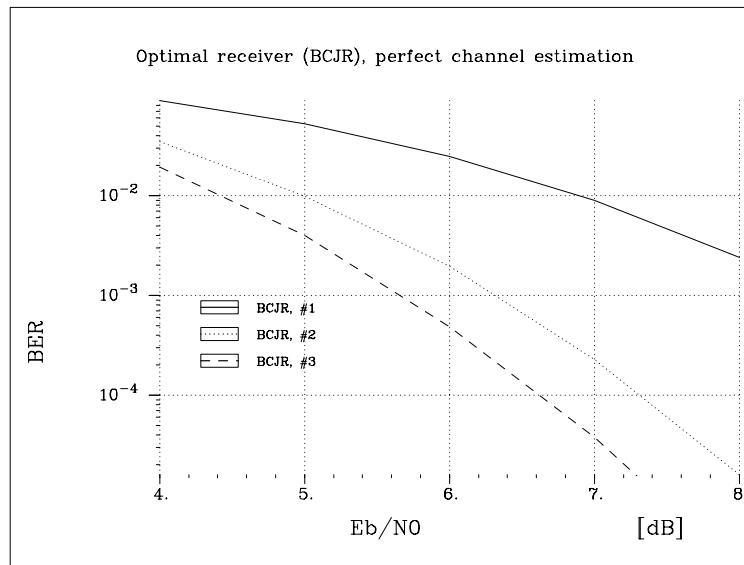


Figure 6.3: Optimal receiver for EQ-3 MIMO ISI channel, perfect channel estimation.

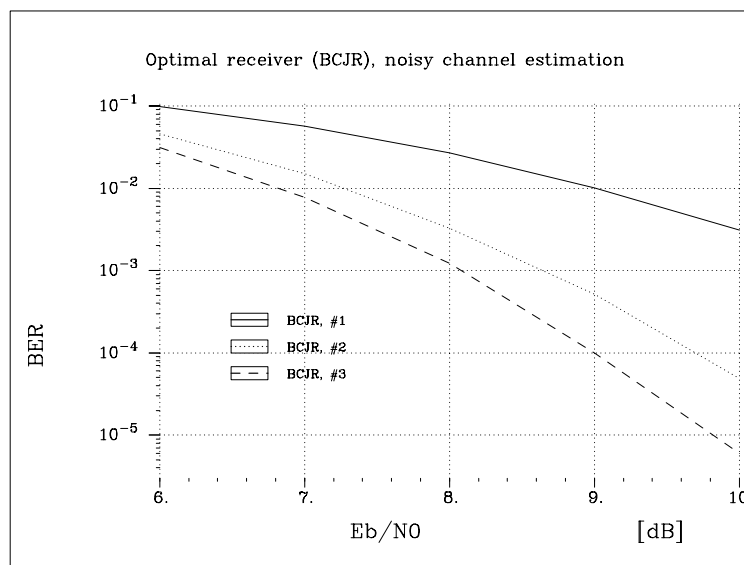


Figure 6.4: Optimal receiver for EQ-3 MIMO ISI channel, noisy channel estimation.

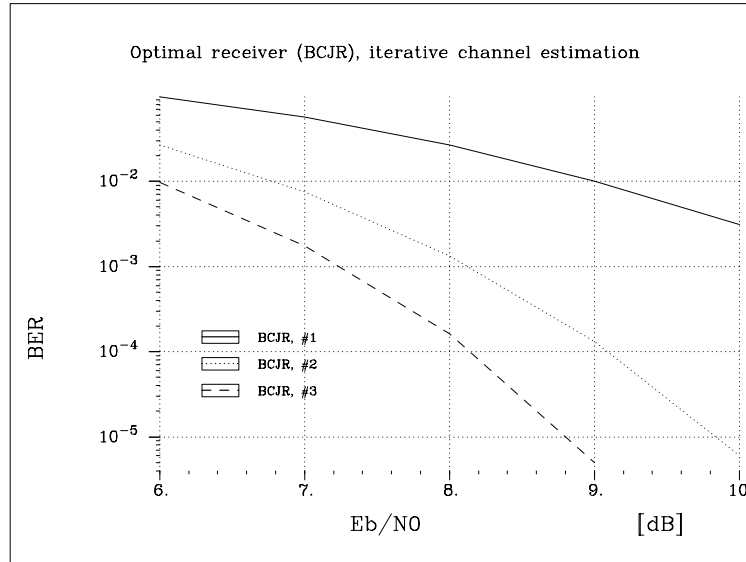


Figure 6.5: Optimal receiver for EQ-3 MIMO ISI channel, with LS-based turbo channel estimation.

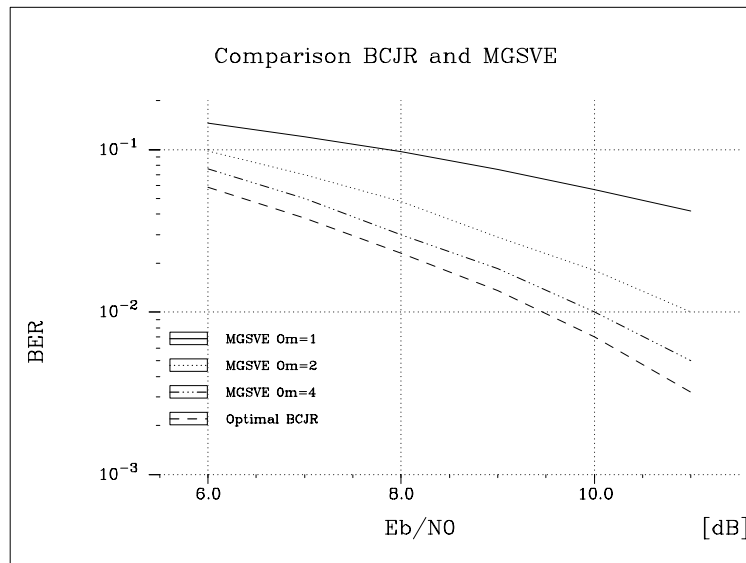


Figure 6.6: Comparison between the optimal receiver and the MGSVE for different values of parameter Ω and EQ-3 MIMO ISI channel.

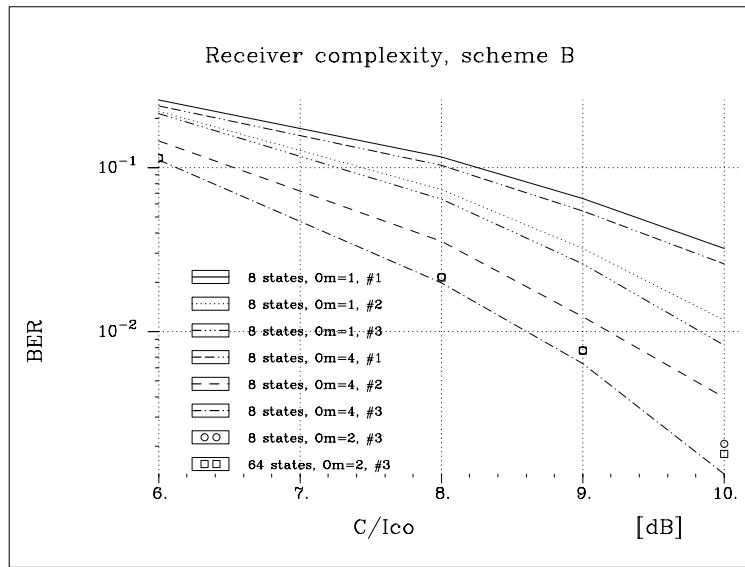


Figure 6.7: Trade off between receiver complexity and performance related to scheme B.

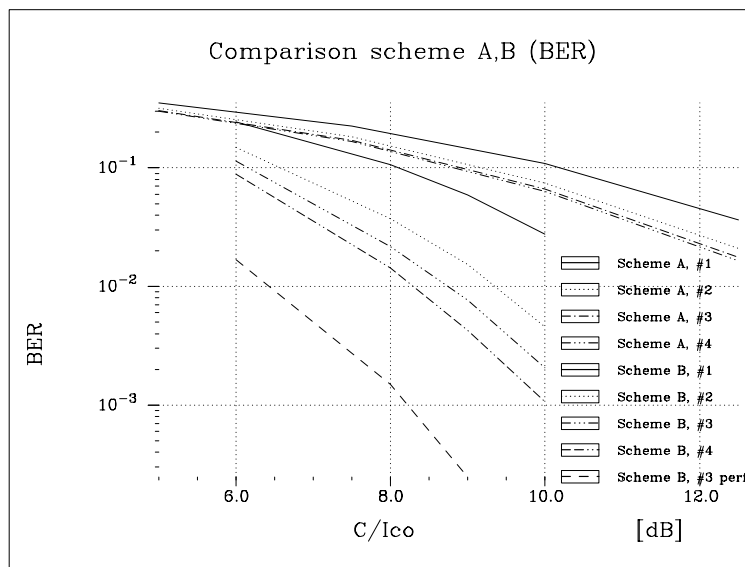


Figure 6.8: Comparison of BER versus C/I_{co} between scheme A and B.

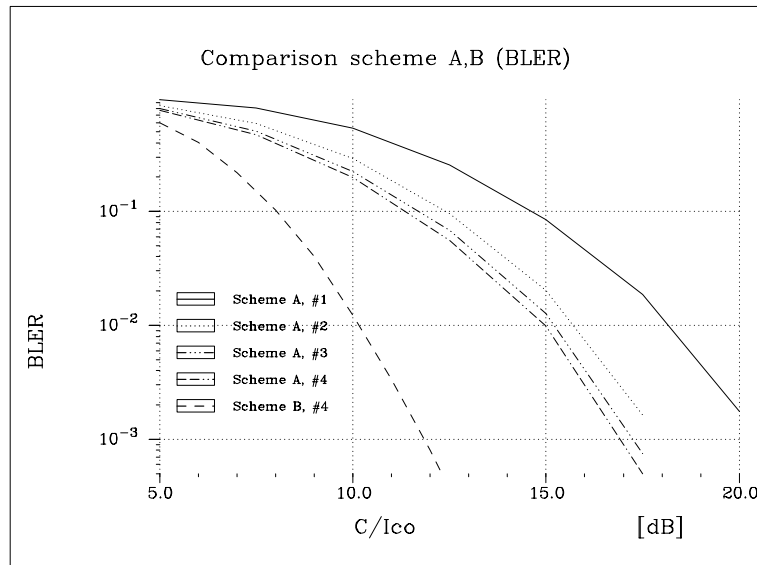


Figure 6.9: Comparison of BLER versus C/I_{co} between scheme A and B.

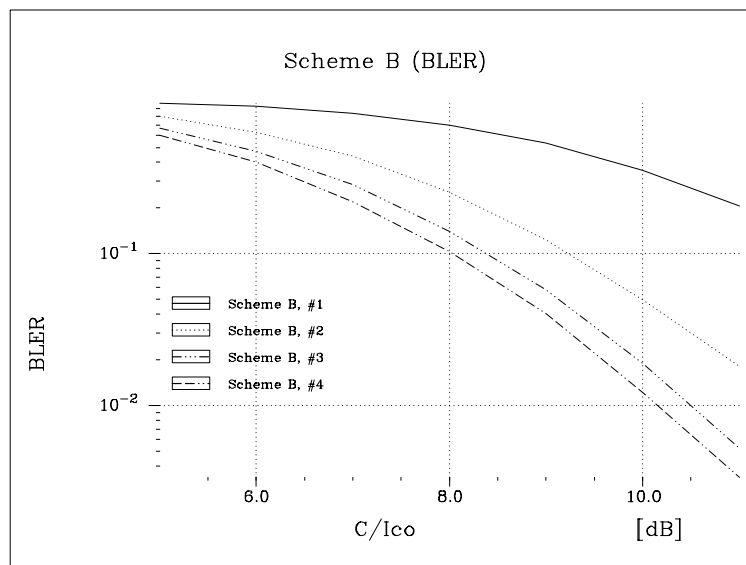


Figure 6.10: performance in terms of BLER versus C/I_{co} of scheme B.

Chapter 7

Iterative Decoding of Serially Concatenated Multilayered Trellis-Coded Modulations in Multipath Rayleigh Fading Environment.

7.1 Introduction

7.1.1 Wireless transmission context

The growing demand of reliable high data rates transmissions over wireless channels has motivated quite intensive research in the design of future generation TDMA mobile systems. As well known, wireless channels are both frequency selective and time-varying. The time variation stems from the mobility of the user and the environment. The frequency selectivity stems from multipath propagation and destructive superposition of received signals coming from different paths. It is responsible of intersymbol interference (ISI). The ISI and the receiver complexity, increase with the data rate. These general characteristics of wireless channels have always driven the design of radio interface and made it particularly difficult, all the more for high data rate and high spectral efficiency. Nonetheless, the frequency selectivity and the time variation, initially impairments, can favourably be exploited via the diversity concept (see [120] and references therein).

7.1.2 Efficiency and limits of full turbo detection

Since their first presentation in 1993, turbo-codes [17] have renewed interest in iterative techniques both from theoretical and practical points of view. Battail first foresaw the three keys of their astonishing success : randomlikeness, concatenation of several low complexity compounds codes, and iterative soft-in soft-out MAP decoding of each constituent code using available information from all others [7]. By extending those concepts, a new approach, called "turbo-principle" has recently emerged in communication theory, as a way of recursively updating randomized a posterior information on data/coded symbols among all concatenated functions in the reception chain. Turbo-detection [39] appears as a promising application of the turbo-principle, for the purpose of fighting against the ISI produced by the wireless channel. By modeling the ISI structure as a time-varying non-recursive non-systematic convolutional code of rate unity, data detection and channel decoding can be formally identified to a serial concatenation of two trellis codes. Optimal maximum-likelihood decoding of the ensemble, conditioned by perfect channel knowledge, is thus reachable through an iterative process similar to [15].

Several domains of interest rise up from past studies on turbo-detection. One of them deals with mismatched channel estimation [10], and has been at least partially solved by designing a "full turbo" receiver [21]. The basic idea consists on superimposing to the turbo-detector architecture an iterative channel reestimation process, which takes advantage of available information on symbols after channel decoding. Another variant of turbo-detection consists in reinforcing the ISI inner code by introducing a trellis coded modulation (TCM), as suggested in [21] [19]. Such a serially concatenated TCM scheme has proved to provide at least two benefits: first, the decoding may start earlier, compared to classical turbo-detection, and the performance is asymptotically better. Second, the computational complexity can be reduced by realizing joint SISO data detection and TCM decoding on the reduced-state TCM trellis only.

Quite by essence, turbo-detection fully exploits (time) coding/interleaving diversity, and consequently, performance is strongly related to interleaver depth. If the concept proves to be efficient even on the worst static ISI configurations, it may not be especially fitted to typical wireless profiles [43], where most of the channel outcomes are easy to equalize, but characterized by deep fades. When the channel impairment caused by time-varying energy distribution overcomes the frequency selective dispersion, turbo-detection remains powerless [93], especially under the constraint of delay sensitive applications. This is the reason why, in order to ensure the best possible performance, TDMA advanced mobile systems should be designed to both fight ISI [19] and encompass other forms of diversity, i.e, antenna diversity.

To benefit from spatial diversity via Space-Time encoding techniques [110] while performing turbo-detection, the basic proposed communication model involves an outer code

(an essential element for the turbo-detection process) interleaved with a *space-time* trellis coded modulation (ST-TCM). In fact, this model should be generically regarded as a serially concatenated space-time trellis coded modulation. It keeps the fundamental advantage to allow joint equalization and inner space-time decoding with sub-optimum low-complexity SISO algorithms, by opposition to the alternative quite complex approach described in [13], where data detection and space-time decoding are performed separately in an iterative fashion.

7.1.3 Improving spectral efficiency of serially concatenated space-time trellis coded modulation

To much of our knowledge, there are only four ways to improve the spectral efficiency of a serially concatenated ST-TCM:

- the first one consists in increasing the coding rate as much as possible of both inner and outer codes;
- the second one consists in increasing the modulation order within the ST-TCM;
- the third one consists in multiplexing several users (or equivalently several distinct data streams) in the same TDMA time-slot, i.e., introducing multi-user communications [72];
- the fourth one consists in demultiplexing one single pre-encoded data stream onto several transmit antennas, conformly to BLAST (Bell Labs Layered Space-Time) approach [48].

Unfortunately, increasing the coding rate of the outer code yields poor turbo-detection performance. Indeed, the extrinsic information provided by the outer code is not sufficiently reliable, and may degrade subsequent inner decoding soft decisions. Similarly, increasing the modulation order over 4, by employing the best known ST-TCM designs, proposed in [110], yields a great loss in performance of the inner code, which results in the combination of the ST-TCM with the ISI code. Since, however, serially concatenated TCM schemes made of simple half-rate trellis coded QPSK modulators prove to be very efficient in various ISI environments [21], the natural following step is to multiplex them in different manners for the purpose of increasing the overall spectral efficiency of the system. One first strategy consists in modeling multi-user communication by multiplexing several purely independent ST-TCM schemes, considering each distinct input data stream as one particular user. It will be verified that such a scheme does not efficiently exploit diversity. Consequently, this chapter rather focuses on a second scenario, called serially concatenated multilayered ST-TCM, where one single pre-encoded data stream is divided onto an arbitrary fixed number of

elementary space-time trellis coded modulators, which all operate and transmit in parallel. This architectural idea, already studied by [111] in conjunction with a new array processing decoding technique, certainly recalls the BLAST approach, apart from the crucial fact that the iterative receiver proposed here is able to cope with severe ISI. Thus, our contribution will be mainly focused on low complexity receiver designs rather than efficient trellis code constructions for wireless frequency selective channels.

7.1.4 Chapter organization

This chapter is organized as follows. In section 2, a very generic serially concatenated multilayered space-time trellis coded modulation scheme is carefully described, as well as its iterative decoding. In section 3, we focus on the inner part of the scheme and analyse the discrete-time finite-state Markov model as well as the associated possibly reduced-state trellis. In section 4, we derive a sub-optimal SISO algorithm for the purpose of performing joint multilayer data detection and inner decoding. In section 5, simulation results are presented and discussed for various cases of our generic communication model. Finally, section 6 is devoted to concluding remarks and future research topics.

7.2 Serially concatenated multilayered space-time trellis coded modulation

7.2.1 Communication model

A binary data vector \mathbf{d} of length τ_o is encoded by an outer channel encoder C_o of rate R_o , made of one single constituent code or, by extension, a code combination (for example, a turbo-code). The produced codeword \mathbf{c} of length $\frac{\tau_o}{R_o}$ is sent into a pseudo-random interleaver Π operating on bit level. The resulting interleaved binary stream is then demultiplexed into N_L binary frames, one for each of the N_L stages of the inner multilayered encoding structure. Each frame is itself split into \mathcal{B} bursts.

On layer $l \in [1, N_L]$, each burst enters a $N_T^{(l)}$ -order space-time encoder Ξ_l . We shall assume a convolutional time encoding, even though cyclic block encoding could be employed as well. The time encoder in Ξ_l associates to any input symbol a coded symbol, whose N_l constituent bits are scattered according to some internal given law and spread by groups of $q_{l,t}$ bits onto $N_T^{(l)}$ distinct transmit branches, so that, at any given time instant:

$$N_l = \sum_{t=1}^{N_T^{(l)}} q_{l,t} \quad . \quad (7.1)$$

Assuming a family of $N_T^{(l)}$ $Q_{l,t}$ -ary modulators $\Psi_{l,t}(\cdot)$, with $Q_{l,t} = 2^{q_{l,t}}$, each group of $q_{l,t}$ bits on each transmit branch $t \in [1, N_T^{(l)}]$ finally enters a modulator producing a complex-valued symbol $z_n^{l,t}$. Note that, in the most general case, neither ST-TCM Ξ_l for all layers $l \in [1, N_L]$, nor employed modulators within one particular ST-TCM are necessarily the same, allowing interesting encoding irregularities and, hence, possible unequal error protection (UEP) of data streams. The transmission part of the communication model is depicted on Fig. 7.1.

The resulting multilayered inner ST-TCM is connected to a network of N_T transmit antennas and N_R received antennas, where:

$$N_T = \sum_{l=1}^{N_L} N_T^{(l)} \quad (7.2)$$

and where the fundamental BLAST constraint $N_R \geq N_T$ is not required.

Due to multipath propagation and mobility, a distinct time-varying frequency selective wireless channel, modeled by an equivalent discrete-time channel impulse response $\mathbf{h}_{l,t,r}$ (including transmit and received pulse shaping filters), links any transmit antenna $t \in [1, N_T^{(l)}]$ of any layer $l \in [1, N_L]$ to any receive antenna $r \in [1, N_R]$. Let \mathbf{H} simply denotes the set of all $N_T \times N_R$ combined discrete-time channel vectors $\mathbf{h}_{l,t,r}$. All channels are supposed to have the same memory μ_c . As mentioned in [13], the assumption is reasonable because the number of individual multipath components is predominantly dictated by large structures and reflecting objects. We consider burst per burst transmission. The channels are static under the duration of a burst and change independently from one burst to another. This describes a suitable model for slow (quasi-static) multipath block fading and frequency hopping. All channel taps $\{h_i^{l,t,r}\}$ are independent complex Gaussian random variables with zero mean and equal mean power, satisfying the normalization constraint:

$$\sum_{i=0}^{\mu_c} E \left\{ \left\| h_i^{l,t,r} \right\|^2 \right\} = 1 \quad . \quad (7.3)$$

At the output of the equivalent discrete-time model, received samples for antenna r are given by:

$$y_n^r = \sum_{l=1}^{N_L} \sum_{t=1}^{N_T^{(l)}} \sum_{i=0}^{\mu_c} h_i^{l,t,r} z_{n-i}^{l,t} + \zeta_n^r \quad , \quad (7.4)$$

where ζ_n^r represents the (considered uncorrelated) zero-mean complex Gaussian noise samples of variance $2\sigma^2$. ζ_n^r is a circularly symmetric complex Gaussian variable (i.e., its real and imaginary parts are uncorrelated and of same power σ^2).

7.2.2 Iterative decoding

The main idea of the proposed receiver consists in iteratively performing joint multilayer coded data detection and inner space-time decoding, together with outer decoding. At first iteration, the SISO joint multilayer data detector and inner ST decoder, processing on each of the \mathcal{B} groups of N_L bursts, computes the corresponding sequences of log *extrinsic* probability ratios on each bit of each input symbol, given the set of the \mathcal{B} complex-valued observed sequences $\{y_1^r, \dots, y_\tau^r\}_{r=1}^{N_R}$ of length τ , on the N_R receive antennas, and given an estimate $\hat{\mathbf{H}}$ of the coefficients of the channels from all transmit antennas to all receive antennas. This computation is done without any *prior* information. Produced sequences are gathered by frames, multiplexed and de-interleaved. The new sequence acts as a sequence of log *intrinsic* probability ratios on coded bits for the outer decoder. The latter (BCJR algorithm, log-domain) evaluates the sequence of log *extrinsic* probability ratios on each bit of each outer coded symbol, which, after re-interleaving Π , frame demultiplexing, and burst segmentation, is passed to the SISO joint multilayer data detector and inner ST decoder as \mathcal{B} sets of N_L sequences of log *prior* probability ratios on bits of input symbols (one for each burst of each layer). This completes an iteration of the data detection and decoding part in the receiver. A recapitulative diagram is shown on Fig. 7.2. We point out that an *iterative estimation* of all distinct ISI channel coefficients can be naturally embedded in the framework of the multilayer turbo data detector, bringing reasonable overhead to the receiver complexity [21] [122].

7.3 Discrete-time finite-state Markov model and associated possibly-reduced trellis

7.3.1 Discrete-time finite-state Markov model for elementary ST-TCM

Let us now consider the discrete-time finite-state Markov process made of the l^{th} $N_T^{(l)}$ -order elementary ST-TCM followed by $N_T^{(l)}$ transversal filters, $\mu_c + 1$ coefficients each. At time n , given the input symbol $\mathbf{u}_n^l = \{u_1^l, \dots, u_{K_l}^l\}$ of K_l bits, the inner time encoder Ξ_l of memory μ_l produces a coded symbol $\mathbf{x}_n^l = \{x_1^l, \dots, x_{N_l}^l\}$ of N_l bits which are scattered into $N_T^{(l)}$ bit-labeled symbols $\{\mathbf{a}_n^{l,t}\}_{t=1}^{N_T^{(l)}}$ and sent in parallel on the $N_T^{(l)}$ transmit branches. On transmit branch $t \in [1, N_T^{(l)}]$, the bit-labeled symbol $\mathbf{a}_n^{l,t}$ is mapped into a complex-valued symbol $z_n^{l,t}$ according to the mapping rule $\Psi_{l,t}(\cdot)$. Hence, the set of transmit symbol $\{z_n^{l,t}\}_{t=1}^{N_T^{(l)}}$ is a function of the time encoder state e_n^l and the input sequence \mathbf{u}_n^l , i.e.,

$$\{z_n^{l,t}\}_{t=1}^{N_T^{(l)}} = \psi(e_n^l; \mathbf{u}_n^l) \quad . \quad (7.5)$$

The states of the final combined Markov model are given by:

$$s_n^l = \left\{ \left\{ z_{n-\mu_c}^{l,t}, \dots, z_{n-1}^{l,t} \right\}_{t=1}^{N_T^{(l)}} ; e_n^l \right\} \quad , \quad (7.6)$$

where the set of complex-valued symbol sequences :

$$\left\{ z_{n-\mu_c}^{l,t}, \dots, z_{n-1}^{l,t} \right\}_{t=1}^{N_T^{(l)}} \quad (7.7)$$

corresponds to a path which takes the combined Markov process from a previous state $s_{n-\mu_c}^l$ to the present state s_n^l in accordance with time encoding laws:

$$e_n^l = \phi_e^l(e_{n-1}^l; \mathbf{u}_n^l) \quad , \quad (7.8)$$

$$\mathbf{x}_n^l = \phi_x^l(e_{n-1}^l; \mathbf{u}_n^l) \quad . \quad (7.9)$$

In the rest of the chapter, encoding laws are supposed to be time-invariant for the sake of simplicity (as it is for convolutional codes). Generalization to time-variant encoding laws is straightforward however. Furthermore, between discrete time $n - 1$ and discrete time n , transitions b_n^l of the combined Markov model are expressed as:

$$s_{n-1}^l : \mathbf{u}_n^l \mapsto s_n^l \quad (7.10)$$

and lead to the transmit symbol set $\{z_n^{l,t}\}_{t=1}^{N_T^{(l)}}$.

Now, thanks to 7.8 and 7.9, the combined state can be expressed in terms of the output coded symbol sequence $\{\mathbf{x}_{n-\mu_c}^l, \dots, \mathbf{x}_{n-1}^l\}$ as:

$$s_n^l = \{ \{ \mathbf{x}_{n-\mu_c}^l, \dots, \mathbf{x}_{n-1}^l \} ; e_n^l \} \quad (7.11)$$

or, equivalently, in terms of the input symbol sequence $\{\mathbf{u}_{n-\mu_c}^l, \dots, \mathbf{u}_{n-1}^l\}$ as:

$$s_n^l = \{ e_{n-\mu_c}^l ; \{ \mathbf{u}_{n-\mu_c}^l, \dots, \mathbf{u}_{n-1}^l \} \} \quad . \quad (7.12)$$

The functioning of the time encoder may also be described by introducing reduced states \mathbf{e}_n^l which consist in memory truncation of the full state e_n^l . Let $\nu_l < \mu_l$ denote the reduced memory of the time encoder. The time encoding laws can be rewritten as:

$$e_n^l = \varphi_e^l(\mathbf{e}_{n-1-(\mu_l-\nu_l)}^l; \{ \mathbf{u}_{n-(\mu_l-\nu_l)}^l, \dots, \mathbf{u}_n^l \}) \quad , \quad (7.13)$$

$$\mathbf{x}_n^l = \varphi_x^l \left(\mathbf{e}_{n-1-(\mu_l-v_l)}^l; \{ \mathbf{u}_{n-(\mu_l-v_l)}^l, \dots, \mathbf{u}_n^l \} \right) \quad . \quad (7.14)$$

Again, thanks to 7.13 and 7.14, the combined state can be expressed in terms of the input symbol sequence $\{ \mathbf{u}_{n-\mu_c-(\mu_l-v_l)}^l, \dots, \mathbf{u}_{n-1}^l \}$ as :

$$s_n^l = \{ \mathbf{e}_{n-\mu_c-(\mu_l-v_l)}^l; \{ \mathbf{u}_{n-\mu_c-(\mu_l-v_l)}^l, \dots, \mathbf{u}_{n-1}^l \} \} \quad . \quad (7.15)$$

7.3.2 Combined trellis associated with elementary ST-TCM

The time progression of the state sequences produced by the combined Markov process described above can be visualized by a trellis diagram T_l whose states and transitions, at any depth or section n , correspond to states and branches s_n^l and b_n^l defined above. Let S_l and B_l denote the state and branch spaces of T_l . Let also S_n^l and B_n^l denote the state and branch spaces at depth and section n respectively. Note that when the trellis is regular, as supposed here, any trellis section B_n^l is sufficient to describe the Markov process evolution from discrete time $n - 1$ to discrete time n . Moreover, at any depth n of the trellis time axis, state space S_n^l can also be identified to one single finite state space, made of all possible states of the combined Markov process. Finally, let $|\cdot|$ denote the space cardinality. Since, at each depth n , $2^{K_l \cdot \mu_c}$ ISI states are combined with each encoder state, the combined trellis state complexity is given by:

$$|S_n^l| = 2^{K_l \cdot \mu_c} |S_n^{l, stc}| \quad (7.16)$$

where $S_n^{l, stc}$ is the state space of the l^{th} ST-TCM trellis. Moreover, since, from each state emerge exactly 2^{K_l} transitions, the combined trellis branch complexity, at each section n , is equal to:

$$|B_n^l| = 2^{K_l} |S_n^l| = 2^{K_l(\mu_c + 1)} |S_n^{l, stc}| \quad . \quad (7.17)$$

7.3.3 Multilayer discrete-time Markov model and multilayer combined trellis

Extending the previous reasoning to the entire multilayer structure is straightforward. States and input sequences of the combined Markov model are simply the concatenation of states or input sequences of the elementary combined Markov processes modeling ST-TCM followed by sub-groups of corresponding ISI channels. The corresponding multilayer combined trellis T^\boxtimes is simply the Cartesian product \boxtimes of the N_L combined trellises $\{T_l\}_{l=1}^L$. Hence, the related complexity measures are given by:

$$|S_n^\boxtimes| = \prod_{l=1}^{N_L} |S_n^l| \quad , \quad (7.18)$$

$$|B_n^\boxtimes| = |S_n^\boxtimes| \cdot \prod_{l=1}^{N_L} 2^{K_l} \quad , \quad (7.19)$$

where S_n^\boxtimes , B_n^\boxtimes , S_n^l and B_n^l denote the state and branch spaces of T^\boxtimes and T_l , at any section $n \in [1, \tau]$.

7.3.4 Reduced-state multilayer combined trellis

For the purpose of iterative decoding, we aim at computing log a posterior probability (APP) ratios on each bit of each input symbol \mathbf{u}_n^l at any time $n \in [1, \tau]$ and for each layer $l \in [1, N_L]$. This can be optimally accomplished by applying the BCJR algorithm [3] on the full multilayer combined trellis $T^\boxtimes (S^\boxtimes, B^\boxtimes)$. The computation and storage requirements of such an optimum algorithm being roughly linear in $|B^\boxtimes|$, this maximum a posteriori (MAP) approach becomes quickly prohibitive in complexity and has to be discarded. One possible way to alleviate the complexity burden consists in restricting all full elementary combined trellises T_l to sub-trellises $T_l(S_l, B_l)$, by truncating the effective overall channel memory μ_c to an arbitrary value v_c in $[0, \mu_c]$ (which could vary from one layer to another) [45] [34] [94]. Since reduction factors on state complexities of elementary combined trellises multiply, the resulting state complexity of the multilayer combined trellis can be considerably lowered by such a process. A particular case we are interesting in is the choice $v_c = 0$, for which elementary combined trellises are restricted to ST-TCM trellises [126]. A further desirable reduction can even be achieved by shortening time encoder memories themselves, as suggested above. Elementary combined trellises are then reduced up to sub-trellises of ST-TCM trellises.

7.4 SISO joint multilayer data detection and inner decoding

7.4.1 Reduced-state trellis search and generalized per-survivor processing

Since only part of the memory of the channels and elementary ST-TCM is kept into the multilayer combined trellis sub-states, transmitted modulated signals involved in Euclidean branch metrics and which are not directly accessible have to be explicitly re-computed

by per-survivor processing (PSP) [94]. In order to limit the well known resulting error propagation effect, the PSP technique requires that the channels from all transmit antennas to all receive antennas be minimum-phase [34].

In 1987, Hashimoto has proposed a list-type reduced-constraint generalization of the Viterbi algorithm (GVA), which in fact, constitutes a broad class of algorithms, including, among others, the most structured Viterbi algorithm and the less structured M -algorithm [61]. The basic idea of the GVA is to compensate the PSP induced performance degradation by retaining $\Omega > 1$ survivor paths per substate. We call this algorithmic property generalized per-survivor processing (GPSP). When applied to joint data detection and channel decoding, the GVA has proved to be very robust to error propagation [123]. In particular, GPSP approach makes the use of a minimum-phase prefiltering *superfluous*. It is all the more important in the MIMO channel context since a prefilter turning every single ISI channel into minimum-phase does not exist [13]. We now describe a one-way SISO algorithm designed to perform joint multilayer data detection and space-time decoding, the last two taking advantage of the generalized per-survivor concept.

7.4.2 A generalized reduced-state SOVA-like algorithm

This section describes the way to extend the Soft-Output Viterbi Algorithm (SOVA) [60][6] to GPSP. In the following derivations, we employ α, γ Greek letters to mimic the BCJR formalism [3], $\bar{\alpha}, \bar{\gamma}$ notations referring to logarithmic approximated probability density functions. Let us assume that, at any time section $n \in [1, \tau]$, to each departure sub-state s , are attached:

- an ordered list $\{\bar{\alpha}_{n-1,\omega}(s), \omega \in [1, \Omega]\}$ of the Ω best forward accumulated sub-state metrics;
- an ordered list $\{\hat{\mathbf{u}}_{i=n-\theta-1}^{n-1, s}, \omega \in [1, \Omega]\}$ of the Ω corresponding survivor paths $\hat{\mathbf{u}}_{i=n-\theta-1}^{n-1, s} = \{\hat{\mathbf{u}}_{n-\theta-1}^s, \dots, \hat{\mathbf{u}}_{n-1}^s\}$ terminating in s . Recall that \mathbf{u}_n denote the set of the N_L concatenated input sequences $\mathbf{u}_n^1, \dots, \mathbf{u}_n^{N_L}$ entering each ST-TCM at time n .
- an ordered list $\{\mathbf{L}_{i=n-\theta-1}^{n-1, s}, \omega \in [1, \Omega]\}$ of the Ω bit-wise unsigned soft sequences $\mathbf{L}_{i=n-\theta-1}^{n-1, s} = \{\mathbf{L}_{n-\theta-1}^s, \dots, \mathbf{L}_{n-1}^s\}$ associated with survivors.

The one-way generalized SOVA-like algorithm performs one single forward recursion. At section $n \in [1, \tau]$, for each branch $b \in B_n^\boxtimes$, and for each rank $\omega \in [1, \Omega]$, it computes non-classified accumulated sub-state metrics as:

$$-\ln \bar{\alpha}_{n,\omega}^{b^-}(b^+) = -\ln \bar{\alpha}_{n-1,\omega}(b^-) - \ln \bar{\gamma}_{n,\omega}(b) \quad . \quad (7.20)$$

Recursion 7.20 is carried out with respect to the boundary conditions:

$$-\ln \bar{\alpha}_{0,1}(0) = 0 \quad -\ln \bar{\alpha}_{0,\omega}(0) = \infty \text{ for } \omega > 1 \quad , \quad (7.21)$$

$$-\ln \bar{\alpha}_{0,\omega}(s) = \infty, \forall s \neq 0, \forall \omega \in [1, \Omega] \quad . \quad (7.22)$$

All sub-state metrics $\bar{\alpha}_{n,\omega}^{b^-}(b^+)$ such that $b^+ = s \in S_n^{\boxtimes}$ are then gathered and classified by increasing order (the smallest the first rank). Again, let:

$$\{-\ln \bar{\alpha}_{n,\omega}(s), \omega \in [1, 2^K \Omega]\}, K = \sum_{l=1}^{N_L} K_l \quad (7.23)$$

denote the temporary set of ordered metrics attached to sub-state $s \in S_n^{\boxtimes}$. Only the Ω best forward accumulated sub-state metrics are actually stored for the next section step. Simultaneously, the past survivor paths are extended according to existing transitions. The new potential survivor paths are temporarily stored and sorted in compliance with the rank of their associated metrics, but only the Ω best ones (in metric sense) will be actually used for constructing the generalized survivor map. Similarly to the path survivors, the past bitwise unsigned soft sequences are extended according to existing transitions. The new potential unsigned soft sequences are temporarily stored, sorted in compliance with the rank of the corresponding survivor path metrics, and updated. After soft updating, only the Ω best unsigned soft sequences need to be stored for next section step.

Now comes the soft updating part of the algorithm. At depth n , at each sub-state s , at each rank $\omega \in [1, \Omega]$, for each layer $l \in [1, N_L]$, and for each input bit $j \in [1, K_l]$, unsigned soft values are initialized as:

$$L_{n,j}^l \overset{s}{\omega} = \infty \quad . \quad (7.24)$$

Bitwise unsigned soft sequences $\underline{L}_{i=n-\theta}^n \overset{s}{\omega}$ are then updated from depth $i = n - 1$ down to depth $i = n - \delta$ according to:

$$L_{i,j}^l \overset{s}{\omega} = f(L_{i,j}^l \overset{s}{\omega}, \Delta_{n,j}^l \overset{s}{\omega}) \quad , \quad (7.25)$$

where $f(\cdot)$ is the updating function, and where:

$$\Delta_{n,j}^l \overset{s}{\omega} = -\ln \bar{\alpha}_{n,\tilde{\omega}_{i,j}^l}(s) + \ln \bar{\alpha}_{n,\omega}(s) \quad , \quad (7.26)$$

with:

$$\tilde{\omega}_{i,j}^l = \min \{ \varsigma \geq \Omega + 1, \hat{u}_{i,j}^l \overset{s}{\varsigma} \neq \hat{u}_{i,j}^l \overset{s}{\omega} \} \quad . \quad (7.27)$$

Following [60][6], the updating function $f(\cdot)$ in 7.25 is defined as:

$$f(L_{i,j}^l, \Delta_{n,j}^l) = \ln \frac{1 + \exp(L_{i,j}^l + \Delta_{n,j}^l)}{\exp(L_{i,j}^l) + \exp(\Delta_{n,j}^l)} \quad (7.28)$$

and may usually be approximated by:

$$f(L_{i,j}^l, \Delta_{n,j}^l) \approx \min \{L_{i,j}^l, \Delta_{n,j}^l\} \quad (7.29)$$

If $n \geq \theta$, the algorithm delivers approximated log APPs on $\mathbf{u}_{n-\theta}^l$, $l \in [1, N_L]$. Those approximated log APPs expressed as:

$$\lambda(u_{n-\theta,j}^l) = (2 \times \hat{u}_{n-\theta,j}^{s_{best}} - 1) \times L_{n-\theta,j}^{s_{best}} \quad (7.30)$$

are calculated for $l \in [1, N_L]$, $j \in [1, K_l]$ using the first rank survivor path $\hat{\mathbf{u}}_{i=n-\theta}^{s_{best}}$ and the corresponding bitwise unsigned soft sequence $\mathbf{L}_{i=n-\theta}^{s_{best}}$, which both terminate, at depth n , into the sub-state s_{best} defined as:

$$s_{best} = \arg \min_{s \in S_n^{\boxtimes}} \{-\ln \bar{\alpha}_{n,1}(s)\} \quad (7.31)$$

Finally, useful approximated log extrinsic probability ratios on bits $u_{n-\theta,j}^l$, $l \in [1, N_L]$, $j \in [1, K_l]$, are computed by bitwise subtracting log *prior* probability ratios $\lambda_p(u_{n-\theta,j}^l)$ coming from outer decoder to approximated log APPs:

$$\lambda_\varepsilon(u_{n-\theta,j}^l) = \lambda(u_{n-\theta,j}^l) - \lambda_p(u_{n-\theta,j}^l) \quad (7.32)$$

7.5 Performance analysis

7.5.1 Serially concatenated TCM (non minimum-phase time-invariant channel)

We first aim at investigating the benefit we get by replacing a conventional modulator by a ST-TCM, assuming constant spectral efficiency. This benefit, expressed both in terms of complexity reduction and performance improvement was already pointed out in [19] [21] for minimum-phase ISI channels and simple half-rate QPSK-based TCM. Here, we extend it to non minimum-phase (highly) frequency selective ISI channels and various ST-TCM. In communication model A, we employ an outer 4-state recursive systematic convolutional (RSC) code C_o of rate $R_o = \frac{1}{2}$ and generator polynomials (7, 5), which generates an encoded sequence \mathbf{c} of size 2048 bits (including tail). The inner coding part of model A is introduced through the use of a coded QPSK-based TCM Ξ , whose time encoder consists in a 4-state

non-recursive non-systematic (NRNS) convolutional code of rate $R = \frac{1}{2}$ and generator polynomials $(7, 5)$. Produced coded bits $\mathbf{x}_n = (x_{n,1}, x_{n,2})$ directly pilot a 4-ary signal mapper $\Psi(\cdot)$ (Gray mapping). Note that Ξ appears as a trivial ST-TCM where space dimension is restricted to 1 (i.e., $N_T = 1$). The outer encoded sequence \mathbf{c} is sent to a pseudo-random interleaver Π . The interleaved bit stream enters the inner TCM Ξ , which produces a sequence of 2048 symbols, segmented into $\mathfrak{B} = 16$ bursts of 128 QPSK symbols each. μ_c tail symbols are added to all bursts before their transmission. The spectral efficiency is 0.5 bit/s/Hz. At reception, channel coefficients are supposed to be perfectly known.

The Bit Error Rate (BER) performance of the overall turbo-receiver has been validated by Monte-Carlo simulation on the worst 6-taps time-invariant ISI channel [92, p. 601]. Fig. 7.3 isolates the BER performance of the inner TCM. The optimal BCJR algorithm processing on a full 128-state combined trellis is confronted with the reduced-state SOVA-like algorithm processing on the much simpler 4-state NRC code trellis. The performance of the latter is dramatically improved by increasing Ω parameter values. For $\Omega = 4$, the reduced-state SOVA-like algorithm is only 1.2 dB away from the optimal joint detection and decoding at BER 10^{-5} , whereas $\Omega = 8$ provides almost optimal performance. In that last case, the reduction in terms of computational complexity reaches a factor 4 compared to optimal BCJR approach. Note that, even with higher memory, a simple SISO Parallel Decision-Feedback Decoder (PDFD) [19] [21] [123] performs extremely bad on such a non-minimum phase ISI channel, highlighting the crucial necessity of GPSP. In order to test the soft quality of the outputs (both log APPs ratios and log extrinsic probability ratios) delivered by the reduced-state SOVA-like algorithm, we have to consider the BER performance of the concatenated system. Fig. 7.4 reveals that, at BER 10^{-5} , the generalized reduced-state SOVA-like algorithm, processing on the 4-state NRC code trellis, is only 1.2 dB away from the optimal joint detection and inner decoding performance for $\Omega = 8$ and $\theta = \delta = 30$.

On Fig. 7.5, iterative decoding performance of various Bit Interleaved Coded Modulations (BICM) is also shown for comparison purpose. The first investigated BICM (model B) involves the best 16-state NRC code C_o of rate $R_o = \frac{1}{4}$ and generator polynomials $(25, 27, 33, 37)$ [92, p. 494] whereas the second (model C) uses a serial concatenation C_o of two 4-state RSC codes of rate $R_o = \frac{1}{2}$ and generator polynomials $(7, 5)$. In both cases, the channel interleaver depth equals 4096 bits and the modulation order is increased up to 4 for achieving spectral efficiency 0.5 bit/s/Hz. Since optimal turbo-detection is assumed, those schemes are of pure theoretical interest because of their prohibitive complexity (1024-state ISI trellis). Surprisingly, the best performance is achieved by model B, although the SCCC is known to clearly outperform a single convolutional code of same rate on the Gaussian channel. We believe that the loss in performance (despite 8 iterations !) is essentially due to the much more pronounced sub-optimality of the iterative decoding process when three

codes are involved instead of two. Additional investigations will be reported on that particular topic soon. Note that, from iterative decoding point of view, model A avoids this drawback as a simpler concatenation of only two encoding/decoding entities.

Another interesting benchmark consists in simulating the performance of a third BICM (model D) made of the same outer part as model A (i.e., 4-state half-rate RSC code, channel interleaver depth of 2048 bits) and a BPSK modulator. Again, the spectral efficiency is 0.5 bit/s/Hz. As observed on Fig. 7.5, a gain of 1.6 dB at BER 10^{-5} can be reached in favor of the serially concatenated TCM, the overall decoding complexity being roughly identical for both schemes. To conclude with, we also underline that the generalized reduced-state SOVA-like algorithm can be employed in pure BICM context by processing on the ISI trellis only [90] [23] [122]. A drastic complexity reduction in the data detection process is then achievable. However, the resulting loss in terms of BER performance makes this approach for highly frequency selective and long delay spread channels (i.e., very high data rate) less attractive than model A at fixed overall computational complexity. Indeed, it appears that the inner Space Time Codes not only improve the performance at low BER (compare to a pure MIMO BICM of same spectral efficiency) but also help to fight back the impairment resulting from the receiver suboptimality.

7.5.2 Design of inner ST-TCM in concatenated systems

We now introduce *space* dimension, being especially interested by designing efficient inner ST-TCM for serially concatenated communication models. As an example, we observe that an outer 4-state RSC code of rate $R_o = \frac{2}{3}$ and generator polynomials (3, 7, 2) begins to decode when fed with an input BER 0.15 (Fig. 7.6). Consequently, the proper criterion for choosing the inner ST-TCM should be mainly focused on the behavior in the region of low SNRs. In this section, we confront two types of ST-TCM at fixed number of transmit antennas, receive antennas, and trellis complexity measures. The first one, called Ξ^2 , is a multilayered TCM ($N_L = 2$ layers). Simple half-rate coded QPSK-based TCM Ξ (previously defined) are chosen on each layer ($N_T^{(l)} = 1$ transmit antenna per layer l). The second one, called Ξ_2 , is the 4-PSK 16-state 2-order ST-TCM proposed by Tarokh [110]. Those two ST-TCM are first evaluated on a flat Rayleigh fading channel (perfect CSI), assuming a BCJR decoding algorithm and $N_R = 2$ antennas at the receiver side. Their performance is depicted on Fig. 7.7. For both schemes, BCJR algorithm processes on a 16 state trellis. We observe that ST-TCM Ξ^2 performs up to 1 dB better than Ξ_2 in the region of low SNRs (-6 to 3 dB). However, the slope of Ξ_2 performance curve is steeper than the one of Ξ^2 , thus leading to an intersecting point at $E_b/N_0 = 3$ dB and BER 10^{-2} . Finally, the Ξ_2 performance is asymptotically far better than Ξ^2 performance. Those observations are not surprising since Ξ_2 has been designed to provide the best tradeoff between data rate, space

diversity advantage and trellis complexity.

As shown on Fig. 7.8, the same type of behavior is witnessed in a MIMO multiple ray fading environment, proving that a space-time code designed for a flat fading channel continues to perform well (at least asymptotically) in various multiple path environments under a variety of mobility conditions. The performance analysis is conducted in the case of a four-ray equally Rayleigh distributed ISI modelization (time-varying EQ-4 ISI channels, perfect CSI). Again, we assume a BCJR decoding algorithm and $N_R = 2$ antennas at the receiver side. For both schemes, the combined trellis on which the BCJR algorithm processes has 1024 states. The performance of Ξ^2 is still far better than the one of Ξ_2 in the region of low SNRs (-6 to 5 dB). The slopes of the performance curves are both increased due to the additional multipath diversity (further investigations have to be done to quantify the diversity gain). The discrepancy between the two slopes is less pronounced than before, however, and the intersecting point occurs at $E_b/N_0 = 5$ dB and BER 10^{-4} .

Since we aim at finding codes that work efficiently in the region of low SNRs, we conclude from this short analysis, that, at fixed transmit and receive antennas number, and at fixed trellis complexity, it seems preferable to employ *multilayer* simple 4-state half-rate QPSK-coded TCM rather than the best ST-TCM found by [110] as inner constituents in concatenated systems.

7.5.3 Serially concatenated multilayered ST-TCM (BLAST-like approach)

As a last step, a new scenario (model E) is investigated, assuming transmission over time-varying EQ-4 ISI channels, antenna diversity, and a targeted spectral efficiency of 2.0 bits/s/Hz. The outer code is a 4-state RSC code of rate $R_o = \frac{2}{3}$ and generator polynomials (3, 7, 2) generating a pre-encoded sequence \mathbf{c} of size 3072 bits (including tail). The inner space-time encoding part is made of a multilayered TCM ($N_L = 3$ layers, $N_T^{(l)} = 1$ transmit antenna per layer l). At each layer, we keep the simple half-rate coded QPSK-based TCM Ξ . This particular choice is motivated by the conclusions of the previous section. The outer encoded sequence \mathbf{c} is sent to a pseudo-random interleaver Π . The interleaved bit stream is de-multiplexed into $N_L = 3$ distinct streams of size 1024 bits. Each of them enters the TCM Ξ , which produces a sequence of 1024 QPSK symbols, segmented into $\mathfrak{B} = 8$ bursts. μ_c tail symbols are added to all bursts before their transmission. At reception, channel coefficients are supposed to be perfectly known. Furthermore, $N_R = 2$ receive antennas are used, allowing Maximum Ratio Combining (MRC). The turbo-receiver employs the generalized reduced-state SOVA-like algorithm to perform joint multilayer data detection and inner decoding. Parameters are $\Omega = 8$ and $\theta = \delta = 20$. The multilayered trellis on which the algorithm processes has been reduced up to 8 states, so that the reduction in terms of

computational complexity reaches a factor 512 compared to optimal BCJR approach on full multilayered combined trellis. The performance in terms of BER is plotted on Fig. 7.9. The performance in terms of Block Error Rate (BLER) is plotted on Fig. 7.10. An impressive decreasing of both BER and BLER can be observed as iterations advance, proving the validity of our approach, i.e., the benefit of mixing antenna diversity, interleaving and coding diversity, and implicit multipath diversity via the energy detection and equalization.

7.6 Conclusion and future research topics

In this chapter, we have proposed a new reduced-complexity receiver. It is suitable for iteratively decoding multilayer trellis-encoded signals transmitted over Multiple-Input Multiple-Output ISI channels. Indeed, a sub-optimal SISO joint multilayer data detector and space-time decoder using reduced-state trellis search and GPSP technique was derived. Its simulated performance is close to optimal, even in the case of highly frequency selective long delay spread ISI channels and huge complexity reduction.

Theoretical investigations still have to be done to measure the reachable optimum performance of this very general communication model on time-varying ISI channels. Besides, exhibiting efficient high-order space-time inner encoders able to compete with multilayered ST-TCM could appear as another challenging topic.

Channel estimation and re-estimation is another topic that has not been investigated here. However, chapter 6, gives already a partial answer to that.

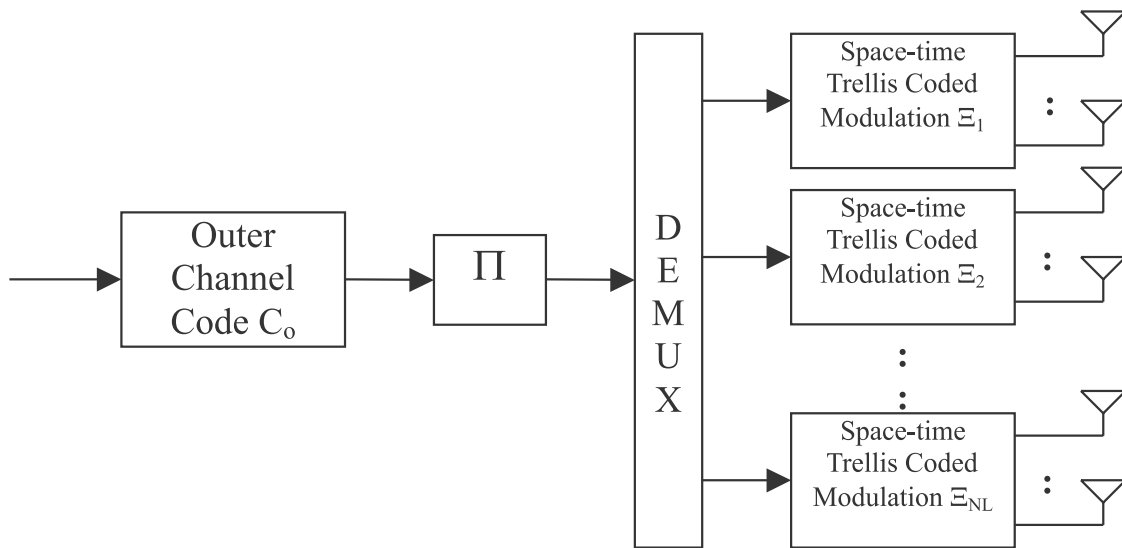


Figure 7.1: Transmitter.

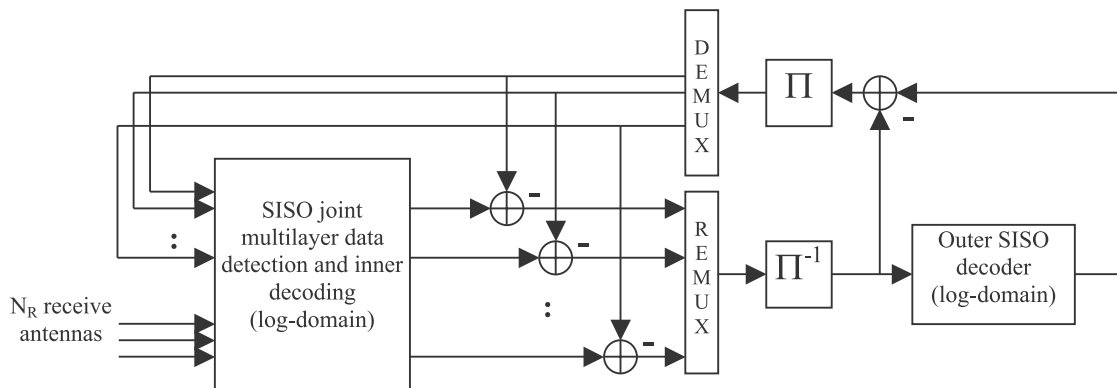


Figure 7.2: Receiver.

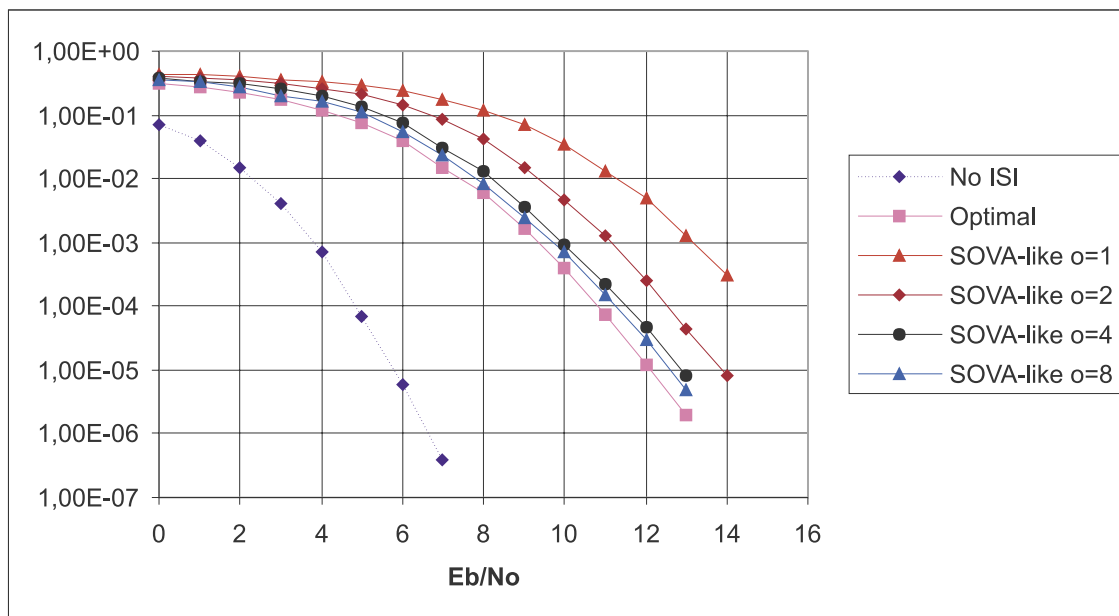


Figure 7.3: BER performance of inner TCM within scheme A (rate 1/2 4-state QPSK-coded TCM Ξ , 1 bit/s/Hz, worst 6-tap time-invariant ISI channel, BCJR versus SOVA-like decoding algorithms, perfect CSI)

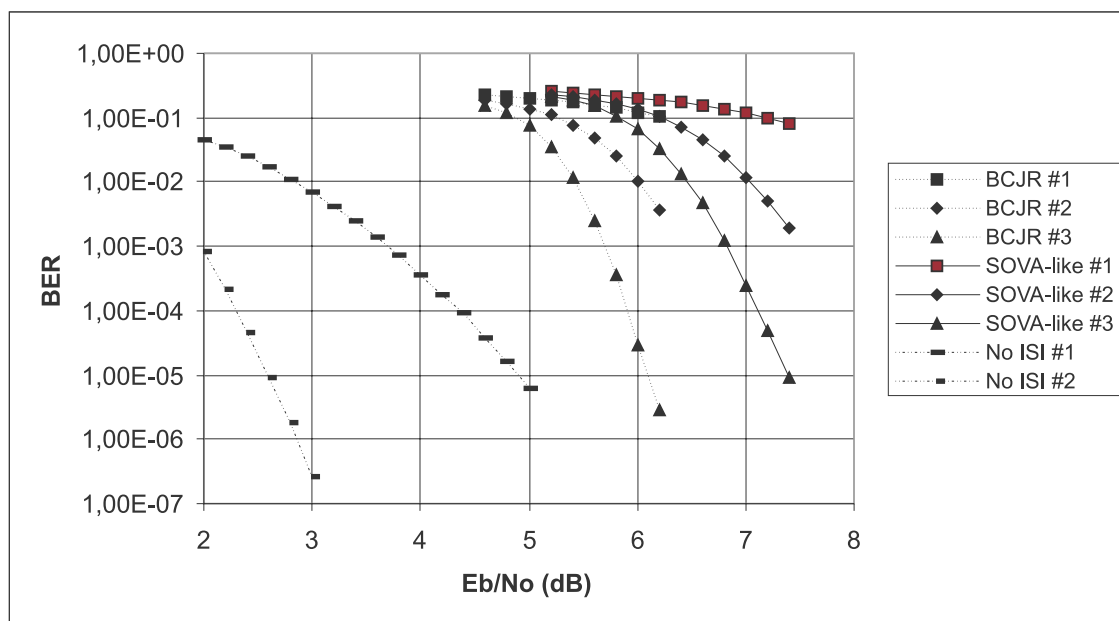


Figure 7.4: BER performance of scheme A (rate 1/2 4-state RSC outer code, rate 1/2 4-state QPSK-coded inner TCM Ξ , 0.5 bit/s/Hz, worst 6-tap static ISI channel, BCJR versus SOVA-like decoding algorithms, perfect CSI)

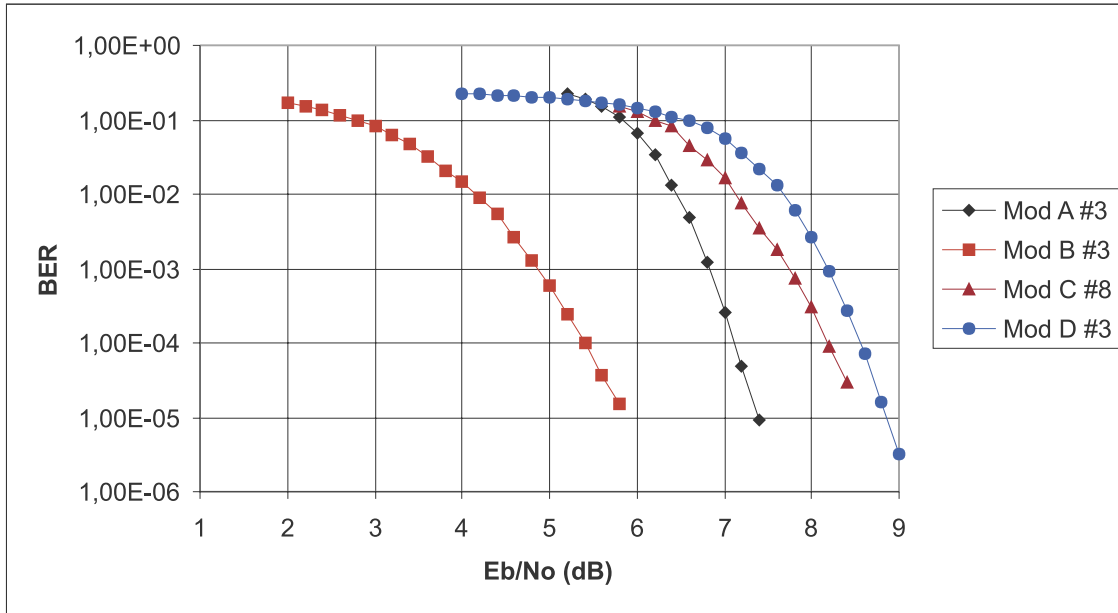


Figure 7.5: BER performance of various communication models (A,B,C,D) over worst 6-tap time-invariant ISI channel (0.5 bit/s/Hz , $N_T = N_R = 1$)

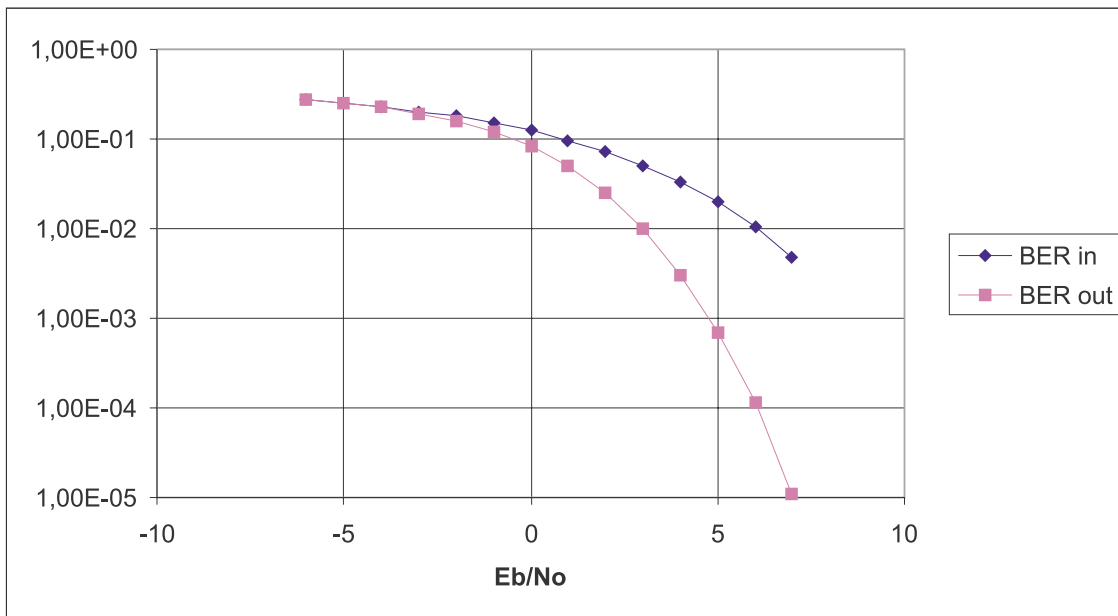


Figure 7.6: BER performance of rate $2/3$ 4-state RSC code over the AWGN channel

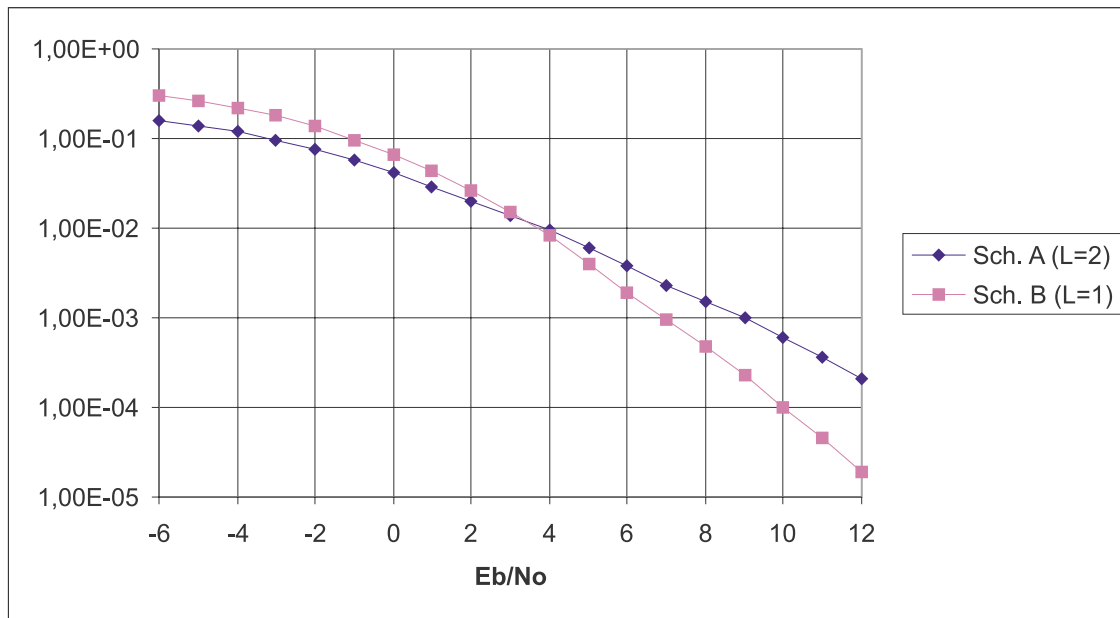


Figure 7.7: BER performance of ST-TCM Ξ^2 ($N_L = 2$, $N_T^{(l)} = 1 \forall l$) and Ξ_2 ($N_L = 1$, $N_T = 2$) over static block flat Rayleigh fading MIMO channel (128 QPSK symbols per block, $N_R = 2$, 2 bits/s/Hz, BCJR decoding algorithm, perfect CSI)

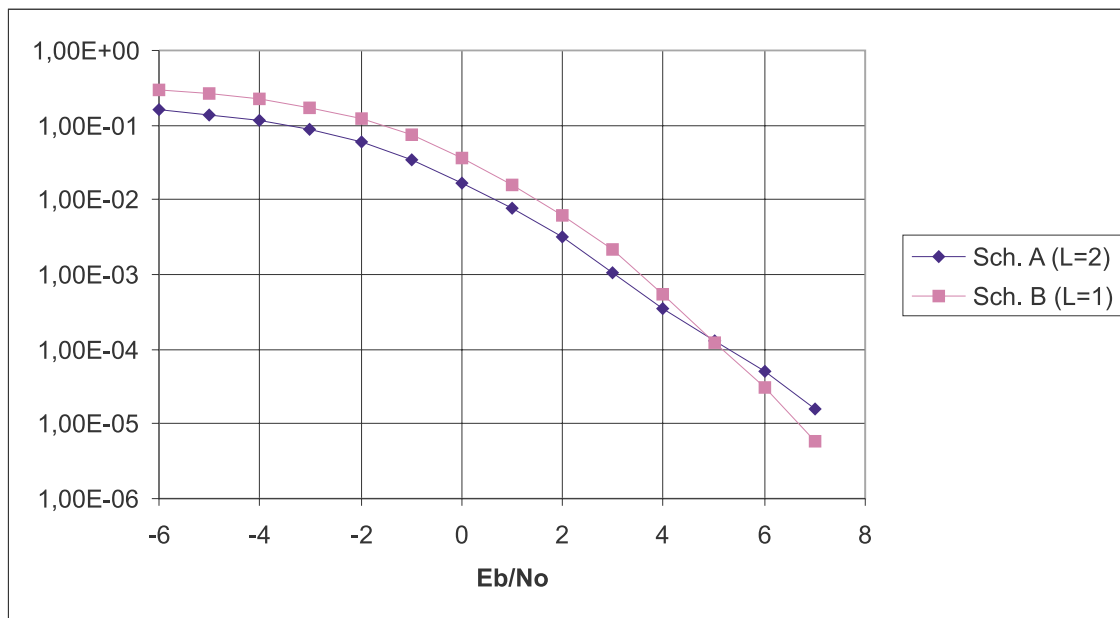


Figure 7.8: BER performance of ST-TCM Ξ^2 ($N_L = 2$, $N_T^{(l)} = 1 \forall l$) and Ξ_2 ($N_L = 1$, $N_T = 2$) over static block MIMO EQ-4 ISI channel (128 QPSK symbols per block, $N_R = 2$, 2 bits/s/Hz, BCJR decoding algorithm, perfect CSI)

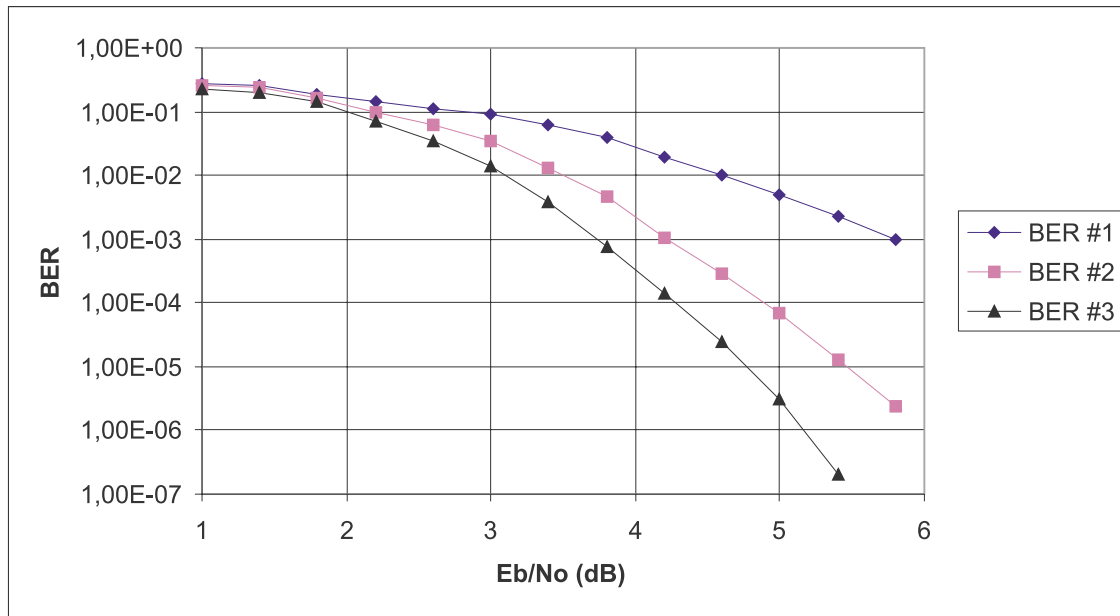


Figure 7.9: BER performance of model E over static block MIMO EQ-4 ISI channel (128 QPSK symbols per block, $N_L = 3$, $N_T^{(l)} = 1 \forall l$, $N_R = 2$, 2 bits/s/Hz, SOVA-like decoding algorithm, perfect CSI)

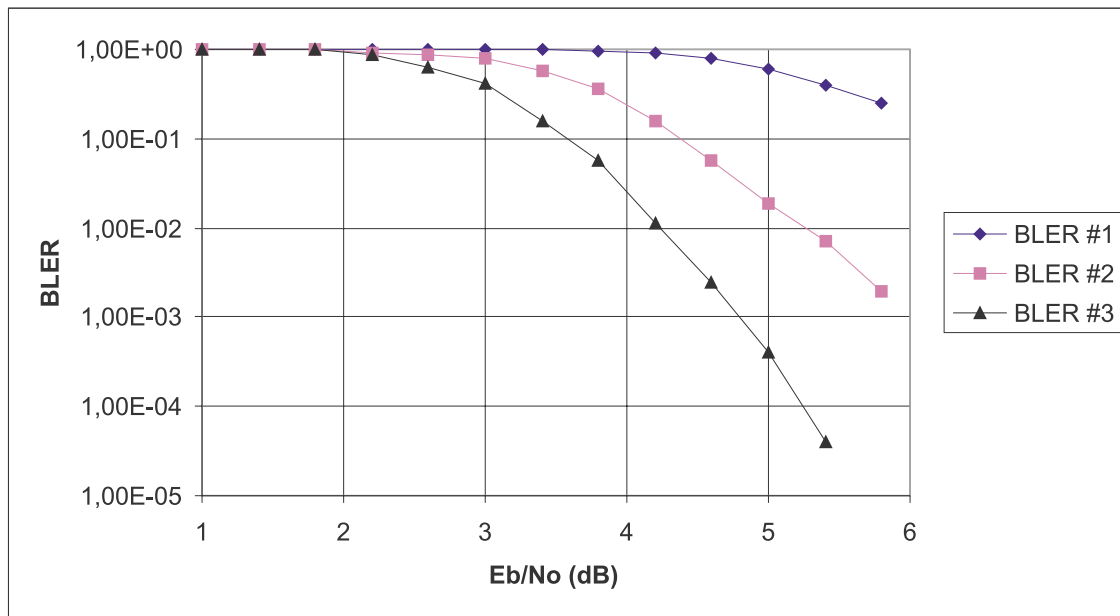


Figure 7.10: BLER performance of model E over static block MIMO EQ-4 ISI channel (128 QPSK symbols per block, $N_L = 3$, $N_T^{(l)} = 1 \forall l$, $N_R = 2$, 2 bits/s/Hz, SOVA-like decoding algorithm, perfect CSI)

Chapter 8

Conclusions

The classical receiver performs separately three tasks, namely, channel estimation, equalization and decoding. The optimal receiver however would treat them jointly but is often non-tractable due to its tremendous complexity.

Throughout this thesis, we identified contexts where this sub-optimality could entail substantial performance loss with the help of the Matched Filter Bound (MFB) introduced in **chapter 2** (this is explicitly the case for chapter 4 and 5, on the other hand the MFB for chapter 6 and 7 was used more as a design tool) .

Three main contexts were pointed out:

- wireless LAN with very high data rate and granularity constraints,
- high data rate CDMA with low spreading factor,
- advanced TDMA systems with high order modulation and/or Multiple Input Multiple Output channel.

Once these contexts identified, we then tried to alleviate this impairment by suggesting low complexity sub-optimal receivers that perform iteratively/jointly channel estimation, equalization and decoding. In order to tackle the complexity issue while keeping the Maximum A Posteriori criterion, efficient reduced state trellis search techniques mainly based on Per Survivor Processing (PSP) were exhaustively described and put into practice for the aforementioned contexts. A generalization of the well known PSP technique consisting quite simply in keeping more than one survivor per state was proved to be very robust to error propagation even in the case of non minimum phase channels. This generalization was first introduced for the Generalized Viterbi Algorithm (GVA) and the technique itself is referred as Generalized Per Survivor Processing (GPSP) in this thesis.

In **chapter 3**, we described a receiver structure for trellis coded signals transmitted through broadband wireless channels based on the GPSP technique. The proposed receiver

performs decoding and equalization jointly, such an approach is particularly appropriate for system where time interleaving is not possible or not needed (very high bit rate and/or granularity constraint). It is optimal in the sense of the blockwise Maximum A Posteriori criteria. The simulation results showed that the proposed receiver structure is suitable for high bit rate wireless applications and gives close to optimal performance with reasonable complexity.

In **chapter 4**, we presented an iterative receiver concept that improves the radio link performance of advanced TDMA systems with high order modulation and channel interleaving. We considered sub-optimal receiver structures comprised of channel estimator, detector and channel decoder, where the performance was improved by iterative data processing among the receiver blocks. As a practical example we considered packet data transmission in GSM and EDGE (Enhanced Data rates for Global Evolution). Low-complexity soft-in-soft-out (SISO) equalizers for EDGE were introduced and its modifications suitable for iterative detection in EDGE were derived. Application of iterative detection and channel estimation techniques in GSM/EDGE showed a significant performance improvement. Furthermore, we showed that re-transmission schemes specified for EDGE also benefited from iterative data processing.

In **chapter 5**, an iterative low-complexity receiver was proposed for Code Division Multiple Access (CDMA) systems with small spreading factor. The UMTS radio interface based on CDMA, has been designed to offer a wide range of data rates using variable spreading factor. It is ongoing standardization effort to include a high data rate packet mode in the downlink direction. This new mode is called High Speed Downlink Packet Access (HSDPA) and is characterized by the giving up of close loop power control, link adaptation using variable constellations (QPSK,MAQ16,MAQ64), and low spreading factor. The proposed receiver is particularly adapted to HSDPA mode since it gives close to optimal performance even in the case of high modulation order and low spreading factor while keeping a reasonable complexity.

In **chapter 6**, a generic model of Bit-Interleaved Coded Modulation (BICM) on a Multipath Rayleigh fading Multiple-Input Multiple-Output (MIMO) channel was derived. A practical low-complexity trellis-based receiver performing iteratively channel estimation, multilayer coded data detection and channel decoding was introduced. The inner multilayer data detector, employing reduced-state techniques together with GPSP, presents two-fold advantages. It enables to cope with severe channel intersymbol interference and allows to use more transmit antennas than receive antennas. Simulations showed that our approach can dramatically improve the downlink performance of Time Division Multiple Access (TDMA)

systems with high order modulation, such as EDGE [52], keeping a reasonable complexity at the receiver side.

In **chapter 7** a communication model made of an outer code interleaved with a space-time trellis coded modulation (ST-TCM) was investigated. Such a scheme is very relevant for highly frequency selective and time-varying channels using turbo-detection at the receiver side, but inherently suffers of a low coding rate. One possible solution to alleviate this impairment (i.e., to increase spectral efficiency) is to use parallel (or multilayered) transmission as done in recent approaches (BLAST). However, parallel transmission and highly frequency selective channels involve tremendous complexity at the receiver side. We propose a low complexity turbo-detector based on reduced-state trellis search and Generalized Per Survivor Processing that proves to be very efficient in this resulting Multiple-input Multiple-Output (MIMO) ISI channel context. Simulations showed that this scheme is very robust to highly frequency selective channels for a more reasonable receiver complexity than the one of a pure MIMO-BICM.

To conclude, simulations tend to show that this approach is very fruitful and can improve the radio performance of existing (GSM, EDGE and UMTS) as well as future radio interfaces (MIMO BICM, Mutilayer ST-TCM) dramatically.

Some interesting research directions that have not been fully exploited in this thesis, notably mentioned in chapter 3 and 7 may serve as a foundation for so-called fourth Generation radio interfaces and are currently being integrated into the France Telecom fourth generation radio interface project.

Appendix A

Wide Sense Stationary (WSS) Random Processes

Let $\mathbf{n}(t) = [n_1(t)n_2(t) \cdots n_K(t)]^T$ be a vector of wide sense stationary band-pass (with respect to f_0) random processes with zero mean and dimension K . $\mathbf{n}(t)$ can be written as $\mathbf{n}(t) = \sqrt{2}\mathcal{R}_e\{\tilde{\mathbf{n}}(t)e^{j2\pi f_0 t}\}$, where $\tilde{\mathbf{n}}(t) = \mathbf{x}(t) + j\mathbf{y}(t)$ is a base-band complex random process of dimension K . First of all, we will demonstrate that $E[\tilde{\mathbf{n}}(t)\tilde{\mathbf{n}}(t)^T] = 0$ (i.e. $\tilde{\mathbf{n}}(t)$ is circularly symmetric). Secondly, we will prove that the circular symmetry of $\tilde{\mathbf{n}}(t)$ and the wide sense stationarity of $\mathbf{n}(t)$ imply the wide sense stationarity of $\tilde{\mathbf{n}}(t)$. For our discussion we use the following notations:

- $\mathbf{K}_x(t + \tau, t) = E\{\mathbf{x}(t + \tau)\mathbf{x}^\dagger(t)\}$ autocorrelation matrix of any K -dimensional random process $\mathbf{x}(t)$
- $\mathbf{K}_{xy}(t + \tau, t) = E\{\mathbf{x}(t + \tau)\mathbf{y}^\dagger(t)\}$ cross-correlation matrix of any K -dimensional random processes $\mathbf{x}(t)$ and $\mathbf{y}(t)$

Note that if $\mathbf{x}(t)$ and $\mathbf{y}(t)$ are wide sense stationary then $\mathbf{K}_x(t + \tau, t) = \mathbf{K}_x(\tau)$ and $\mathbf{K}_{xy}(t + \tau, t) = \mathbf{K}_{xy}(\tau)$. In that case we can define the spectral density matrices \mathbf{S}_x and \mathbf{S}_{xy} which are the Fourier transform with respect to τ of $\mathbf{K}_x(\tau)$ and of $\mathbf{K}_{xy}(\tau)$ respectively.

It is well known that the complex envelope of $\mathbf{n}(t)$ can be written $\tilde{\mathbf{n}}(t) = \sqrt{2}[\mathbf{h}_+(t) * \mathbf{n}(t)]e^{-j2\pi f_0 t}$ where the Fourier transform $\mathbf{H}_+(f)$ of $\mathbf{h}_+(t)$ is the step function

$$\begin{cases} \mathbf{H}_+(f) = 1 & \text{if } f > 0 \\ \mathbf{H}_+(f) = \frac{1}{2} & \text{if } f = 0 \\ \mathbf{H}_+(f) = 0 & \text{if } f < 0 \end{cases} \quad (\text{A.1})$$

We then have

$$\begin{aligned}
E[\tilde{\mathbf{n}}(t)\tilde{\mathbf{n}}^T(s)] &= 2E([\mathbf{h}_+(t) * \mathbf{n}(t)]e^{-j2\pi f_0 t}[\mathbf{h}_+(s) * \mathbf{n}(s)]^T e^{-j2\pi f_0 s}) \\
&= 2 \int du dv \mathbf{h}_+(u)e^{-j2\pi f_0 t} \mathbf{K}_n(t-u-s+v) \mathbf{h}_+^T(v) e^{-j2\pi f_0 s} \\
&= 2e^{-j2\pi f_0(t+s)} \int df df' df'' du dv \mathbf{H}_+(f') \mathbf{S}_n(f) \mathbf{H}_+^T(f'') e^{j2\pi f(t-s)} \\
&\quad e^{j2\pi(f'-f)u} e^{j2\pi(f''+f)v} \\
&= 2e^{-j2\pi f_0(t+s)} \int df \mathbf{H}_+(f) \mathbf{S}_n(f) \mathbf{H}_+^T(-f) e^{j2\pi f(t-s)} \\
&= 0 \text{ if } \mathbf{S}_x(0) \text{ is finite .}
\end{aligned}$$

Finally

$$E[\tilde{\mathbf{n}}(t)\tilde{\mathbf{n}}^T(s)] = \mathbf{K}_x(t, s) - \mathbf{K}_y(t, s) + j[\mathbf{K}_{yx}(t, s) + \mathbf{K}_{xy}(t, s)] = 0. \quad (\text{A.2})$$

Now let us calculate $\mathbf{K}_n(\tau)$

$$\begin{aligned}
\mathbf{K}_n(\tau) &= E[\mathbf{n}(t+\tau)\mathbf{n}^\dagger(t)] \\
&= \{\mathbf{K}_x(t+\tau, t) - \mathbf{K}_y(t+\tau, t)\} \cos(4\pi f_0(t+\tau)) \\
&\quad + \{\mathbf{K}_x(t+\tau, t) + \mathbf{K}_y(t+\tau, t)\} \cos(2\pi f_0\tau) \\
&\quad - \{\mathbf{K}_{yx}(t+\tau, t) + \mathbf{K}_{xy}(t+\tau, t)\} \sin(4\pi f_0(t+\tau)) \\
&\quad - \{\mathbf{K}_{yx}(t+\tau, t) - \mathbf{K}_{xy}(t+\tau, t)\} \sin(2\pi f_0\tau).
\end{aligned}$$

Using (A.2), we obtain

$$\mathbf{K}_n(\tau) = 2 \{\mathbf{K}_x(t+\tau, t) \cos(2\pi f_0\tau) + \mathbf{K}_{xy}(t+\tau, t) \sin(2\pi f_0\tau)\} \quad (\text{A.3})$$

or equivalently

$$\mathbf{K}_n(\tau) = 2 \{\mathbf{K}_y(t+\tau, t) \cos(2\pi f_0\tau) - \mathbf{K}_{yx}(t+\tau, t) \sin(2\pi f_0\tau)\}. \quad (\text{A.4})$$

Obviously, for (A.3) and (A.4) to be valid, the wide sense stationarity of $\mathbf{n}(t)$ implies the wide sense stationarity of \mathbf{x} and \mathbf{y} , and consequently the wide sense stationarity of $\tilde{\mathbf{n}}(t)$. The circular symmetry of $\tilde{\mathbf{n}}(t)$ implies useful properties for the correlation between its components. Considering any two components $\tilde{n}_i(t) = x_i(t) + jy_i(t)$ and $\tilde{n}_j(t) = x_j(t) + jy_j(t)$, the circular symmetry (A.2) implies $E[x_i(t)y_i(t)] = 0$ and $E[x_j(t)y_j(t)] = 0$. It follows that either $E[x_i(t)y_j(t)] = E[x_j(t)y_i(t)] = 0$ or $E[x_i(t)x_j(t)] = E[y_i(t)y_j(t)] = 0$. The first case is commonly chosen. As a result $\mathbf{K}_{xy} = 0$ and $\mathbf{K}_{\tilde{n}}$ is real.

Appendix B

Karhunen-Loève Expansion for Circularly Symmetric Complex Variables

This annex follows the problem 4.8 of [63, page 135]. Let \mathbf{v} be a K -dimensional circularly symmetric complex random variable, and \mathbf{V} defined as $\mathbf{V} = [\mathcal{R}_e(\mathbf{v}), \mathcal{I}_m(\mathbf{v})]^T$. From (A.2), we have

$$\mathbf{K}_V = \frac{1}{2} \begin{bmatrix} \mathcal{R}_e(\mathbf{K}_v) & -\mathcal{I}_m(\mathbf{K}_v) \\ \mathcal{I}_m(\mathbf{K}_v) & \mathcal{R}_e(\mathbf{K}_v) \end{bmatrix} \quad (\text{B.1})$$

Consider any eigenvector $\mathbf{U} = [\mathbf{u}_r, \mathbf{u}_i]^T$ of \mathbf{K}_V with eigenvalue λ' . $F(\mathbf{U}) = [-\mathbf{u}_i, \mathbf{u}_r]$ is another eigenvector, perpendicular to \mathbf{U} , having the same eigenvalue λ' . Moreover $\mathbf{u} = \mathbf{u}_r + j\mathbf{u}_i$ is a complex eigenvector of \mathbf{K}_v with eigenvalue $\lambda = 2\lambda'$. It follows that \mathbf{V} has a Karhunen-Loève expansion of the form

$$\mathbf{V} = \sum_{k=1}^K y_{r,k} \mathbf{U}_k + y_{i,k} F(\mathbf{U}_k) \quad (\text{B.2})$$

where $y_{r,k}$ and $y_{i,k}$ are uncorrelated, and have the same variance λ'_k . Equation (B.2) can be written as

$$\mathbf{v} = \sum_{k=1}^K y_k \mathbf{u}_k \quad (\text{B.3})$$

where $\mathbf{u}_k = \mathbf{u}_{r,k} + j\mathbf{u}_{i,k}$ are orthonormal complex vectors, and $y_k = y_{r,k} + jy_{i,k}$ are uncorrelated complex random variables of variance $E|y_k|^2 = \lambda_k = 2\lambda'_k$.

Appendix C

Calculus of U_n

We reproduce from a previous work [14] the proof that

$$U_n = \sum_{i=1}^K \frac{\pi_i}{\mu_i^n} \quad (\text{C.1})$$

has the following properties:

$$\begin{cases} U_n = 1 & n = 0 \\ U_n = 0 & n = 1, \dots, K-1 \\ U_n = \frac{(-1)^{K+1}}{\prod_{i=1}^K \mu_i} & n = K \end{cases} \quad (\text{C.2})$$

Let us introduce $g(x)$ defined by

$$g(x) = \frac{x^{K-1-n}}{\prod_{i=1}^K (x - \mu_i)} \quad (\text{C.3})$$

- Case 1: $n \leq K-1$

$g(x)$ can be decomposed into elementary fractions such as

$$g(x) = \sum_{k=1}^K \frac{a_k}{x - \mu_k} \quad (\text{C.4})$$

with

$$a_k = \frac{\mu_k^{K-1-n}}{\prod_{i=1, i \neq k}^K (\mu_k - \mu_i)}. \quad (\text{C.5})$$

As a result, $U_n = \sum_{k=1}^K a_k$ can be now evaluated as the following limit

$$[xg(x)]_{x \rightarrow \infty} = \left[\frac{x^{K-n}}{\prod_{i=1}^K (x - \mu_i)} \right]_{x \rightarrow \infty} = \sum_{k=1}^K a_k = U_n \quad (\text{C.6})$$

From the previous expression it is obvious that $U_n = 1$ if $n = 0$ and $U_n = 0$ if $n = 1, \dots, K-1$.

- Case 2: $n = K$

In this case, we have

$$g(x) = \frac{b}{x} + \sum_{k=1}^K \frac{a_k}{x - \mu_k}. \quad (\text{C.7})$$

As for the previous case, let us multiply $g(x)$ by x and take the limit as $x \rightarrow \infty$. We obtain

$$U_K = \sum_{k=1}^K a_k = -b. \quad (\text{C.8})$$

The computation of b is

$$b = [xg(x)]_{x=0} = \frac{(-1)^K}{\prod_{i=1}^K \mu_i} \quad (\text{C.9})$$

and consequently

$$U_K = \frac{(-1)^{K+1}}{\prod_{i=1}^K \mu_i}. \quad (\text{C.10})$$

Appendix D

CRLB for Iterative Channel Estimation

Let's consider AWGN channel with noise samples $w_n = \mathcal{N}(0, \sigma_n^2)$ and a constant variance σ^2 during the received block \mathbf{y}_m , i.e. $\sigma_n^2 = \sigma^2, n = 1 \dots \tau$. The variance of the estimate $\hat{\mathbf{h}}$ based only on the training sequence \mathbf{m} may be bounded by Cramer-Rao lower bound (CRLB) [67] as $\text{var}(\hat{h}_i) \geq [\mathbf{I}(\mathbf{h})]_{ii}^{-1}$, where $\mathbf{I}(\mathbf{h}) = \{I_{ij}\}$ is the $(v_c+1) \times (v_c+1)$ Fisher information matrix with elements $I_{ij} = -\frac{\partial^2 \ln \Pr(\mathbf{y}_m | \mathbf{m}, \mathbf{h})}{\partial h_i \partial h_j}$.

In our case CRLB may be written as

$$\text{var}(\hat{h}_i) \geq [\mathbf{M}^H \mathbf{R}^{-1} \mathbf{M}]_{ii}^{-1} \approx \frac{1}{\sum_{n=1}^P \frac{1}{\sigma_n^2}} = \frac{\sigma^2}{P} \quad (\text{A.1})$$

where $i=0 \dots v_c$.

For the "extended" training sequence \mathbf{y} it gives

$$\text{var}(\hat{h}_i^{\text{extend}}) \geq [\mathbf{Z}^H \mathbf{R}^{-1} \mathbf{Z}]_{ii}^{-1} \approx \frac{1}{\sum_{n=1}^{\tau} \frac{1}{\sigma_n^2}} = \frac{1}{\frac{P}{\sigma^2} + \frac{\tau - P - L}{\sigma_d^2}} = \frac{\sigma^2}{P + (\tau - P - L) \frac{\sigma^2}{\sigma_d^2}} \quad (\text{A.2})$$

where σ_d^2 is the variance associated with the "extended" data $\check{\mathbf{c}}$ provided by the decoder.

To evaluate (A.2) let's denote p_n as an error probability for n^{th} complex symbol \check{z}_n after decoding/re-encoding operations, $\check{z}_n \in \check{\mathbf{z}}, \check{\mathbf{z}} = \Psi(\check{\mathbf{c}})$. The probabilities p_n are calculated by averaging over a number of received blocks. Let's consider the antipodal signalling ($z_n = 1, \bar{z}_n = -1$), the generalization to Q -ary modulation is straight forward. We can treat symbols $\check{\mathbf{z}}$ forming the extension of training sequence as a set of random variables with the mean and the variance as follows

$$E[\check{z}_n] = (1 - p_n)z_n + p_n\bar{z}_n$$

$$\text{var}[\check{z}_n] = E[|\check{z}_n|^2] - |E[\check{z}_n]|^2 = |z_n|^2 - p_n(|z_n|^2 - |\bar{z}_n|^2) - (z_n - p_n(z_n - \bar{z}_n))^2,$$

where $\bar{z}_n \neq z_n$.

Assuming a time-invariant channel during the transmitted block (i.e. $p_n = p$, $n=0, \dots, \tau - P - L - 1$) for antipodal signalling it results in

$$\text{var}[\check{z}_n] = 4p(1 - p) \quad (\text{A.3})$$

The variance of the "extended" data is

$$\sigma_d^2 = \text{var}[\check{z}_n + w_n] = \text{var}[\check{z}_n] + \text{var}[w_n] + 2\text{cov}[\check{z}_n w_n] \quad (\text{A.4})$$

Taking into account that more errors appear after decoding/re-encoding operations at high noise levels (i.e. larger σ^2 results in larger p , and hence, in larger $\text{var}[\check{z}_n]$), the correlation term in (A.4) $\text{cov}[\check{z}_n w_n] \geq 0$, therefore $\sigma_d^2 \geq \text{var}[\check{z}_n] + \text{var}[w_n]$. As can be seen from (A.4) the CRLB (A.2) is a function of $\text{cov}[\check{z}_n w_n]$, and it achieves its minimum $\text{var}(\hat{\underline{h}}_i^{\text{extend}})$ if $\text{cov}[\check{z}_n w_n] = 0$. Based on (A.2) and (A.3) this minimum may be presented as

$$\text{var}(\hat{\underline{h}}_i^{\text{extend}}) \geq \frac{\sigma^2}{P + \frac{(\tau - L - P)\sigma^2}{4p - 4p^2 + \sigma^2}} \quad (\text{A.5})$$

Bibliography

- [1] J.R. Abeysinghe and J.A. Roberts, "Bit Error Rate of Antenna Diversity Systems with Channel Correlation," in *Proc. IEEE GLOBECOM'95 Conference*, pp. 2022–2026, Nov. 1995.
- [2] F. Adachi, M.T. Feeny, A.G. Williamson, and J.D. Parsons, "Cross-correlation Between the Envelopes of 900MHz Signals Received at a Mobile Radio Base Station Site," *Proc. IEE*, vol. 133, Pt. F, no. 6, pp. 506–512, Oct. 1986.
- [3] L.R. Bahl, J. Cocke, F. Jelinek, and J. Raviv, "Optimal Decoding of Linear Codes for Minimizing Symbol Error Rate," *IEEE Trans. Inform. Theory*, vol. IT-20, pp. 284–287, March 1974.
- [4] P. Balaban and J. Salz, "Dual Diversity Combining and Equalization in Digital Cellular Mobile Radio," *IEEE Trans. Veh. Technol.*, vol. 40, no. 2, pp. 342 – 354, May 1991.
- [5] P. Balaban and J. Salz, "Optimum Diversity Combining and Equalization in Digital Data Transmission with Applications to Cellular Mobile Radio – Part I: Theoretical Considerations," *IEEE Trans. Commun.*, vol. 40, No 5, pp. 885 – 894, May 1992.
- [6] G. Battail, "pondération des symboles décodé par l'algorithme de Viterbi," *Ann. Télécommun., Fr.*, vol. 42, no. 1-2, pp. 31-38, Jan. 1987.
- [7] G. Battail, "We can think of good codes and even decoded them," *Eurocode 92*, Udine, October 26-30 1992, CISM courses and lectures no. 339, P. Camion, P. Charpin, and S. Harari, Eds, pp. 353-358, Springer, 1993.
- [8] G. Bauch, H. Khorram, and J. Hagenauer, " Iterative Equalization and Decoding in Mobile Communications Systems ," *Proc. EPMCC'97 conference*, pp. 307-312, Bonn, Germany, Sept. 1997
- [9] G. Bauch and V. Franz, "Iterative Equalization and Decoding for the GSM-System," *Proc VTC'98*, May 1998, pp. 2262-2266.

- [10] G. Bauch and V. Franz, "A comparison of Soft-In Soft-Out Algorithms for Turbo-Detection," *Proc. ICT'98*, vol.2, pp. 259-263, Portos Carras, Greece, June 1998.
- [11] G. Bauch and N. Al-Dhahir, "Iterative equalization and decoding with channel shortening filters for space-time coded modulation," *Proc. IEEE VTC'2000 Fall*, pp.1575-1582, Sept.2000.
- [12] G. Bauch and N. Al-Dhahir, "Reduced-Complexity Turbo Equalization with Multiple Transmit and Receive Antennas over Multipath Fading Channels," in *Proc., 2000 conference on Inform. Sciences and Systems*, Princeton University, USA, March 15-17, 2000.
- [13] G. Bauch, N. Naguib, "MAP Equalization and Space-Time Coded Signals over Frequency Selective Channels," in *Proc. IEEE WCNC'99*, Sept. 1999.
- [14] E. Bejjani, "Techniques de transmission pour les canaux très dispersifs," *École Nationale Supérieure des Télécommunications - Paris*, Thèse de doctorat (PhD Thesis), ENST 97 E 044, France, 1997.
- [15] S. Benedetto, D. Divsalar, G. Montorsi, and F. Pollara, "Serial Concatenation of Interleaved Codes: Performances, Analysis, Design and Iterative Decoding," *TDA Progress Report 42-126*, August 1996.
- [16] S. Benedetto, G. Montorsi, and F. Pollara, "A Soft-Input Soft-Output APP Module for Iterative Decoding of Concatenated Codes," *IEEE Communications Letters*, vol. 1, no. 1, pp. 22-24, Jan. 1997.
- [17] C. Berrou, A. Glavieux, and P. Thitimajshima, "Near Shannon Limit Error-Correcting Coding and Decoding: Turbo-codes," *Proc. ICC'93*, Geneva, Switzerland, pp. 1064-1070, May 1993.
- [18] A.O. Berthet, J. Fang, and P. Tortelier, "Heuristics for Optimizing in Complexity SISO Trellis-Based Decoding of Linear Block Codes," in *proc., GRETSI'99*, Vannes, France, Sept. 1999
- [19] A.O. Berthet, R. Visoz, B. Ünal, and P. Tortelier, "A Comparison of Several Strategies for Iteratively Decoding Serially Concatenated Convolutional Codes in Multipath Rayleigh Fading Environment," in *Proc., IEEE GLOBECOM'2000*, San Fransisco, USA, Nov. 2000.
- [20] A.O. Berthet, R. Visoz, and B. Ünal, "Iterative Decoding of Serially Concatenated Multilayered Trellis Coded Modulations in the presence of InterSymbol Interference and Noise," *IEEE GLOBECOM'2001*, San Antonio, Nov. 2001.

- [21] A.O. Berthet, B. Ünäl, and R. Visoz, "On Iterative Decoding of Trellis-Encoded Signals over Multipath Rayleigh Fading Channels," *IEEE J. Select. Areas Commun.*, vol. 19, sept. 2001.
- [22] A.O. Berthet, R. Visoz, and P. Tortelier, "Sub-Optimal Turbo-Detection for coded 8-PSK Signals over ISI Channels with Application to EDGE Advanced Mobile System," *Proc. IEEE PIMRC'2000*, pp. 151-157, London, UK, Sep. 2000.
- [23] A.O. Berthet, B. Penther, R. Visoz, and J.J. Boutros, "A New Reduced Complexity Turbo-Detector for Highly Selective Long Delay Spread ISI Channels: A Solution for 4G Mobile Systems ?," *Proc., IEEE VTC2001, Spring*, Rhodes Island, Greece, May 2001.
- [24] A.O. Berthet and R. Visoz, "procédé et système de codage-décodage itératif de flux de données numériques codées par combinaisons spatio-temporelles, en émission et réception multiple," Patent filed by France Telecom with reference number 0102343, Feb. 2001.
- [25] A.O. Berthet and R. Visoz, " Procédé de codage/décodage d'un flux de données numériques codées avec entrelacement sur bits en émission et en réception multiple en présence d'interférence intersymboles et système correspondant," patent filed by France Telecom with reference number 9911411, Apr. 2001.
- [26] E. Biglieri, D. Divsalar, P.J. McLane, and M.K. Simon, "Introduction to Trellis-Coded Modulation with Applications," *New York: MacMillan*, 1991.
- [27] E. Biglieri, G. Caire, and G. Taricco, "Recent results on Coding for Multiple-Antenna Transmission Systems," *Proc. IEEE ISSSTA '2000*, NJIT, New Jersey, USA, Sept. 2000.
- [28] H. Boujemaa and M. Siala, "On the performance of the Rake receiver," VTC 2000 Fall, Boston, USA.
- [29] J. Brossier, "Signal et communication numérique: égalisation et synchronisation," Paris:Hermès, 1997.
- [30] C. Brutel, J.J. Boutros, and P. Mege, "Iterative Joint channel estimation and Detection of Coded CPM," *Proc. Broadband Communications I2S'2000*, Zurich, Switzerland, pp. 287-292, 2000.
- [31] G. Caire, G. Taricco, and E. Biglieri, "Bit-Interleaved Coded Modulation," *IEEE Trans. Inform. Theory*, vol. 44, no. 3, pp. 927-946, May 1998.

- [32] A.R. Calderbank, G.D. Forney, and A. Vardy, "Minimal Tail-Biting Trellises: the Golay Code and more," *IEEE Trans. Inform. Theory*, vol. 45, no.5, pp. 1435-1455, July 1999.
- [33] K-H. Chang, and C.N.Georghiadis, "Iterative Joint Sequence and Channel Estimation for Fast Time-Varying Intersymbol Interference Channels," *Proc. ICC'95*, pp.357-361, Seattle, 1995.
- [34] P. Chevillat and E. Eleftheriou, "Decoding of trellis-encoded signals in the presence of intersymbol interference and noise," *IEEE Trans. Commun.*, vol. 37, pp. 669-676, July 1989.
- [35] M. V. Clark, L. J. Greenstein, K. Kennedy, and M. Shafi, "Matched filter performance bounds for diversity combining receivers in digital mobile radio," *IEEE Trans. Veh. Technol.*, vol. 41, no. 4, pp. 356-362, Nov. 1992.
- [36] COST 207, "Digital Land Mobile Radio Communications: Final Report," Luxembourg: *Office for Official Publications of the European Communities*, 1989.
- [37] J. De rosnay, "L'homme symbiotique, regards sur le troisième millénaire," *collection points*, nouvelle edition, Seuil, sept. 2000.
- [38] A. Duel-Hallen and C. Heegard, "Delayed Decision-Feedback Sequence Estimation," *IEEE Trans. on Commun.*, vol. 37, pp. 428-436, May 1989.
- [39] C. Douillard, M. Jézéquel, C. Berrou, A. Picard, P. Didier, and A. Glavieux, "Iterative correction of intersymbol-interference: Turbo-equalization," *Europ. Trans. on Telecom.*, vol. 6, pp. 507-511, Sept-Oct 1995.
- [40] D. Durand, "La systématique," *que sais je?*, no 1795, 9th edition, jan. 2002.
- [41] ETSI BRAN 3ERI074A, "Radio Wave Propagation Characteristics at 5 GHz with Modeling Suggestions for HIPERLAN/2," J. Medbo, Jan. 1998.
- [42] *ETSI Digital cellular telecommunications system (Phase 2+). GSM 05 series*, rel.1999.
- [43] ETSI. GSM Recommendations, 05.05, Version 5.8.0, December 1996.
- [44] M.V. Eyuboglu and S.U. Qureshi, "Reduced-state sequence estimation for coded modulation on intersymbol interference channels," *IEEE J. Sel. Areas Commun.*, vol. 7, pp. 989-995, Aug. 1989.
- [45] M.V. Eyugoblu and S.U. Qureshi, "Reduced-State Sequence Estimation with Set Partitioning and Decision Feedback," *IEEE Trans. on Commun.*, vol.36, pp.13-20, Jan. 1988.

- [46] S. A. Fechtel and Heinrich Meyr, "Matched Filter Bound for Trellis-Coded Transmission over Frequency-Selective Fading Channels with Diversity," *European Transactions on Telecommunications*, vol. 4, no. 3, pp. 109 – 120, May/June 1993.
- [47] G.J. Foschini, Jr, and M.J. Ganz, "On limits on Wireless Communication in a Fading Environment when using Multiple Antennas," *Wireless Personal Commun.*, vol. 6, no. 3, pp. 311-335, March 1998.
- [48] G.J. Foschini, G.D. Golden, R.A. Valenzuela, and P.W. Wolaniansky, "Simplified Processing for High Spectral Efficiency Wireless Communication Employing Multi-element Arrays," *IEEE J. Select. Areas Commun.*, vol. 17, no. 11, pp. 1841-1852, November 1999.
- [49] M. Fossorier et al., "On the Equivalence Between SOVA and Max-Log-MAP Decoding," *IEEE Commun Letters*, vol. 2, pp. 137-139, May 1998.
- [50] France Telecom (R. Visoz), "Preliminary results on turbo equalization for GERAN trellis based sub-optimal receiver," Tdoc 053, 3GPP TSG GERAN AdHoc on release 2000 and beyond, Helsinki, Aug. 2000.
- [51] V. Franz and G. Bauch, "Turbo-Detection for Enhanced Data GSM Evolution," *Proc. IEEE VTC'1999 Fall*, vol. 4, pp. 2954-2958, Amsterdam, Sept. 1999.
- [52] A. Furuskär, S. Mazur, F. Müller, and H. Olofsson, "EDGE, Enhanced Data Rates for GSM and TDMA/136 Evolution," *IEEE Pers. Commun. Mag.*, pp. 56-66, 1999.
- [53] W.H. Gerstacker and J.B. Huber, "Improved Equalization for GSM Mobile Communications," *Proc. ICT'96*.
- [54] W.H. Gerstacker and R. Schober, "Equalization for EDGE Mobile Communications," *IEEE Electronics Letters*, vol. 36, pp.189-191, No. 2, Jan. 2000.
- [55] W.H. Gerstacker, R. Müller, and J.B. Huber, "Iterative Equalization with Adaptive Soft Feedback," *IEEE Trans. Comm.*, vol.48, pp.1462-1466, Sept. 2000.
- [56] I. Ghauri and D. T. M. Slock, "Linear receivers for the DS-CDMA downlink exploiting orthogonality of spreading sequences," *Proc. 32th Asilomar Conf. On Signals, Systems and Comp.*, Asilomar, CA, Nov. 1-4 1998 .
- [57] 3GPP TSG-RAN #1 (01)0430, March 2001, TR 25.848 v6.0.0 (1999-10), "High Speed Downlink Packet Access".

- [58] 3GPP TSG RAN #5 (99)587, October 1999, TS 25.211 v3.0.0 (1999-10), "Physical channels and mapping of transport channels onto physical channels (FDD)".
- [59] J. Hagenauer, E. Offer, and L. Papke, "Iterative Decoding of Binary Block and Convolutional Codes," *IEEE Trans. Inform. Theory*, vol. 42, no. 2, pp. 429-445, Mar. 1996.
- [60] J. Hagenauer and P. Hoeher, "A Viterbi Algorithm with Soft-Decision Outputs and its applications," in *Proc. IEEE GLOBECOM'89*, pp. 1680-1686, Dallas, USA, Nov. 1989.
- [61] T. Hashimoto, "A List-Type Reduced-Constraint Generalization of the Viterbi Algorithm," *IEEE Trans. Inform. Theory*, vol. IT-33, no. 6, pp. 866-876, Nov. 1987.
- [62] M. Heikkilä, P. Komulainen, and J. Lilleberg, "Interference Suppression in CDMA Downlink through Adaptive Channel Equalization," *Proc. IEEE VTC 99 Fall*, Tokyo, Japan.
- [63] P. Humblet, *Telecommunications*, class notes of Institut Eurécom Sophia Antipolis, spring 1996.
- [64] W.C. Jakes, *Microwave Mobile Communications*, New York: John Wiley and Sons, chapter I, 1974.
- [65] S.H. Jamali and T. Le-Ngoc, "Coded Modulation Techniques for Fading Channels," *New York: Kluwer*, 1994.
- [66] V. Kaasila and A. Mammela, "Bit Error Probability of a Matched Filter in a Rayleigh Fading Multipath Channel," *IEEE Trans. Commun.*, vol. 42, no. 2/3/4, pp 826 – 828, Feb./March/April 1994.
- [67] S.M. Kay, "*Fundamentals of Statistical Signal Processing: Estimation Theory*," Prentice Hall, vol.1, NJ,1998.
- [68] W. Koch, A.Bair, "Optimum and Sub-Optimum Detection of Coded Data Disturbed by Time-Varing Intersymbol Interference," *Proc.GLOBECOM'90*, pp.1679-1684.
- [69] R. Krenz and K. Wesolowski, "Comparative Study of Space-Diversity Techniques for MLSE Receivers in Mobile Radio," *IEEE Trans. Veh. Technol.*, vol. 46, no. 3, pp. 653–663, August 1997.
- [70] F.R. Kschichang, V. Sorokine, "On the Trellis Structure of Block Codes," *IEEE Trans. Inform Theory*, vol. 41, no. 6, pp. 1924-1937, Nov. 1995
- [71] H. Kubo, B. Penther, "Single Carrier Modulation Scheme Employing Modified List-Output Equalizers," ETSI EP BRAN#9, Sophia Antipolis, July 1998.

- [72] E. Kurtas and T.M. Duman, "Iterative Decoders for Multiuser ISI channels," *?*, 1999
- [73] A. Lafourcade, A. Vardy, "Optimal Sectionalization of a Trellis," *IEEE Trans. Inform. Theory*, vol. 42, pp. 689-703, 1996.
- [74] C. Lamy, F. Boixadera and J.J. Boutros, "Iterative APP Decoding and Channel Estimation for Multiple-Input Multiple-Output Channels," *to be published in IEEE Trans. Commun.*, Jan. 2000.
- [75] P.A. Laurent, "Exact and Approximate Construction of Digital Phase Modulations by Superposition of Amplitude Modulated Pulses," *IEEE Trans. Commun.*, vol. 34, no. 2, pp. 150-160, Feb. 1986.
- [76] W.C.Y. Lee and Y.S. Yeh, "Polarization Diversity System for Mobile Radio," *IEEE Trans. Commun.*, vol. 20, no. 5, pp. 912-923, Oct. 1972.
- [77] E. A. Lee and D. G. Messerschmitt, *Digital communication*, Kluwer Academic Publishers, 2nd edition, 1994, pp. 448-450.
- [78] F. Ling, "Matched Filter-Bound for Time-Discrete Multipath Rayleigh Fading Channels," *IEEE Trans Commun.*, vol. 43, No. 2/3/4, pp. 710-713, Feb./March/April 1995.
- [79] F. Lotse, J.-E. Berg, U. Forssen, and P. Idahl, "Base Station Polarization Diversity Reception in Macrocellular Systems at 1800 MHz," in *Proc. IEEE VTC'96 Conference*, pp. 1643-1646, 1996.
- [80] A.A. Luna, F.M. Fontaine, S.B. Wicker, "iterative Maximum-Likelihood Trellis Decoding of Block codes," *IEEE Trans. Commun.*, vol. 47, no.3, pp. 338-342, March 1999.
- [81] C. Luschi *et al.*, "Performance of soft-output space-time equalization for EGPRS," *Proc. IEEE VTC'2000 Fall*, pp. 2325 -2332, Sept. 2000.
- [82] M. Mouly and M. B. Pautet, *The GSM system for mobile communications*, Published by the authors, Palaiseau, France, 1992.
- [83] T. Nagayasu *et al.*, "A Soft-Output Viterbi Equalizer Employing Expanded Memory Length Trellis," *IEICE Trans. on Comm.*, pp.381-385, vol.E80-B, No.2, Feb.1997.
- [84] N. Nefedov and M. Pukkila "Iterative Channel Estimation for GPRS," *Proc. IEEE PIMRC'2000*, London UK, Sep 2000.
- [85] N. Nefedov and M. Pukkila "Turbo Equalization and Iterative (Turbo) Estimation Techniques for Packet Data Transmission," *Proc. of Int. Symp. on Turbo Codes (ISTC'2000)*, pp.423-426, Brest, France, Sept. 2000.

- [86] N. Nefedov, M. Pukkila, R. Visoz, and A.O. Berthet, "Iterative Equalization and Estimation for Advanced TDMA Systems," *submitted to IEEE Trans. Commun.*
- [87] C. Nill and C.E. Sundberg, "List and Soft Symbol Output Viterbi Algorithms: Extensions and Comparison," *IEEE Trans. Commun.*, vol. 43, no. 2/3/4, pp. 277-287, February/March/April 1995.
- [88] S. Pasupathy, "Minimum Shift Keying: a Spectrally Efficient Modulation," *IEEE Communications Magazine*, vol. 17, pp. 14-22, July 1979.
- [89] B. Penther, H. Kubo, "Viterbi Equalization Technologies for Samba Project and Broadband Radio Access Network," ETSI EP BRAN#7, WG3 Temporary document 3MEL071.doc, Dec. 1998.
- [90] B. Penther, D. Castelain, and H. Kubo, "A Modified Turbo-Detector for Long Delay Spread Channels," in *Proc., 2nd International Symposium on Turbo-Codes*, Brest, France, Sept. 2000.
- [91] A. Picart, P. Didier, A. Glavieux, "Turbo-Detection: A new approach to combat channel frequency selectivity," *Proc. ICC'97*, pp.1498-1502.
- [92] J.G. Proakis, *Digital communications*, New York: McGraw-Hill, 2nd edition, 1989.
- [93] M. Pukkila, "Turbo Equalisation for Enhanced GPRS System," *Proc. IEEE PIMRC'2000*, London UK, Sep 2000.
- [94] R. Raheli, A. Polydoros, and C. Tzou, "Per-Survivor Processing: A General Approach to MLSE in Uncertain Environments," *IEEE Trans. Commun.*, 1995.
- [95] B. Risløw *et al.*, "Soft Information in Concatenated Codes," *IEEE Trans. Commun.*, vol. 44, pp. 284-286, March 1996.
- [96] P. Robertson, E. Villebrun, and P. Hoeher, "A Comparaison of Optimal and Sub-Optimal MAP Decoding Algorithms Operating in the Log Domain," in *Proc., IEEE ICC95*, Seattle, Washington, pp. 1009-1013, June 1995.
- [97] R. Robertson, P. Hoeher, and E. Villebrun, "Optimal and Sub-Optimal a Posterior Algorithms Suitable for Turbo Decoding," *European Trans. Telecommun.*, vol. 8, no. 2, pp. 119-125, March/April 1997.
- [98] J. Salz and J.H. Winters, "Effect of Fading Correlation on Adaptive Arrays in Digital Mobile Radio," *IEEE Trans. Veh. Technol.*, vol. 43, no. 4, pp. 1049 - 1057, Nov. 1994.

- [99] M. Sandell et al, "Iterative Channel Estimation Using Soft Decision Feedback," *Proc. Globecom'98*, pp. 3728 - 3733, Dec. 1998.
- [100] C.Schlegel, "Error Probability for Multibeam Rayleigh Channels," *IEEE Trans. Commun.*, vol. 44, no. 3, pp. 290-293, March 1996.
- [101] M. Schwartz, W.R. Bennet, and S. Stein, *Communications Systems and Techniques*, New York: McGraw-Hill, chapter 10, p. 479, 1966.
- [102] N. Seshardi, "Joint Data and Channel Estimation Using Blind Trellis Search Techniques," *IEEE Trans. Comm.*,v.42,No.2/3/4, 1994, pp.1000-1011.
- [103] N. Seshadri and C.E. Sundberg, "List Viterbi Decoding Algorithms with Applications," *IEEE Trans. on Communications*, vol. 42, no. 2/3/4, pp. 313-319, February/March/April 1994.
- [104] N. Seshadri and P. Hoeher, "On post-decision Reliability Generation," in *Proc., ICC'93*, Geneva, Switzerland, pp. 741-745, May 1993.
- [105] A.S. Stefanov and T.M. Duman, "Turbo-Coded Modulation for Systems with Transmit and Receive Antenna Diversity," *Proc. IEEE GLOBECOM99*, Rio de Janeiro, Brazil, pp. 2336-2340, Dec. 1999.
- [106] B. Steiner and P. Jung, "Optimum and Suboptimum Channel Estimation for the Uplink of CDMA Mobile Radio Systems with Joint Detection," *Europ. Trans. Telecommun.*, vol. 5, pp 39-50, Jan.-Feb. 1994.
- [107] P. Strauch *et al.*, "Turbo Equalization for an 8-PSK Modulation Scheme in a Mobile TDMA Communication System," *Proc.IEEE VTC'1999 Fall*, pp. 1605-1609, Amsterdam, Sept. 1999.
- [108] P. Strauch *et al.*, "Iterative Channel Estimation for EGPRS," *Proc. IEEE VTC'2000 Fall*, pp. 2271 -2277, Sept.2000.
- [109] S. Tantikovit and A.U.H. Sheikh "Joint multipath combining and MLSE equalization (rake-MLSE Receiver) for WCDMA systems," *VTC 2000 Spring*, Tokyo, Japan.
- [110] V. Tarokh, N. Seshadri, and A.R. Calderbank, "Space-Time Codes for High Data Rate Wireless Communication: Performance Criterion and Code Construction," *IEEE Trans. Inform. Theory*, vol. 44, no. 2, March 1998.
- [111] V. Tarokh, A. Naguib, N. Seshadri, and A.R. Calderbank, "Combined Array Processing and Space-time Coding," *IEEE Trans. Inform. Theory*, vol. 45, no. 4, pp. 1121-1128, May 1999.

- [112] V. Tarokh, H. Jafarkhani and A.R. Calderbank, "Space-time Block Codes from Orthogonal Designs," *IEEE Trans. Inform. Theory*, vol. 45, no. 5, pp. 1456-1467, July 1999.
- [113] E. Telatar, "Capacity of Multi-antenna Gaussian Channels," *AT&T Bell Laboratories Internal Tech. Memo.*, June 1995.
- [114] TIA/EIA/IS-95, "Mobile Station - Base Station Compatibility Standard for Dual-Mode Wideband Spread Spectrum Cellular System," July 1993.
- [115] P. Tortelier, and A. Berthet, "Décodage par le treillis des codes polynomiaux : un écueil à éviter," *submitted to Annals of Telecommunications*
- [116] G. Ungerboeck, "Channel Coding with Multilevel/phase Signals," *IEEE Trans. Inform. Theory*, vol. 28, pp. 56-67, Jan. 1982.
- [117] R.G. Vaughan, "Polarization Diversity in Mobile Communications," *IEEE Trans. Veh. Technol.*, vol. 39, no. 3, pp. 177 – 186, August 1990.
- [118] R. Visoz, P. Tortelier, and A. Berthet, "A Generalized Viterbi Algorithm for Trellis Coded Signals transmitted through Broadband Wireless Channels," *IEEE Electronic Letters*, vol. 36, no. 3, Feb. 2000.
- [119] R. Visoz, A.O Berthet, and P. Tortelier "Joint Equalization and Decoding of Trellis-Encoded Signals using the Generalized Viterbi Algorithm," in *Proc. IEEE VTC'2000*, Boston, USA.
- [120] R. Visoz and E. Bejjani, "Matched Filter Bound for Multichannel Diversity over Frequency-Selective Rayleigh-Fading Mobile Channels," *IEEE Trans. on Veh. Technol.*, vol. 49, No. 5, Sept. 2000.
- [121] R. Visoz, A.O. Berthet, A. Saadani, and B. penther, "Turbo Equalization and Incremental Redundancy for advanced TDMA systems," *proc. IEEE VTC'2001* spring conf., 6-9 May, Rhodes, Greece.
- [122] R. Visoz, A.O. Berthet, and J.J. Boutros, "Iterative Receivers for Bit-Interleaved Coded Modulation over Wireless frequency Selective Channels," *submitted to PIMRC2002*
- [123] R. Visoz, A.O. Berthet, and J.J. Boutros, "Joint Equalization and decoding using the Generalized Viterbi Algorithm for broadband wireless applications," *submitted to IEEE Transactions on commun.*, February 2001.

- [124] J.-F. Wagen and M. Keer, "Comparison of Diffraction Coefficients for Propagation Prediction in Microcell," *European cooperation in the field of scientific and technical research*, COST231 TD(93)80, Grimstad, Norway, May 1993.
- [125] A. Wautier, J.C. Dany, and C. Mourot, "Filtre correcteur de phase pour égaliseurs sous-optimaux," *Ann. Télécommun.*, no. 9-10, 1992.
- [126] K. Wesolowski, "Efficient digital receiver structure for trellis-coded signals transmitted through channels with intersymbol interference," *Electron. Lett.*, pp. 1265-1267, Nov. 1987.
- [127] J.H. Winters, J. Salz, and R.D. Gitlin, "The Impact of Antenna Diversity on the capacity of wireless Communications," *IEEE Trans. Commun.*, vol. 42, no. 2/3/4, pp. 1740-1751, Feb./March/April 1994.
- [128] J. Wolfmann, "Almost Perfect Autocorrelation Sequences," *IEEE trans. Inform. Theory*, vol. 38, No.4, July 1992.
- [129] K.W Yip and T.S. Ng, "Matched Filter Bound for Multipath Rician-Fading Channels," *IEEE Trans. Commun.*, vol. 46, no. 4, pp. 441 - 445, April 1998.
- [130] E. Zehavi, "8-PSK Trellis Codes for a Rayleigh Channel," *IEEE Trans. Commun.*, vol. 40, pp. 873-884, May 1992.

Publication list

Revue papers

- [131] R. Visoz and E. Bejjani " Matched Filter Bound for Multichannel Diversity over Frequency-Selective Rayleigh-Fading Mobile Channels ," *IEEE Trans. on Veh. Technol.*, vol. 49, No. 5, Sept. 2000.
- [132] A.O Berthet, B. Ünäl, and R. Visoz " On Iterative Decoding of Trellis-Encoded Signals over Multipath Rayleigh Fading Channels ," *IEEE J. Select. Areas Commun.*, vol. 19, sept. 2001.
- [133] R. Visoz, P. Tortelier, and A.O Berthet " A Generalized Viterbi Algorithm for Trellis Coded Signals transmitted through Broadband Wireless Channels ," *IEE Electron. Lett.*, March 2000, pp. 227-228.
- [134] N. Nefedov, M. Pukkila, R. Visoz, and A.O. Berthet " Iterative Equalization and Estimation for Advanced TDMA Systems " (co-operation with Nokia), submitted to *IEEE Transactions on communications*.
- [135] R. Visoz, A.O Berthet, and J.J. Boutros " Joint Equalization and decoding using the Generalized Viterbi Algorithm for broadband wireless applications ," submitted to *IEEE Transactions on communications*.
- [136] R. Visoz and A.O. Berthet "Iterative Receivers for Bit-Interleaved coded Modulation over wireless frequency selective channels," submitted to *IEEE Transactions on communications*.
- [137] A.O. Berthet and R. Visoz "Iterative Decoding of Serially Concatenated Multilayered Trellis-Coded Modulations in Multipath Rayleigh Fading Environment," submitted to *IEEE Transactions on communications*.

Conference papers

- [138] R. Visoz, E. Bejjani, and V. Kumar " Matched Filter Bound for Equalization and Antenna Diversity over Mobile Radio Channels ," IEEE International Conference on Universal Personal Communications, *Proc. IEEE ICUPC'98*, Oct. 1998 Florence Italy.
- [139] A.O Berthet, R. Visoz, B. Unal, and P. Tortelier " A Comparison of Several Strategies for Iteratively Decoding Serially Concatenated Convolutional Codes in Multipath Rayleigh Fading Environment ," *Proc. IEEE GLOBECOM'2000*, San Francisco, California, USA.
- [140] R. Visoz, A.O. Berthet, and P. Tortelier " Joint Equalization and Decoding of Trellis-Encoded Signals using the Generalized Viterbi Algorithm ," *IEEE VTC'Fall 2000*, Boston, USA.
- [141] A.O Berthet, R. Visoz, and P. Tortelier " Turbo-Equalization for Coded 8-PSK Signals over ISI Channels with application to EDGE Advanced Mobile System ," *Proc. IEEE PIMRC'2000*, London, UK, Sept. 2000.
- [142] R. Visoz, A.O. Berthet, A. Saadani, and B. Penther "Turbo Equalization and Incremental Redundancy for advanced TDMA systems," *Proc. IEEE VTC'2001 spring*, 6-9 May, Rhodes, Greece.
- [143] A.O Berthet, B. Penther, R. Visoz, and J.J. Boutros " A new reduced complexity Turbo detector for highly selective long delay spread ISI channels : a solution for 4G Mobile Systems ? ," *Proc. IEEE VTC'2001 spring*, 6-9 May, Rhodes, Greece.
- [144] B. Unal, A.O. Berthet, and R. Visoz "Iterative Channel Estimation and Coded Symbol Detection for Dispersive Channels," *Proc. IEEE PIMRC'2001*, 30-3 Oct., San Diego, USA.
- [145] A.O. Berthet, R. Visoz, and B. Unal " Iterative Decoding of Serially Concatenated Multilayered Trellis Coded Modulations in the presence of InterSymbol Interference and Noise," *IEEE GLOBECOM'2001*, 25-29 Nov., San Antonio, USA.
- [146] R. Visoz, A.O. Berthet, and J.J. Boutros "Iterative Decoding of Bit-Interleaved Coded Modulation over Wireless Frequency-Selective Channels," submitted to *IEEE PIMRC'2002*.
- [147] H. Boujemaa, R. Visoz, and A.O. Berthet, "Rake-DFSE (Decision Feedback Sequence Estimator) Equalizer for the UMTS Downlink," selected for oral presentation at *IEEE VTC'2002 spring*.

Normalisation

- [148] France Telecom (R. Visoz) ” Preliminary results on turbo equalization for GERAN trellis based sub-optimal receiver ,” Tdoc 053, presented to 3GPP TSG GERAN AdHoc on release 2000 and beyond, Helsinki, Aug. 2000.

Patents

- [149] Patent 99 11411 filed on Sept. 99 by France Telecom, P. Tortelier, R. Visoz ” Procédé de décodage et d'égalisation conjointe d'un signal numérique protégé par un code défini par un treillis ”.
- [150] Patent 00 06246 filed on May 2000 by France Telecom, A.O. Berthet, R.Visoz ” Procédé et système de détection et de décodage itératif couplé à une ré-estimation des coefficients du canal de transmission ”.
- [151] Patent 01 02343 filed on Feb. 2001 by France Telecom, A.O. Berthet, R.Visoz ” Procédé et système de codage-décodage itératif de flux de données numériques codées par combinaisons spatio-temporelles, en émission et réception multiple ”.
- [152] Patent 01 05037 filed on Apr. 2001 by France Telecom, A.O Berthet, R. Visoz ” Procédé de codage/décodage d'un flux de données numériques codées avec entrelacement sur bits en émission et en réception multiple en présence d'interférence inter-symboles et système correspondant ”.
- [153] Patent 01 11549 filed on Sept. 2001 by France Telecom, R. Visoz, H. Boujemaa ” Procédé et système de réception itérative sous optimale pour système de transmission haut débit CDMA”.